Copyright Warning & Restrictions

The copyright law of the United States (Title 17, United States Code) governs the making of photocopies or other reproductions of copyrighted material.

Under certain conditions specified in the law, libraries and archives are authorized to furnish a photocopy or other reproduction. One of these specified conditions is that the photocopy or reproduction is not to be "used for any purpose other than private study, scholarship, or research." If a, user makes a request for, or later uses, a photocopy or reproduction for purposes in excess of "fair use" that user may be liable for copyright infringement,

This institution reserves the right to refuse to accept a copying order if, in its judgment, fulfillment of the order would involve violation of copyright law.

Please Note: The author retains the copyright while the New Jersey Institute of Technology reserves the right to distribute this thesis or dissertation

Printing note: If you do not wish to print this page, then select "Pages from: first page # to: last page #" on the print dialog screen

ABSTRACT

ANALYTICAL AND EXPERIMENTAL STUDY OF INVESTMENT CASTING WITH LASER STEREOLITHOGRAPHY MODELS

by
Wen-Long Yao

This dissertation presents an analytical and experimental investigation of ceramic shell cracking during the burnout process in investment casting with internally webbed laser stereolithography (SLA) patterns. Included in the consideration are the cracking temperature of the ceramic shell, the web link buckling temperature, and the glass transition temperature of the epoxy resin. The hypothesis is that shell cracking will occur when the cracking temperature is lower than the glass transition temperature and the web buckling temperature.

An analytical and experimental study has been conducted, with the cross-sectional area, the span length of the web structure, and the shell thickness being the variables. It is found that the ceramic shell cracking and the internal web structure buckling are related to the cross-sectional area, the span length of the web structure, and the shell thickness. A finite element analysis (FEA) model is developed to simulate the burnout process in investment casting with an SLA webbed pattern. The numerical results show that the shell cracking in investment casting can be prevented by the buckling of epoxy webbed pattern in early stages of the burnout process. A strain gauge based experimental study validates the trend of the computational prediction from FEA of the burnout process in investment casting with SLA webbed epoxy patterns. The thermal insulation property of

ANALYTICAL AND EXPERIMENTAL STUDY OF INVESTMENT CASTING WITH LASER STEREOLITHOGRAPHY MODELS

by
Wen-Long Yao

A Dissertation
Submitted to the faculty of
New Jersey Institute of Technology
in Partial Fulfillment of the Requirements for the Degree of
Doctor Philosophy

Department of Mechanical Engineering

May 1998

APPROVAL PAGE

ANALYTICAL AND EXPERIMENTAL STUDY OF INVESTMENT CASTING WITH LASER STEREOLITHOGRAPHY MODELS

Wen-Long Yao

Dr. Ming C. Leu, Dissertation Advisor — Date
New Jersey State Sponsored Chair in Manufacturing/Productivity
Professor of Mechanical Engineering, NJIT

Dr. Bernard Koplik, Committee Member — Date
Professor of Mechanical Engineering, NJIT

Dr. Rong-Yaw Chen, Committee Member — Date
Professor of Mechanical Engineering, NJIT

Dr. Denis Blackmore, Committee Member — Date
Professor of Mathematics, NJIT

Dr. Zhiming Ji, Committee Member — Date
Associate Professor of Mechanical Engineering, NJIT

BIOGRAPHICAL SKETCH

Author: Wen-Long Yao

Degree: Doctor of Philosophy

Date: May 1998

Undergraduate and Graduate Education:

- Doctor of Philosophy in Mechanical Engineering
  New Jersey Institute of Technology, Newark, NJ, USA, 1998

- Master of Science in Mechanical Engineering
  New Jersey Institute of Technology, Newark, NJ, USA, 1990

- Bachelor of Mechanical Engineering
  Feng Chia University, Taichung, Taiwan, 1980

Major: Mechanical Engineering

Publications:

W. L. Yao, M. C. Leu, and B. Yang
"Shell Cracking in Investment Casting with Laser Stereolithography Patterns," accepted by the Ninth Annual Solid Freeform Fabrication Symposium, U. of Texas at Austin, August, 1998.

W. L. Yao, H. Wong, M. C. Leu, and D. H. Sebastian
"An Analytical Study of Investment Casting with Webbed Epoxy Patterns," Proceedings of the 1996 ASME Manufacturing Science and Engineering Winter Conference and Annual Meeting, MED-Vol. 4, Atlanta, GA, November, 1996.

W. L. Yao and M. C. Leu
"Analysis of Thermal Stresses in Investment Casting with Epoxy Patterns," Proceedings of North America Stereolithography User Group 1996 Conference and Annual Meeting, San Diego, CA, March, 1996.

M. C. Leu, W. L. Yao and D. H. Sebastian
"An Investigation into the Use of Laser Stereolithography in Rapid Prototyping, and Tooling," Technical Report of Center of Manufacturing Systems, New Jersey Institute of Technology, August, 1996.

M. C. Leu, B. Yang, and W. L. Yao
"A Feasibility Study of EDM Tooling Using Metalized Stereolithography Models," Proceeding of North America Manufacturing Research Conference, May 19-22, 1998, Atlanta, GA.

M. C. Leu, W. Zhang, L. A. Hanesian, and W. L. Yao
"Effect of Stereolithography Process Parameters on Part Curl Distortion," submitted to ICRPM, Beijing, China, April, 1998.

W. Zhang, M. C. Leu, Z. Ji, W. L. Yao, B. Yang and Y. N. Yan
"Rapid Freezing Prototyping with Water," accepted by the Ninth Annual Solid Freeform Fabrication Symposium, U. of Texas at Austin, August, 1998.

W. L. Yao and K. J. McDermott
"Developing a Hybrid Programmable Logic Controller Platform for a Flexible Manufacturing System," The International Journal of Flexible Manufacturing Systems, Vol. 9, No. 4, October, 1997.

W. L. Yao and K. J. McDermott
"A PC-based Programmable Logic controller Platform for a Flexible Manufacturing System," Proceedings of 1996 ASME Japan/USA Symposium, Vol. 1, Boston, MA, July, 1996.

W. L. Yao
"Development of a Flexible Control and Automatic Data Acquisition System for Wear Testing," Master's Thesis, Mechanical Engineering, New Jersey Institute of Technology, Newark, New Jersey, 1990.

Presentations

W. L. Yao
"A Feasibility Study of EDM Tooling Using Metalized Stereolithography Models," North America Manufacturing Research Conference, May 19-22, 1998, Atlanta, GA.

W. L. Yao
"Study of Ceramic Shell and Stereolithography Pattern Using FEA,"
ANSYS Local User Group Meeting and Conference, Lucent Technologies, Holmdel, New Jersey, May, 1997.

W. L. Yao

"An Analytical Study of Investment Casting with Webbed Epoxy Patterns," NJIT & Drew Graduate Student Research Forum, New Jersey Institute of Technology, Newark, New Jersey, April, 1996.

W. L. Yao

"A PC-based Programmable Logic controller Platform for a Flexible Manufacturing System," NJIT & Drew Graduate Student Research Forum, New Jersey Institute of Technology, Newark, New Jersey, April, 1996.

W. L. Yao

"A PC-based Programmable Logic controller Platform for a Flexible Manufacturing System," The 1996 ASME Japan/USA Symposium, Boston, MA, July, 1996.

Awards and Honors:

Licensed Professional Engineer, Connecticut, No. 00019667, 1996.
Teaching Fellowship, New Jersey Institute of Technology, 1998 Spring.
Research Assistantship, New Jersey Institute of Technology, 1994 Fall-1998 Spring.
Teaching Assistantship, New Jersey Institute of Technology, 1994 Fall-1996 Spring.
Who's Who in America in Science and Engineering, 1997.

This dissertation is dedicated to
my parents, in-laws,
wife Shu-chuan and son Jason for
their love, patience, courage and support.

ACKNOWLEDGMENT

I would like to express my appreciation and sincere gratitude to my research advisor, Dr. Ming C. Leu, for introducing me to solid freeform fabrication technology and his valuable guidance, counsel, research assistantship (RA: 96F, 97S and 97F) and friendship throughout this study.

I am very grateful to the Department of Mechanical Engineering and Dr. R. Y. Chen for teaching assistantship support (TA: 94F, 95S - 96S, and Teaching Fellow: 98S). I also express my special thanks to Drs. B. Koplik, D. Blackmore, R. Y. Chen and Z. Ji for their fruitful suggestions to this dissertation and for serving as members of the committee. Thanks are also due to Sandia National Laboratories for performing ceramic coating on epoxy samples used in the burnout experiments. Also acknowledged are timely help and valuable suggestions from many good friends: S. Wong, Dr. S. C. Chang and Drs. H. Wong, H. T. Liao, K. Naruse and W. Zhang who are members of the Robotics and Intelligent Manufacturing Laboratories. The work of author was partially supported by the Multi-Lifecycle Engineering Research Center (MERC) and 3D Systems, Inc., Valencia, CA.

Specially, I thank my wife Shu-chuan and my son Jason for their patience, comfort, and support. I also extend my thanks to my parents and the members of family for their support throughout my life.

TABLE OF CONTENTS

TABLE OF CONTENTS
(Continued)

Chapter **Page**

TABLE OF CONTENTS
(Continued)

Chapter **Page**

LIST OF TABLES

LIST OF FIGURES

LIST OF FIGURES
(Continued)

LIST OF FIGURES
(Continued)

LIST OF FIGURES
(Continued)

LIST OF FIGURES
(Continued)

LIST OF SYMBOLS

P_L	laser power
W_0	Gaussian half width
V_s	scan speed
D_p	penetration depth of resin where the irradiance is about 37% or 1/e of the surface irradiance
C_d	the maximum cure depth or thickness of the solidified layer
E	the exposure energy used to solidify the resin mixture
E_{crit}	the critical exposure at which solidification starts to occur
L_w	the full-width of a laser cured line
B	laser spot diameter
l	layer thickness
t	ceramic shell thickness
P	generated contact pressure
δ_1	deformation of resin pattern due to temperature rise
δ_2	deformation of ceramic shell due to temperature rise
Δ_1	deformation of epoxy pattern due to contact pressure
Δ_1	deformation of ceramic shell due to contact pressure
L	web link length
b	web link width
h	web link height
ε_c	induced strain on ceramic shell

LIST OF SYMBOLS
(Continued)

σ_c	induced stress on ceramic shell
E_c	Young's modulus of ceramic
E_r	Young's modulus of epoxy resin
α_c	coefficient of thermal expansion of ceramic
α_r	coefficient of thermal expansion of epoxy resin
R	radius of circular pattern
ΔT	temperature rise
MOR	modulus of rupture of ceramic material
T_g	glass transition temperature of the epoxy resin
T_u	cracking temperature of the ceramic shell
T_b	buckling temperature of the web link
P_{cr}	critical load per unit area to cause web link buckle
I	moment inertia of web structure
A	cross-sectional area of web structure
σ_θ	hoop or circumferential stress of walled cylinder
σ_{rad}	radial stress of walled cylinder
$\delta_{r,T}$, $\delta_{c,T}$	elongation of resin and ceramic due to temperature rise
$\delta_{r,p}$, $\delta_{c,p}$	elongation of resin and ceramic due to generated contact pressure
ν_r, ν_c	Poisson ratio of epoxy resin and ceramic
$\{\sigma\}$	stress tensor

LIST OF SYMBOLS
(Continued)

$\{\varepsilon\}$	strain tensor
[D]	elasticity matrix
[B]	strain-displacement matrix
$\{u\}$	nodal displacement vector
$\sigma_1, \sigma_2, \sigma_3$	principal stresses
σ_x, σ_y	compressive stresses

CHAPTER 1

INTRODUCTION

The investment casting process, also known as the lost wax process, is a precision casting and ancient metal forming process. This process offers good surface finish, complex geometry, and cast features without the necessity of extensive machining or finishing work. Its products are everywhere and its processes are diverse. The processes have the following points in common: (1) Expendable patterns are used - usually produced from wax through injection of liquid wax into a precision engineered pattern die, (2) Shell mold is done with a tedious slurry coating process, (3) The ceramic shell is hardened in contact with the pattern, providing precise reproduction of the pattern, (4) The mold is heated to remove the pattern and drive off all gases, and (5) Molten metal is poured into the cavity to form metal parts. Traditional methods for producing prototypes in the foundry are frequently very expensive and time-consuming, resulting in a limited number of possible design iterations. It is an industry that is in great need of modernization.

Complex models can be produced without shaping tools, automatically and without human intervention, by a new, rapid prototyping technology. Rapid Prototyping (RP), sometimes referred to as Layered Manufacturing (LM) or Solid Freeform Fabrication (SFF), is a relatively new technology. All SFF systems convert a computer-aided design of a three-dimensional object to a physical model by sequentially stacking thin, two-dimensional laminates. The development of RP methods currently revolutionizes a new product development cycle. A complex model, which usually took

weeks to manufacture, is now available in a few hours or days via the rapid provision of models. RP models allow a concurrent, iterative examination of the quality and functionality of a product. A main strength of RP is its ability to make patterns for investment casting. RP lends itself well to mitigate a bottleneck of the investment casting industry.

The most popular of RP technologies is using the stereolithography apparatus (SLA). It is valued for its exceptional dimensional accuracy, building speed, and ability to fabricate parts of complicated shape. SLA in conjunction with investment casting provides a rapid route to fabricate functional metal parts as well. In a globally competitive market, this casting method can be used as an instrument to reduce production time and cost. However, despite the many advances of SLA, several inherent shortcomings have prevented foundries from achieving the same success in using SLA patterns as thermally expendable patterns as the conventional wax patterns in shell investment casting.

The major deficiency of applying the SLA technology to shell investment casting tooling is the property of the photopolymer. The thermoset material of the SLA model does not melt under heating during the pattern burnout process. The expansion of the cured resin creates stresses on the ceramic wall that may cause the investment ceramic shell to crack. Although, in conventional investment casting, the investment casting wax also has a high coefficient of thermal expansion, it does not cause stress build-up since wax melts at low temperatures. The early attempt to replace wax models with solid SLA models as thermally expendable models did not show impressive results. Nonetheless, investment casters found good success with these solid SLA patterns by using a solid

plaster investment mold. The solid plaster mold offers greater strength and smaller mismatch in thermal expansion. Although this older technique is less accurate than the shell investment mold, it is the preferred route for use with solid plastic patterns.

The replacement of wax patterns in the investment casting process with solid acrylate SLA models, provided the investment caster in early process development with many challenging problems. Recently quasi-hollowed build styles and newer SLA epoxy resins were developed by the SLA manufacturer and resin suppliers to make the SLA technology more applicable to rapid manufacturing. With the advances in resins and build styles coupled with increased experiences, more metal parts are being produced from SLA models via the shell investment casing route. However, despite the improvements, the ceramic shell, using rapid SLA prototypes as thermally expendable patterns, may still crack during the epoxy pattern burnout process.

At present the process knowledge of the user grows primarily on the basis of ineffective "trial-and-error" procedure. The present understanding about fundamental thermal effects on the webbed pattern and ceramic shell is not sufficient. A research team at 3D Systems Inc., the SLA manufacturer, studied quasi-hollow webbed patterns in investment casting. Jacobs observed the yield of casting as a function of the pattern void ratio, defined as the fraction of air space in a pattern [Jacobs, 1995]. He stated that under such a situation the SLA webbed patterns would collapse inwards under the influence of heat, rather than cracking the ceramic shell by expanding outwards. Hague and Dickens indicated that the SLA pattern is likely to soften under heat [Hague and Dickens, 1995 and 1996]. They observed shell cracking at temperatures below the glass transition temperature of the epoxy material. They did not observe buckling of the hollow SLA

pattern in their burnout experiments. Our hypothesis is that shell cracking will occur when the cracking temperature is lower than the temperature of glass transition and the temperature of web buckling. We observe that the cracking of the shell can be prevented if either the material softened or the web links buckled during the burnout process. The web link buckling and shell cracking are correlated to the cross-sectional area of web structure, web link space, and thickness of ceramic shell.

This doctoral study is aimed at determining why quasi-hollowed models are cracking the investment ceramic shells, what causes the webbed pattern to collapse, and how to design an optimal web structure to prevent cracking. The dissertation includes both analysis and experimentation. Chapter 2 discusses the fundamentals of SLA and rapid routes for making investment casting prototypes. Chapter 3 presents the statement of the problem, research objectives, and project tasks, and reviews related studies. A numerical simulation model using finite element analysis is presented in Chapter 4. The analysis of the equivalent force technique is also presented. A model of the web structure is derived to describe the variables related to the cracking of investment shells and the buckling of web links. Chapter 5 describes the experimental results of the SLA pattern burnout process in investment casting. It provides the evidence of shell cracking in investment casting obtained from the computational simulation and supports the shell cracking hypothesis in this study. A strain gauge based experiment is then performed to validate the computer simulation results. Chapter 6 shows the design and simulation of a hexagonal honeycomb internal web structure via rheological and geometrical studies. Finally, concluding remarks and recommended process improvements are given in Chapter 7.

CHAPTER 2

SOLID FREEFORM FABRICATION

This chapter reviews the current RP technologies (especially on SLA), functional principles, rapid tooling applications, and research activities. It describes the use of the SLA pattern in the prototype investment casting process. Also discussed are the fundamental operating principles and process of SLA. The purpose of this chapter is to help identify the research problem.

2.1 Rapid Prototyping Methods

In engineering practice, making physical prototypes from a design concept in a new product development is often costly and time consuming. Changes made after a production run are very costly. A limited number of prototypes are necessary in the early design stage for form, fit, and function testing or tooling checking. Physical prototypes have many advantages over a sketch, engineering drawing, or computer representation of a part. Being able to view and touch models of a product can be an extremely valuable step in the design process. This helps correct design errors and optimize the product design before tooling fabrication and product manufacturing, thus minimizing costly engineering changes and time to market, and assuring product quality. Conventionally, physical prototypes are either machined or cast. In either case, the time and cost associated with product redesign or tooling rework can be considerable. Flexible and inexpensive prototype and tooling fabrication methods are urgently needed.

Generally speaking, fabrication processes can be categorized into three groups: subtractive, additive, and conservative [Burns, 1993]. Machining processes such as milling, turning and grinding are subtractive processes. In these processes, a block of raw material is carved out to produce the desired shape and heat treated for desired strength. The methods to produce internal cavities or complex geometric parts are difficult. Conservative processes, including casting and molding, are also conventional. In these processes, a semi-solid or liquid material is forced into a pre-formed mold of desired shape, which is pre-fabricated by a machining process. The inherent problems are the same as those in the subtractive process. Unlike subtractive and compressive processes, an additive process builds an object by joining materials in layered fashion. Additive processes are often referred to as rapid prototyping (RP), layered-manufacturing (LM), or solid freeform fabrication (SFF). The process is especially useful for creating complex three-dimensional models quickly and accurately, with details hard to match by CNC machining.

About a decade ago, several RP processing technologies were developed to convert the CAD data of an object into a physical model. Taking advantages of computer hardware and software technologies, the CAD data of a three-dimensional object was sliced into multiple two-dimensional layers (see Figure 2.1) [Menon 1991]. RP fabricators generate a three-dimensional physical model by stacking thin layer cross-sections of the sliced part geometry from the CAD data.

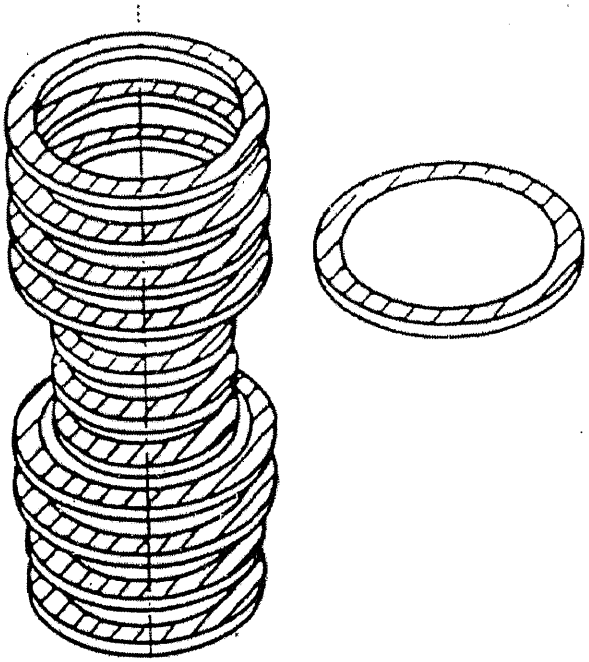

Figure 2.1 Sliced thin cross-sectional layers of a three-dimensional part.
Source: [Menon, 1991]

The goal of RP technology is rapid and accurate translation of CAD model data to create, without tooling or cutting, a physical prototype in a fraction of the time required by conventional methods. RP systems can quickly create a complex model of high accuracy (e.g. about 1.8 mils in SLA), with internal cavity (e.g. ship in a bottle), small features and fine details not matched by CNC machining. They allow the engineers to create a physical prototype without machining or tooling, and often within hours or days, instead of months. If any improvements or revisions are necessary, the part can be redesigned easily before it is prototyped again, and the process can be repeated as many times as desired over a period of just days to arrive at the final design, before making expensive investments in tooling for part fabrication. RP technology has been

documented by a diverse array of companies and organizations in an attempt to provide major benefits in engineering visualization, verification, and design iteration and optimization, with substantial productivity gains and cost savings. RP technology has added "One real prototype is worth a thousand pictures" to the old saying "A picture is worth a thousand words" [Jacobs, 1992].

RP fabrication processes can be classified according to the method of controlling layer fabrication [Johnson, 1994]. Raw material and energy are used to build each layer using information in the layer description. Interaction of raw material mass (m) and energy (W) produces the physical layer in a total variation occurring as:

$$\Delta(mW) = m\Delta W + W\Delta m \tag{2.1}$$

RP processes can produce a model by selectively activating a uniform mass m acted on by a variable energy ΔW controlled by the layer description, or by acting a constant energy on a variable mass Δm controlled by layer information. RP fabrication processes can be classified as variable energy processes $m\Delta W$, such as Laser Stereolithography (SLA), Selective Laser Sintering (SLS), Laminated Object Manufacturing (LOM) and 3-D Printing (3DP) (or Direct Shell Production Casting, DSPC), and variable mass processes $W\Delta m$, such as Ballistic Particle Manufacturing (BPM), Sander Prototype (SPI), Laser-Engineered-Net-Shaping (LENS), and Fused Deposition Manufacturing (FDM). These RP technologies are either laser related or non-laser related (see Figures 2.2 and 2.3). They use various materials, such as light sensitive resins, ceramic powders, wax, plastics and paper, etc. They use the same principle of building a rapid prototype in an additive manner.

SLA technology fabricates physical parts by controlling a laser beam generated ultra-violet light to selectively cure photopolymer resins layer by layer. In SLS layers of powder are sintered one at a time. In FDM a filament of wax or nylon is melted and re-solidified in layers. In LOM the cross-section of each layer is cut by a laser beam from a continuous sheet of material. In 3DP the ink-jet printer technology has been modified to selectively bind layers of powder to produce the physical part. In LENS metal powders are injected into a pool of molten metal created by a focused laser beam while the substrate below is slowly moved to trace out the geometry of the desired part. [Ashley, 1991, 1997; Burns, 1991; Conley and Marcus, 1997; Deckard and Beaman, 1988; Jacobs, 1992; Menon and Dickens, 1992; and Sachs, 1991].

The collective features of these new RP techniques can be summarized as follows:

- The production of the structural parts takes place layer by layer automatically without human intervention, and with no fixture needed.
- For most methods, the manufacture of parts is the result of conversion of a liquid, powder, filament or film starting material into a solid state.
- The manufacture of parts occurs directly from computer based three dimensional description of the part geometry.

Each RP process has restrictions in terms of accuracy, material coverage, part size, and cost. None of the existing RP systems excels over others in all aspects. For example: although SLA is limited in materials, it is widely used for concept visualization, form and fit analysis, and secondary tooling creation. A major distinction of SLS is the capability of using a variety of materials for final functional parts. The ease of support

removal and the variety of selective materials led to a substantial increase of FDM market shares. Table 2.1 summarizes a comparison of major commercial RP processes.

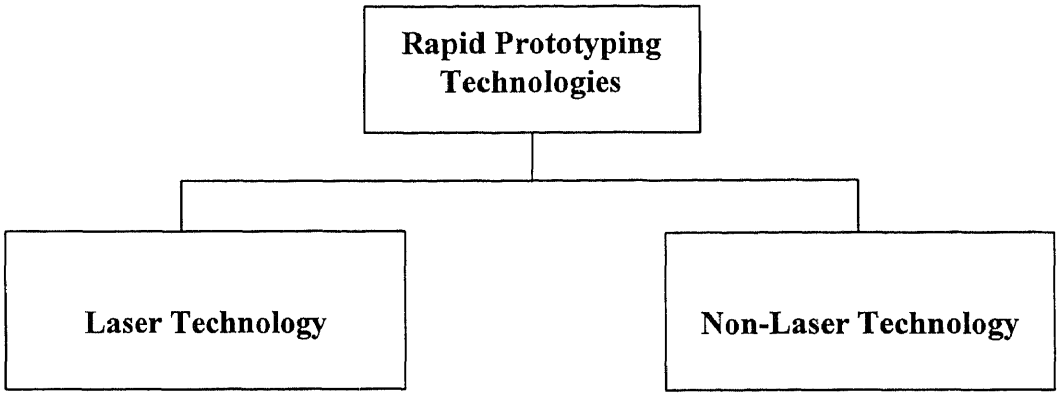

- 3D Systems - SLA
  Stereolithography Apparatus
- DTM/U.T., Austin - SLS
  Selective Laser Sintering
- Helisys - LOM
  Laminated Object Manufacturing
- Sandia National Lab. - LENS
  Laser-Engineered Net Shaping
- Stratasys Inc. - FDM
  Fused Deposition Modeling,
  Controlled Nozzle Extrusion.
- Soligen/M.I.T. - 3DP or DSPC
  Ink-Jet Printing,
  Direct Shell Production
- Carnegie Mellon University -SDM
  Shape Deposition Manufacturing
- BPM Technology - BPM Ballistic
  Particle Manufacturing

Figure 2.2 RP&M alternative technologies.

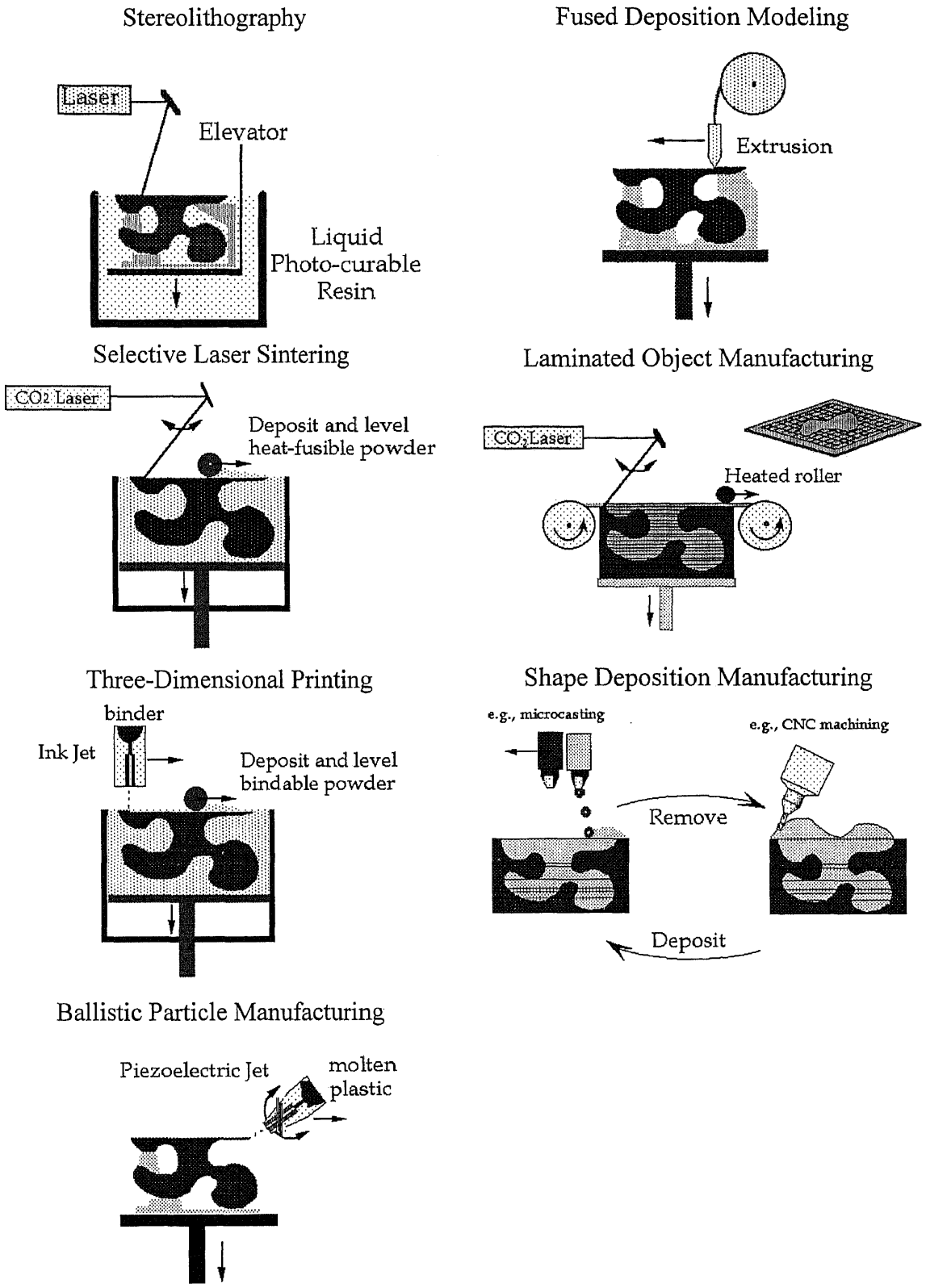

Figure 2.3 Operating principles of solid freeform fabrication technologies. Source: [Beaman, 1997]

Table 2.1 A comparison of some RP technologies.

Maker	3D Systems	Stratasys	DTM/U. T., Austin	Sanders Prototype	Soligen/MIT	Helisys
Technology	Laser Curing Stereolithography	Fused Deposition Modeling	CO_2 Laser Sintering	Liquid Jetting Deposition	3D Ink-Jet Printing of Binder	CO_2 Laser Cutting and Adhesive Stacking
Material	Liquid Photopolymer: Epoxy Acrylate	Filament of Thermoplastic: Nylon, ABS Casting Wax	Powder of Nylon, Polycarbonate, Casting Wax Metal	Low-Melting Thermoplastic and Wax for Support	Powder of Ceramic and Adhesive Binder	Adhesived Sheet Paper, Polyester
Support Requirement	Need Supports	Need Supports	Powder Self - Supporting	Separate Wax for Support	Powder Self - Supporting	No
Layer Thickness	0.004 - 0.020 in	0.002 - 0.030 in	0.003 - 0.020 in	0.0005 - 0.005 in		0.008 inch
Post Process	Support Removal, Postcuring	Support Removal	Sintering	Support Removal	Sintering/Firing	None
Build Size	SLA 250: 10"x10"x12" SLA 500: 20"x20"x24"	10"x10"x10"	12 Diameter x 15 in	12"x6"x9"	16"x16"x16"	LOM 1015: 10"x15"x14" LOM 2030: 22"x32"x20"
Achievable Accuracy	0.0018 in	0.005 in	0.005 in	0.0005 in		0.01 in
File Format	STL and SLC	STL, NC Code and IGES	STL and IGES	STL, SLC, and DXF	STL	STL

2.2 Stereolithography Apparatus

SLA was first commercialized in 1988. It is the most widely used RP technology today. SLA is an optical fabrication process that translates CAD solid model data into a physical model by successively laser-curing liquid photopolymeric resin to build the cross sections of a part layer by layer. The computer controlled SLA system consists of an open-top vat of photocurable polymer resin, computer controlled automatic elevating platform and leveling device, and an ultraviolet (UV) or visible wavelength laser and optical mirror system. A schematic illustration of the SLA machine is shown in Figure 2.4. The process of production of an SLA part starts from a 3-D CAD design. In the pre-processing, a three-dimensional object is developed using a CAD system and its surface is approximated by triangular facets in STL format. The object is then sliced into a number of two-dimensional cross-sections. The part is built from bottom to top by a computer controlled laser and elevator. The process is illustrated in Figure 2.5.

As noted above, SLA builds a part by controlling a laser beam to selectively cure liquid photopolymer layer by layer. So, the principle of polymerization and exposure of laser beam play important roles in SLA technology. In the following sections, the principles of photo polymerization and laser beam in SLA will be reviewed to provide a solid understanding of the process.

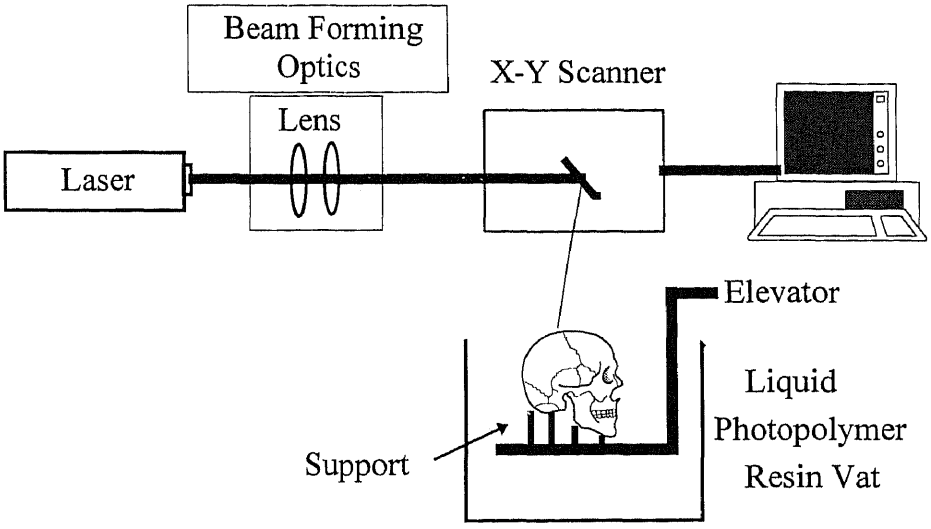

Figure 2.4 The SLA system.

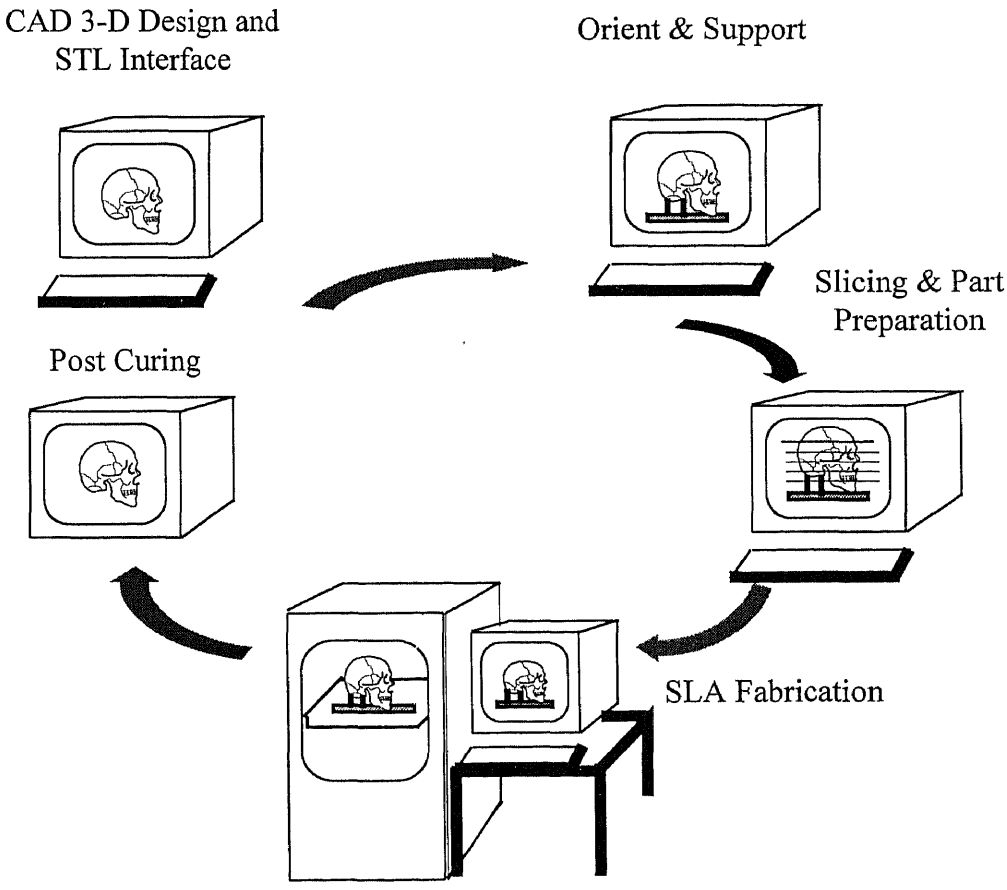

Figure 2.5 Fabrication sequence of SLA prototype.

2.2.1 Photocurable Resin and Photo Polymerization

The materials used in the SLA method are photocurable polymer resins, such as acrylate or epoxy resins. Epoxies are attractive because of their higher mechanical strength and lower volumetric shrinkage compared to acrylates. The requirements for the resins are:

- high reactivity in order to achieve high degrees of polymerization
- unchanged viscosity in order to allow for equal layering
- good susceptibility to aging
- low sensitivity to process parameter variation
- low toxicity
- low shrinkage
- high rigidity and impact toughness.

The forming of photocurable thermoset resins is more sophisticated. Polymerization is the process of linking small liquid monomers into larger solid polymers using the catalyst energy of absorbed photons. The radicals may be generated either thermally or photochemically. In SLA, the forming of thermoset polymers is photoinitiated radical polymerization. Actinic photon is the catalyst for transformation of the liquid monomer to solid polymer. Three essential steps in polymerization for SLA are initiation, propagation, and termination. A radical process of photopolymerization of ethylene is shown in Figure 2.6.

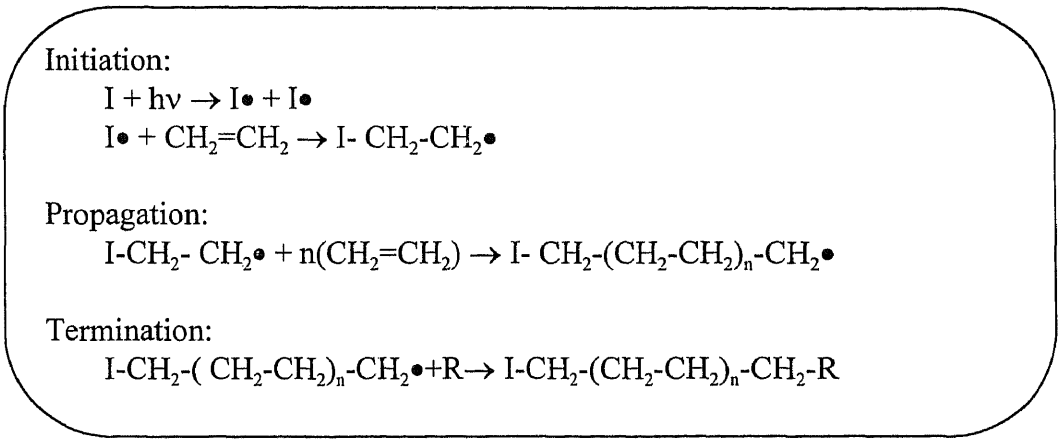

Figure 2.6 Photopolymerization process: initiation, propagation, and termination.

2.2.2 Laser Exposure

SLA is able to rapidly direct focused radiation of appropriate power and wavelength onto the surface of a liquid photocurable resin to form a two dimensional layer of a solid part. The use of a laser beam with a continuous wave emitting radiation of power P_L at a suitable wavelength λ is the source of radiation with very high radiance to provide a tightly focused spot on the surface of the photopolymer located at a substantial distance. Excellent features of an SLA part rely greatly on the features of laser. For example, the minimum feature size of a part is determined by the diameter of the focused laser spot on the photopolymer surface. The resolution of a part depends on the angular accuracy of the galvanometers, the ability to control the intensity distribution, and the laser power.

The solidification of the liquid resin depends on the optical energy per unit area, also known as the exposure. The volumetric exposure equation for any arbitrary point is

$$E_{crit} = \sqrt{\frac{2}{\pi}} [P_L/W_o\ V_s] \exp [-(2y^2 / W_o^2 + z/ D_p)] \qquad (2.2)$$

When the exposure is less than a critical value, E_{crit}, the resin remains liquid. When the exposure is greater than E_{crit}, the resin polymerizes. When the exposure is equal to E_{crit}, the polymer is at the gel point, corresponding to the transition of the liquid from monomers to polymers. The critical exposure energy at a locus of points (y^*, z^*) is:

$$E_{crit} = \sqrt{\frac{2}{\pi}} [P_L/W_o\ V_s] \exp [-(2y^{*2} / W_o^2 + z^* / D_p)] \tag{2.3}$$

where P_L is laser power, W_o is Gaussian half width of the laser spot, V_s is scan speed, and D_p is penetration depth of resin where the irradiance is about 37% or 1/e of the surface irradiance [Jacobs, 1995]. After an algebraic operation equation (2.3) becomes:

$$2y^{*2} /W_o^2 + z^* / D_p = \ln \{\sqrt{\frac{2}{\pi}} [P_L/W_o\ V_s\ E_c]\} \tag{2.4}$$

Note that W_o, D_p, P_L, V_s, and E_c are constants. Equation (2.4) can be written in the form

$$a\ y^{*2} + b\ z^* = c \tag{2.5}$$

where a, b, and c are all positive constants. Equation (2.5) is a parabolic equation. Figure 2.7 shows a schematic view of a cured line having the parabolic cross-section.

In SLA, the relationship between the thickness of the exposed layer and the applied energy is called the "working curve" of a given resin. The equation representing the working curve is [Jacobs, 1995]

$$C_d = D_p \times \ln (\frac{E}{E_{crit}}) \tag{2.6}$$

where C_d is the maximum cure depth or thickness of the solidified layer, D_p is the penetration depth, E is the exposure energy used to solidify the resin mixture and E_{crit} is

the critical exposure energy at which solidification starts to occur. Equation (2.6) states five fundamental points of laser exposure in the SLA process:

- The cure depth is proportional to the natural logarithm of the exposure on the centerline of the scanned laser beam.
- The semi-log plot of C_d versus E is a straight line. This line is known as the working line of a given resin.
- The slope of the working curve is the penetration depth, D_p, of that resin at the laser wavelength.
- The intercept of the working curve is the critical exposure, E_{crit}, of that resin.
- The D_p and E_{crit} are resin parameters, which are independent of laser power.

The maximum linewidth can be derived from equation (2.4). When $z^* = 0$, y^* equals y_{max}, and linewidth, L_w, equals $2y_{max}$, plus the working curve (2.6) and the maximum critical exposure energy (2.2), E, at y=z=0. Equation (2.4) becomes

$$L_w = W_o [2 C_d / D_p]^{1/2} \tag{2.7}$$

where W_o is the Gaussian half-width of laser irradiance distribution, and L_w is defined as the full-width of a laser cured line. The laser spot diameter is $B = 2W_o$. The cured linewidth becomes

$$L_w = B \sqrt{C_d / 2D_p} \tag{2.8}$$

The cured linewidth is directly proportional to the laser spot diameter, B. The cured linewidth is also proportional to the square root of the ratio of the cured depth to the resin

penetration depth (C_d / D_p). Thus curing deeper will also result in increased linewidth. The scan of a line and a layer are shown in Figures 2.7 and 2.8.

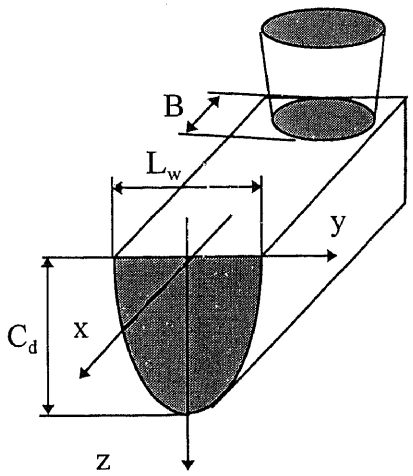

C_d: Cure depth

L_w: Line width

B: Laser spot diameter

Figure 2.7 Laser exposure of a line.

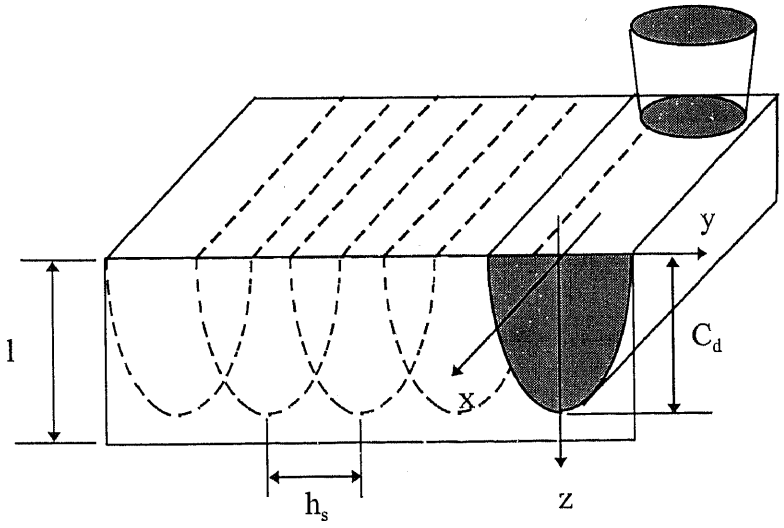

C_d: Cure depth

l : layer thickness

h_s : hatch space

Figure 2.8 Laser exposure of a layer.

2.3 Investment Casting Using Rapid Prototype Technology

Investment casting, or the lost wax process, has been utilized through history for some 5000 years. It is not an industry that is likely to disappear soon but it is one that is in great need of modernization. Its products are everywhere and its processes are diverse. The process can fabricate complex work pieces to meet near-net shape reproduction without certain machining, finishing and assembly steps. Complicated internal configurations and exterior shapes such as thin walls, blind pockets, internal seats, fillets and radii can be achieved. It is not only the oldest metal forming process, but also the most advanced technology in the sphere of metal forming techniques employed by the manufacturing industry today. A main strength of RP is its ability to make patterns, and a main need of the foundry is for such patterns, where the current/traditional pattern making process is expensive and time consuming. Using RP built models in investment casting has gained rapid attention from foundry. The output of RP can be used directly as an expendable pattern or to produce investment wax patterns from RP made molds. RP has the potential to be a provision of precision patterns and cores for sand casting and flask casting. RP is capable of generating thermally expendable patterns, or toolings for fabricating permanent dies or molds for injection of investment wax patterns for shell investment casting. It provides a sharp tool for global competition by saving time and cost.

2.3.1 Shell Investment Casting

The investment casting process, also known as the lost wax process, is one of precision casting. It is possible that the first investment casting was produced in Thailand around 4500 BC [Taylor, 1986]. It was not until World War II that it attained industrial

importance for making jet turbine blades from metals that were not readily machinable. The process runs as follows. Investment casting begins with the formation of an expendable pattern - usually produced from wax through injection of liquid wax into a precision engineered pattern die. The wax patterns are assembled with a gating and feeding system and cleaned prior to their investment with the ceramic coating. This ceramic coating is built up through successive stages of dipping and stuccoing. This procedure is repeated until the required shell thickness is obtained. The formation of this investment shell is usually carried out over three days to dip into a ceramic slurry six to eight times to generate a 6 to 8 mm thick ceramic shell. On completion of the coating stage the expendable wax pattern is removed at 140 °C and 300 psi, in a steam autoclave or flash furnace, and the ceramic shell is fired to around 1000°C (1832°F) prior to casting. After the molten metal is poured and solidified, the shell is broken away and the castings are removed from the runner system. Figure 2.9 illustrates the conventional lost wax shell investment casting process [Kalpakjian, 1991].

With the better dimensional accuracy and surface finish, the use of SLA patterns in conjunction with the investment casting process becomes a rapid and economic route for the replacement of wax patterns. The process runs as follows. Build SLA patterns by an SLA fabricator. The SLA patterns are assembled with the gating and feeding system and cleaned prior to their investment with the ceramic coating. After completion of the shell investment, the SLA pattern is burned out in a steam autoclave or flash furnace. The process flow is shown in Figure 2.10.

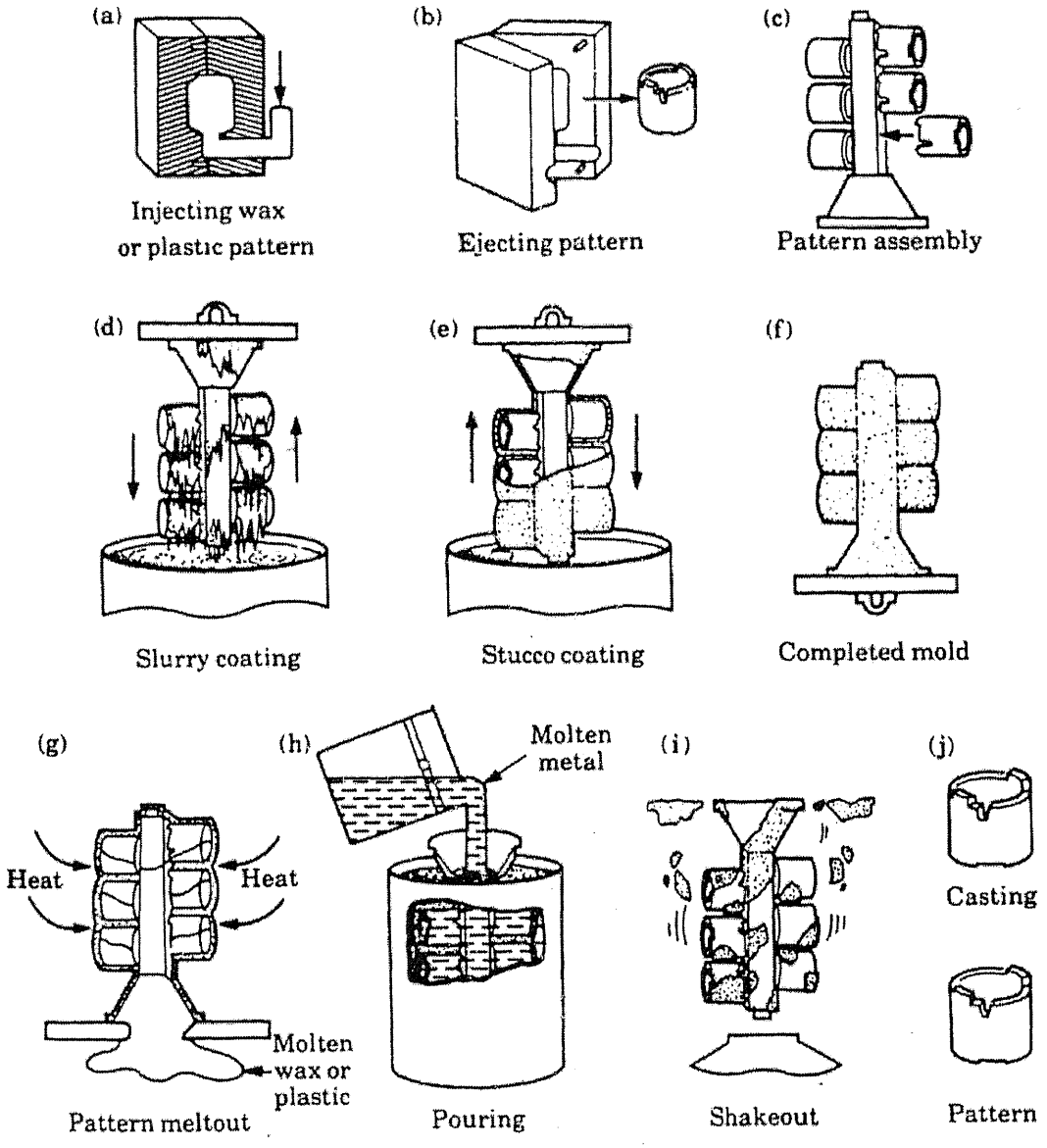

Figure 2.9 Conventional lost wax shell investment casting process [Kalpakjian, 1991].

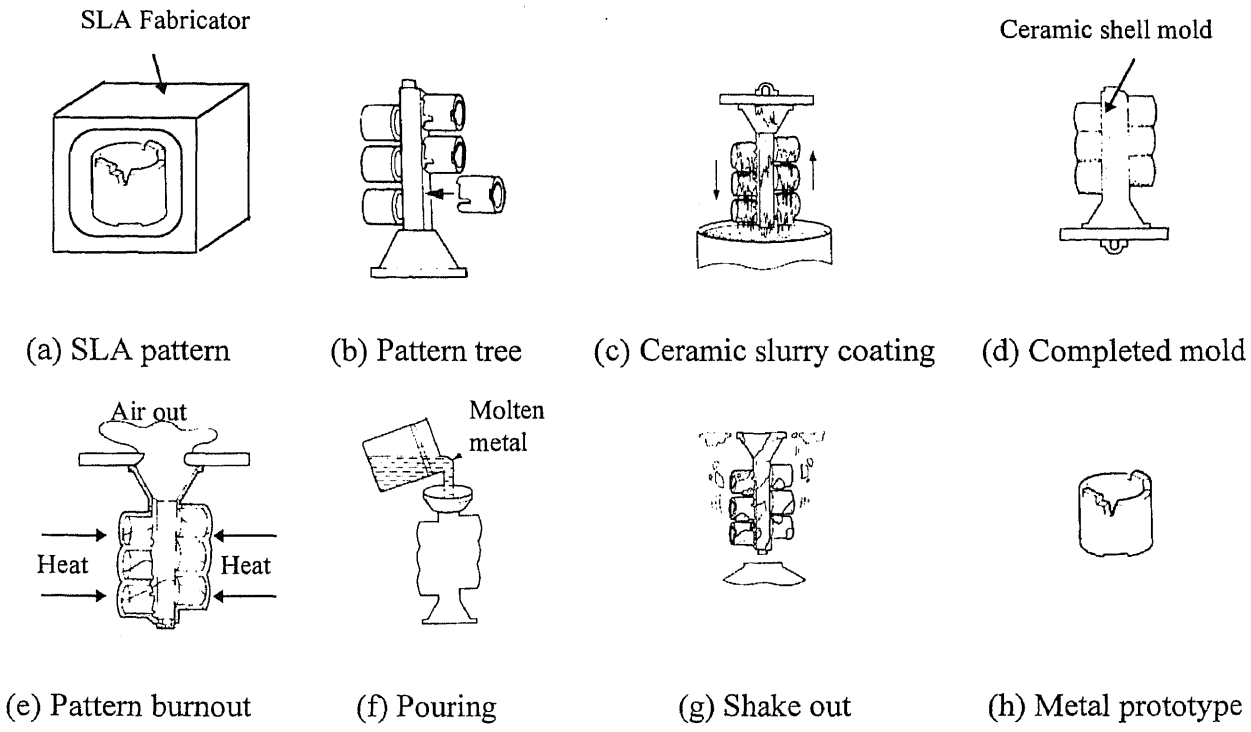

Figure 2.10 Rapid SLA prototype shell investment casting procedure.

2.3.2 Rapid Prototyping Route

Investment casting is expendable pattern casting. Traditional methods for producing prototypes in the foundry are expensive and time-consuming, resulting in a limited number of possible design iterations. As with many industries, one of the most pressing needs is reducing the time and cost of the product development cycle. The current method for prototyping is to make the wax injection tool [Koch, 1994]. If the prototype is acceptable then this tool is used for production. However, in the design stage of a product development cycle, redesign and/or tooling rework is a commonplace. As a result, the process is very lengthy and expensive. It offers a unique opportunity for RP because a main strength of RP is its ability to make patterns quickly. The use of RP models in

conjunction with investment casting has the potential to produce truly functional metal prototypes quickly. There are several alternatives for involving RP processes in investment casting. Some RP processes can fabricate expendable patterns for casting. Other RP processes can produce mold tooling for injection of investment wax patterns. Furthermore, some RP processes can make ceramic shells directly for investment casting. However, the outputs of those RP systems have inherent problematic characteristics. Table 2.2 shows the compatibility of various RP technologies with investment casting. It includes the material availability, pattern accuracy, toxicity and the transferability of pattern removal.

Table 2.2 The compatibility of RP processes with investment casting.

RP Process	Material	Accuracy	Transferability	Material toxicity
SLA	Epoxy	Excellent	Thermal expansion	Yes
SLS	Casting wax, ploycarbonate	Poor	Material shrinkage	Yes
FDM	Casting wax	Good	Similar to "Lost-wax"	No
SPI, Model Maker	Low-melting thermoplastic	Excellent	Negligible thermal expansion	No
DSPC	Casting ceramic	Poor	Material shrinkage	Yes
LOM	Sheet paper	Fair	Residual ash	Yes

2.3.3 Direct Casting of RP Pieces as Expendable Patterns

RP models can be used directly as the expendable investment patterns. The replacement of wax pattern eliminates the need for a precision machined wax injection mold and thus eliminates the cost of tooling. A diverse array of documented reports have shown successful generation of RP parts by various RP systems, such as SLA, SLS, FDM, SPI, DSPC, and LOM processes. A comparison table is shown in Table 2.2. Wax based RP models, such as those made by SLS, SPI, and FDM, by all means, are the easiest patterns to generate for investment casting use. However, these wax models generally yield castings with surface finish inferior to those produced from SLA patterns. The use of paper patterns from the LOM process, so-called the "lost paper" process, is also reported to work well with investment casting.

2.3.4 RP for Injection Tooling and Investment Shell Making

Another alternative of using RP systems to make expendable patterns is that of using the RP to make a mold for wax injection. There are: (1) direct tooling, tools made from the RP process, and (2) indirect tooling, tools made from RP masters. The use of direct AECS injection molding (AIM) of the SLA process can produce a medium volume of wax patterns. The masters from the LOM process also have the capability for doing this. Additionally, the spray metal method can be used effectively to produce injection tools from RP masters. Another approach, so-called the hard tooling, is that of using RP to make permanent dies and molds to produce expendable wax patterns for prototyping or manufacturing.

Another use of RP is for direct casting shell production. The DSPC of Soligen can produce actual ceramic molds for direct metal castings. This process does not require tooling and patterns. DSPC uses the 3-D printing technology developed at MIT, to produce the ceramic casting molds including the gating system.

CHAPTER 3

HYPOTHESIS AND RESEARCH OBJECTIVES

This chapter describes the problem of using SLA patterns as thermally expendable patterns in the shell investment casting process. It reviews current research activities on shell cracking in investment casting with SLA patterns. The hypothesis and objectives of the dissertation study are presented.

3.1 Statement of the Problem

Since investment casting is expendable pattern casting, the focus of this study is on the use of RP built patterns, especially on SLA built epoxy patterns, as thermally expendable patterns in investment casting. The use of SLA generated patterns in conjunction with investment casting has the potential to provide a rapid route for fabricating metal prototypes. However, the photopolymers used in SLA are thermosets which do not melt on heating. Removing the epoxy pattern is more challenging than losing the wax pattern in the conventional investment casting process. By subjecting the epoxy model to a high temperature furnace or an autoclave for a sufficient amount of time, it is possible to burn out the thermoset material. However, many early attempts of using SLA patterns in investment casting experienced unsatisfactory results, because the investment shells are subjected to considerable stresses during the burnout process, which can easily break the shell mold.

When an investment casting shell with an SLA epoxy pattern inside is placed in an autoclave or a flash-fire oven during the burnout process, it is subjected to high temperature rise, thermal expansion, and large strains. Since the difference between the coefficient of thermal expansion of epoxy and that of investment ceramic is more than one order of magnitude, the epoxy pattern exerts considerable stress on the ceramic shell. From Hooke's Law, the ceramic shell stress, in the elastic deformation regime, is proportional to the ceramic shell strain. In turn, the strain is proportional to the thermal expansion of the epoxy pattern, and the thermal expansion of the pattern is proportional to the size of the pattern. Hence, thicker sections of a pattern will induce greater shell stresses. Consider a long cylindrical epoxy pattern coated with a ceramic shell, but open on the two ends. During the pattern burnout process, the inner epoxy pattern is expanding much more than the outer ceramic shell. As a result, pressure between the ceramic shell and the epoxy pattern is formed. The induced pressure causes compressive stress to the inner epoxy pattern and tensile stresses to the outer ceramic shell. The tensile stresses may cause shell cracking.

The development of the QuickCast build style and the improvement in epoxy resins make the webbed SLA pattern more compatible with the shell investment casting process to produce functional metal parts [Jacobs, 1995; Pang, 1996]. The idea behind the QuickCast build style is enabling the pattern to collapse and buckle inwards under the influence of heat, rather than cracking the ceramic shell as a result of expanding outwards. Figure 3.1 depicts the square quasi-hollow structure. Despite the advancements in the build style and resin, the ceramic shell, with a quasi-hollow pattern inside, may still crack during the burnout process.

Under the influence of heat, whether an investment shell will crack or not depends upon factors governed by the epoxy web structure and the investment shell. The primary hypothesis of this work is as follows: which of the shell cracking, pattern buckling, and epoxy softening occurs first depends on which of the pattern buckling temperature, the glass transition temperature of the resin, and the shell cracking temperature is the lowest. If the epoxy resin softens or the internal epoxy web structure buckles first, the exerted stress upon the shell wall will drop dramatically, thus keeping the shell intact. On the other hand, cracking of the ceramic shell in investment casting will occur if the shell cracking temperature is lower than both the pattern buckling temperature and the glass transition temperature of the resin. This dissertation study will provide a good understanding of shell cracking with use of SLA patterns in investment casting and investigate how to prevent the cracking.

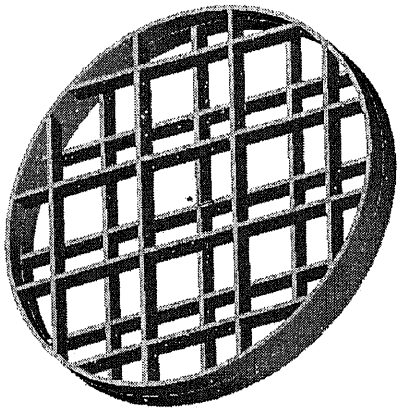

Figure 3.1 Typical offset layers of internal web structure in an SLA quasi-hollow pattern.

3.2 Related Research

There have been some studies about how to prevent the ceramic shell cracking during the pattern burnout process. The main research activities included investment casting process adjustment, build style invention, new resin development, and analysis of induced stresses on the ceramic shell and SLA generated epoxy pattern.

The use of SLA pattern in solid plaster casting has shown a good yield rate. However, this old technology is less popular than shell investment casting because of its relatively poor production quality. Jacobs [1995] observed the foundry yield of casting shells as a function of the SLA pattern void ratio, R_v, defined as the fraction of volume with air space. The early attempts to use SLA solid patterns, $R_v = 0$, to replace investment casting wax patterns met with very limited success. Engineering calculations and experimental tests show that a "critical solid pattern thickness" exists for an investment casting shell. Blake et al. [1994] calculated that the critical solid pattern sectional thickness, which is just a few millimeters. Practically, the cross-section is always larger than a few millimeters. It became clear that solid SLA patterns could not be compatible with real investment casting. A completely hollow pattern, $R_v = 1$, could result in good yields of rapid investment castings. However, a completely hollow pattern deforms too easily under normal handling and is likely to collapse inwards during the slurry coating process. A research team of 3D Systems Inc. has developed a quasi-hollow build style "QuickCast™" for investment casting [Jacobs, 1995]. QuickCast builds a pattern with a relatively thin skin, supported by a "simple, topologically connected" internal web hatch structure. The idea behind QuickCast is expecting the pattern to collapse inwards under

the influence of heat, rather than cracking the ceramic shell as a result of expanding outwards.

Hague and Dickens [1995, 1996] conducted a study of the shell cracking issue. Their experimental observations showed that the ceramic shell stayed intact with completely hollow patterns in the burnout process. The observations also indicated that the SLA epoxy pattern is likely to soften due to the heat. They did not observe buckling occurrence of their hollow samples inside the investment shell.

Jacobs [1995] hypothesized that the ceramic shell cracking can be prevented if the epoxy pattern buckles at a temperature that is lower than the ceramic shell cracking temperature. Hague and Dickens [1995, 1996] concluded from their experimental observation that the shell cracking can be prevented if the glass transition temperature of the epoxy resin is lower than the shell cracking temperature. The hypothesis of this study is thus: which of the shell cracking, the pattern buckling, and the epoxy softening occurs first depends on which of the pattern cracking temperature, the resin glass transition temperature, and the shell cracking temperature is the lowest.

The results from the previous studies of the shell cracking in rapid SLA prototype investment casting can be summarized as follows:

1. The "critical" sections of solid SLA patterns are too small for practical shell investment casting.
2. Hollow SLA patterns deform easily during the subsequent handling and processing.

3. The quasi-hollow build style with newly developed epoxy resins improves the feasibility of shell investment casting with SLA patterns. The internal web structure in the quasi-hollow pattern is expected to buckle under heating.
4. Investment shells with webbed SLA patterns are still cracking. Shell cracking occurs at low temperatures which are below the epoxy glass transition temperature (60 -70 °C).

3.3 Research Objective and Tasks

The main objective of this research is to provide a comprehensive knowledge about the mechanism of the ceramic shell cracking during the burnout process in investment casting with an SLA built epoxy pattern. It is highly valuable to discover whether the prevention of ceramic shell cracking can be achieved by buckling of the epoxy pattern, or by softening of the epoxy material, or by both. The result of this study is vital to developing new pattern build styles and determining the dimensions of the pattern and shell for prevention of shell cracking during the pattern burnout process.

The following is the list of research tasks:

1. To develop a computational simulation model used to simulate and analyze the burnout process in investment casting with webbed SLA patterns,
2. To conduct an experimental study in conjunction with the computer simulation and analysis to better understand the mechanisms of shell cracking and web structure collapsing, and

3. To compare various internal web structure designs for prevention of shell cracking during the pattern burnout process with the consideration of pattern deformation during the coating of ceramic slurries and resin drainage during the pattern build process.

CHAPTER 4

MODELING AND ANALYSIS

This chapter presents and discusses modeling of the burnout process in investment casting with a webbed SLA pattern, so as to understand the cracking of the ceramic shell and the buckling of the internal web link. Due to the complexity of the internal web structure, it is necessary to perform numerical simulations corresponding to the pattern burnout process. The parameters that govern the shell cracking and the web link buckling are described. Structural and finite element models are presented, so that the influence of various design and process parameters can be quantitatively studied. A series of computational simulations is performed to predict the temperatures of shell cracking and web link buckling for various pattern parameter values and shell thicknesses. The simulated predictions are then compared with strain gauge based measurements during the burnout process, to be reported in the next chapter.

4.1 Feasibility of Investment Casting with SLA Pattern

Using solid SLA prototype models as thermally expendable patterns has not been very successful in shell investment casting, due to the fact that the thermal expansion coefficients of photopolymer and ceramic materials are one order of magnitude different. The maximum thickness of a solid SLA pattern is only a few millimeters. A simple model of shell investment casting with a solid SLA prototype pattern is shown in Figure 4.1. Consider a circular solid pattern of radius R invested with a ceramic shell of

thickness t. Due to the influence of temperature, ΔT, the strain in the ceramic shell has the following relation [Blake, 1994]:

$$\varepsilon_c = \frac{\sigma_c}{E_c} = \frac{(\alpha_r - \alpha_c)R\Delta T}{t} \tag{4.1}$$

where ε_c and σ_c are, respectively, the induced strain and stress on the ceramic shell, E_c is Young's modulus of the ceramic, α_r and α_c are, respectively, coefficients of thermal expansion of the epoxy resin and the investment ceramic, R is the pattern radius, ΔT is the temperature rise, and t is the thickness of ceramic shell.

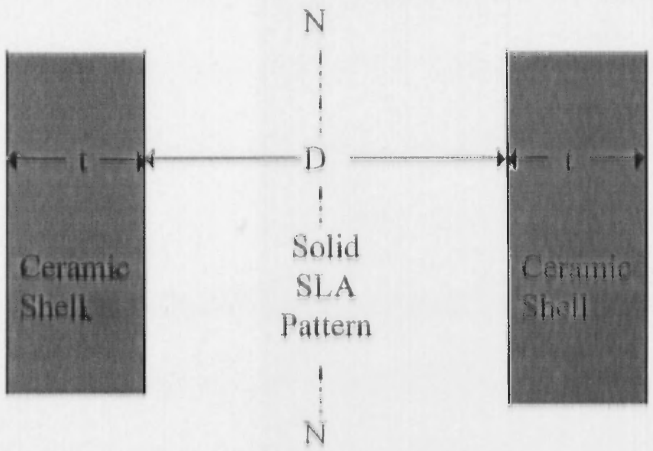

Figure 4.1 Model of shell investment casting with solid SLA pattern.

For instance, assume that the material properties of the photopolymer epoxy and the fused ceramic are as follows:

α_r = 90 × 10^{-6} mm/mm-°C	MOR, ceramic = 30 Mpa
α_c = 7 × 10^{-6} mm/mm-°C	t = 6 mm
E_c = 8200 MPa	ΔT = 140 °C

and let σ_c = MOR (Modulus of Rupture), then

$$D_{max} = 3.78 \text{ mm}$$

This critical solid pattern thickness is far smaller than the cross-section of a practical casting part. It is thus clear that solid SLA patterns should not be used in real investment casting. Experiments with solid pattern thickness values of 1, 2, 3, 4 and 5 mm have been made by foundries. The results showed that distinct shell cracks occurred when the section of the solid pattern was larger than about 3 mm; a 4 mm thick pattern caused major shell cracking; with a 5 mm thickness, the shell cracking caused catastrophic explosion.

A quasi-hollow build style for SLA technology has been devised by 3D Systems for shell investment casting. The idea is to increase the void ratio, i.e. the ratio of air space in the part, of the SLA pattern. The quasi-hollow SLA pattern has a thin outer skin (0.014 - 0.018 inch or 0.35 - 0.45 mm) with a simple, topologically connected internal web support structure. The internal web structure has a hatch structure. The new layer of internal web structure is built on the top of the previous layer for a specified height and with an offset (see Figure 4.2). An internal web structure with triangular or square lattice increases the rigidity of the SLA model over a hollow pattern while it decreases the thermal expansion compared with a solid pattern. The semi-hollow pattern may collapse

inwards instead of expanding outwards under heating during the burnout process in investment casting.

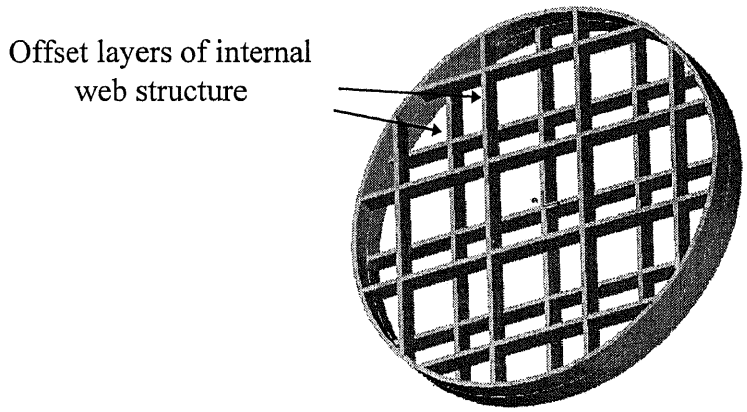

Figure 4.2 Layers of quasi-hollow SLA pattern.

The summary of the features and advances of the quasi-hollow pattern build style is as follows:

1. A quasi-hollow SLA pattern has a thin outer skin (0.014 - 0.018 inch or 0.35 - 0.45 mm) with a simple, topologically connected internal web support structure.
2. The simple, topologically connected web structure has an offset internal hatch structure. Two consecutive layers of the internal web structure are simply piled on top of each other.
3. The quasi-hollow SLA pattern increases the void ratio of the SLA pattern compared with a solid SLA pattern.
4. The simple, topologically connected web structure allows uncured liquid resin at any location within the pattern to flow to other locations.

5. The internal web support structure increases the rigidity of quasi-hollow SLA pattern, compared with a hollow pattern, the later handling and operating process.
6. The uncured resin is easily drained out of the pattern with gravity, viscous drag, and surface tension forces.
7. The internally supported web structure is fragile enough to buckle and break down due to the heat of the burnout process in investment casting.

4.2 Analytical Approach

4.2.1 Structural Analysis

Consider a typical layer of an SLA pattern with internal square web structure as shown in Figure 4.3a. Since the skin of SLA pattern is so thin, the effect of the outer thin skin can be negligible in the analysis. The internal square web structure can be treated as a girder type rigid planar frame with fixed ends (see Figure 4.3b). The internal web structure is composed of straight members connected by rigid joints. A rigid joint prevents relative translations and rotations of the member ends connected to it, so that the joint is capable of transmitting two force components and a couple between the connected members. Under the action of external loads, the members of the frame may be subjected to bending moments, and axial compression.

This structural model in Figure 4.3a is used to study the shell cracking mechanism and web pattern collapsing mechanism, which are correlated with the dimensions of web structure and the thickness of the ceramic shell. "L" is denoted as the web link span length of the web structure. "A" is the cross-sectional area of the web link which has the

width of "b" and depth of "h". Different values of these parameters will give different thermal stresses to the ceramic shell during the burnout process. The following section will define the elements related to web buckling, epoxy softening and shell cracking.

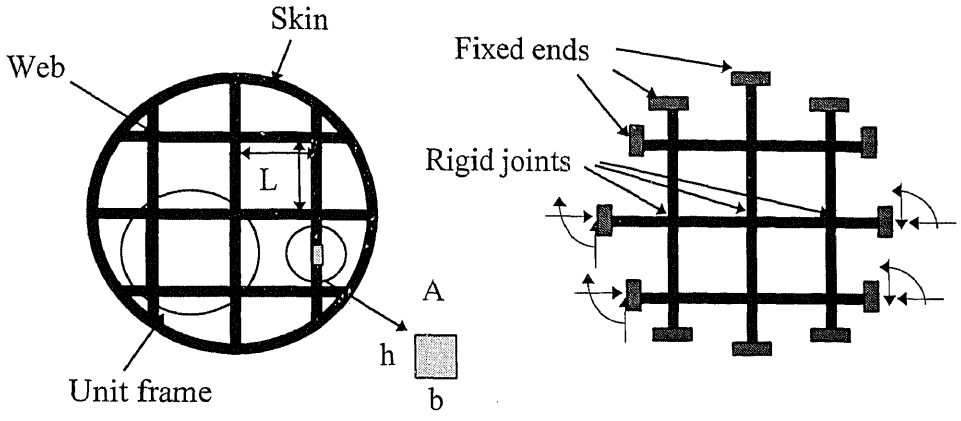

Figure 4.3 (a) A typical layer of SLA pattern with internal web structure.
(b) Internal web structure as a rigid planar frame with fixed ends.

4.2.2 Notation and Definition of Parameters

"Inwards collapsing" during pattern burnout is the primary intent of the quasi-hollow SLA pattern for investment casting. The collapse is due to the glass transition of the epoxy or buckling of the web link. Thus, the hypothesis of this study is that whether shell cracking, pattern buckling, and epoxy softening occurs first depends on which of the shell cracking temperature (T_u), the pattern buckling temperature (T_b), and the resin's glass transition temperature (T_g) is the lowest. T_u is the temperature at which the induced stress is greater than the modulus of rupture (MOR) of the shell ceramic material; MOR = S_u = 3.0 MPa in this study [Sandia, 1995]. T_g is the glass transition temperature of the epoxy resin, a material property; T_g = 60 - 70°C for SL5170 epoxy from Ciba-Geigy [Hague and

Dickens, 1995]. T_b is the temperature at which the compressive pressure causes the web link to buckle. The temperatures of shell cracking and web link buckling are related to the dimensions of the internal web structure and the ceramic shell, such as the cross-sectional dimensions of the web structure and the thickness of the investment ceramic shell. Several values for each questioned parameter are chosen in this study as follows. Test samples are named with a group number and the thickness of ceramic shell; for instance, "Part1t1" stands for sample Part1 coated with 1 mm ceramic shell.

Table 4.1 Dimensions of samples.

(mm)	Part1	Part2	Part3	Part4	Part5
Web length (L)	6.35	9.525	6.35	3.175	6.35
Web width (b)	0.3048	0.3048	0.4572	0.3048	0.3048
Web height (h)	1.4732	1.4732	1.4732	1.4732	0.7366

As can be seen from Figure 4.3a, the internal web structure consists of a number of square grids. The rigid joints resist bending moments and preserve the angles between the various members as observed in later experiments in Chapter 5. The SLA pattern is subjected to an internal pressure from the wall of the ceramic shell under the thermal expansion. The frame is likely to buckle under the induced compressive load (see Figure 4.4). The critical pressure to cause the square frame to buckle is [Wang, 1953]:

$$P_{cr} = \frac{16.47EI}{AL^2} \tag{4.2}$$

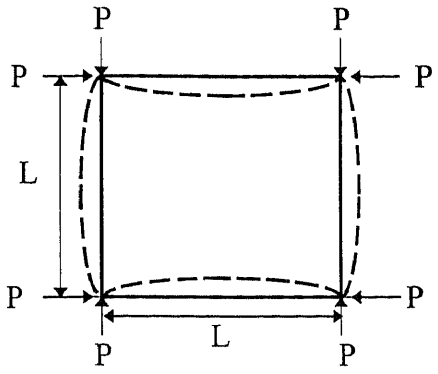

Figure 4.4 The buckling of the frame under compressive loads.

where P_{cr} is the critical pressure (load per unit area) to cause the web link buckling, E is Young's modulus of the epoxy, I is the moment of inertia of the web structure, A is the cross-sectional area of the web structure, and L is the web link length of the web structure.

4.2.3 Lames Equations

An investment casting with a circular solid SLA pattern can be modeled as a walled cylinder problem. It can be a thin-walled or a thick-walled cylinder depending on the wall thickness-to-diameter ratio. If the wall thickness-to-diameter ratio is less than 10 percent, the model is a thin-walled cylinder, otherwise it is a thick-walled cylinder. In this study the samples have 25.4 mm diameter in the pattern with 6 mm thickness of ceramic coating. The thick-walled cylinder model is thus used in the analysis. In the theory of thick-walled cylinders (see Figure 4.5), Lames solutions provide a set of equations to

calculate the circumferential stress (σ_θ) and radial stress (σ_{rad}) on the ceramic shell when the contact pressure is formed under heating. The general form of equations for stress is given in (4.3). The maximum stresses occurred at the bore of the thick-walled cylinder, r = r_i. Here we neglect the external pressure, P_o, and let P_i, the internal pressure, equal the induced contact pressure, P. Equation (4.3) can be simplified to equation (4.4) [Ugural and Fenster, 1995]. This model is used to verify the FEA model.

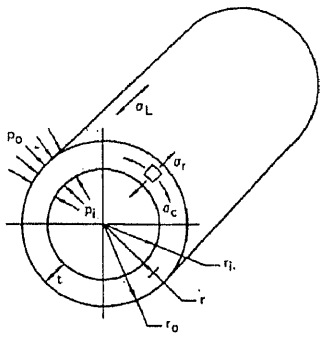

General Stresses in Thick Walled Cylinder

$$\sigma_\theta = \frac{r_i^2 p_i - r_o^2 p_o + \frac{(p_i - p_o) r_i^2 r_o^2}{r^2}}{r_o^2 - r_i^2} \qquad (4.3)$$

$$\sigma_{rad} = \frac{r_i^2 p_i - r_o^2 p_o - \frac{(p_i - p_o) r_i^2 r_o^2}{r^2}}{r_o^2 - r_i^2}$$

$$\delta = \frac{1-\nu}{E} \frac{(r_i^2 p_i - r_o^2 p_o) r}{r_o^2 - r_i^2} + \frac{1+\nu}{E} \frac{(p_i - p_o) r_i^2 r_o^2}{(r_o^2 - r_i^2) r}$$

Internal Pressure Only

At $r = r_i$

$$\sigma_{\theta,\,max} = \frac{(r_i^2 + r_o^2) p}{(r_o^2 - r_i^2)} \qquad (4.4)$$

$$\sigma_{rad,\,max} = -P$$

Figure 4.5 Thick-walled cylinder and Lames equations.

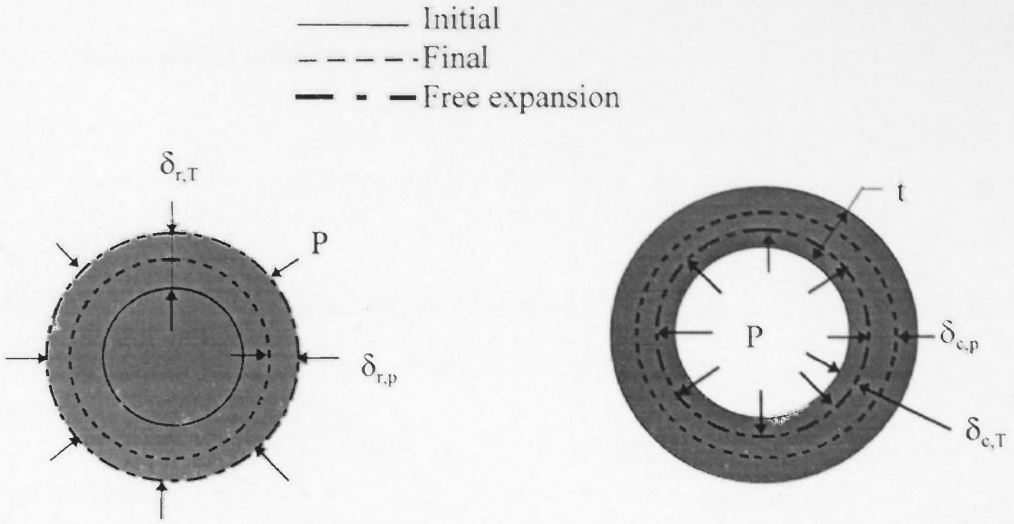

Figure 4.6 Solid pattern-shell model.

The first step is to find the contact pressure between the pattern and the ceramic shell under the thermal expansion. Based on the theory of thick-walled cylinders, the solid pattern-shell can be modeled as follows (see Figure 4.6). The elongations of resin and ceramic, due to the temperature rise ΔT, are denoted as $\delta_{r,T}$ and $\delta_{c,T}$, respectively. The elongation of resin and ceramic, due to the generated pressure at the interface, are denoted as $\delta_{r,p}$ and $\delta_{c,p}$, respectively.

$$\delta_{r,T} = \alpha_r \times R \times \Delta T \tag{4.5}$$

$$\delta_{c,T} = \alpha_c \times R \times \Delta T \tag{4.6}$$

The pattern is subjected to a compression,

$$\delta_{r,p} = \frac{pR}{E_r}(1 - \nu_r) \tag{4.7}$$

The ceramic shell is subjected to a tension,

$$\delta_{c,p} = \frac{R^2 pR}{E_c[(R+t)^2 - R^2]}[(1-v_c) + (1+v_c)\frac{(R+t)^2}{R^2}] \tag{4.8}$$

At the interface of pattern and ceramic shell the total elongation, δ_{total} is balanced. That is,

$$\delta_{total} = \delta_{r,T} - \delta_{c,T} = \delta_{r,p} + \delta_{c,p} \tag{4.9}$$

Then the pressure p is:

$$p = \frac{(\alpha_r - \alpha_c)\Delta T}{\frac{1}{E_r}(1-v_r) + \frac{1}{E_c}(k+v_c)} \tag{4.10}$$

where $k = \frac{(R+t)^2 + R^2}{(R+t)^2 - R^2}$. The radial stress ($\sigma_{rad}$) and hoop stress ($\sigma_\theta$) of the ceramic shell are as follows:

$$\sigma_{rad} = -p \tag{4.11}$$

$$\sigma_\theta = kp \tag{4.12}$$

They are both principal stresses. The calculated values are examined and compared with the results of the finite element computation in Section 4.4.1.

4.3 Numerical Modeling and Analysis

4.3.1 General

The finite element method for stress analysis fully utilizes the advantages of computer capacity in performing speedy and reliable calculations for a wide range of engineering design problems. This is particularly true when the problem is difficult to solve by using

a traditional mathematical model or when the geometry is too complex. In this study, a finite element package, ANSYS version 5.3, is utilized for simulation and prediction.

From the mechanics of materials, the stresses are related to the strains by:

$$\{\sigma\} = [D]\ \{\varepsilon^{el}\} \tag{4.13}$$

where $\{\sigma\}$ is the stress tensor; $[D]$ is the elasticity matrix; $\{\varepsilon^{el}\}$ equals $\{\varepsilon\}$ - $\{\varepsilon^{th}\}$, where $\{\varepsilon\}$ is the total strain tensor, and $\{\varepsilon^{th}\}$ is the thermal strain vector. The $\{\varepsilon^{th}\}$ is:

$$\{\varepsilon^{th}\} = \Delta T\ [\alpha_x\ \alpha_y\ \alpha_z\ 0\ 0\ 0]^T \tag{4.14}$$

where α is the coefficient of thermal expansion, ΔT is the temperature rise. In turn, the strain is related to the nodal displacements by

$$\{\varepsilon\} = [B]\ \{u\} \tag{4.15}$$

where $[B]$ is the strain-displacement matrix, and $\{u\}$ is the nodal displacement vector. ANSYS solves (4.13) and the following equation

$$\{\varepsilon^{el}\} = [B]\ \{u\} - \{\varepsilon^{th}\} \tag{4.16}$$

The highest stress is shown by the equivalent stress σ_e. The equivalent stress is computed as:

$$\sigma_e = \frac{1}{\sqrt{2}}[(\sigma_1 - \sigma_2)^2 + (\sigma_2 - \sigma_3)^2 + (\sigma_3 - \sigma_1)^2]^{1/2} \tag{4.17}$$

where σ_1, σ_2, and σ_3 are the principal stresses. On the ceramic shell, we examine the principal stresses, while in the webbed structure we examine the compressive stresses in the x- or y-direction, i.e. σ_x or σ_y.

An ANSYS analysis consists of three phases: preprocessing, solution, and postprocessing. In the preprocessing phase, the data needed to perform a solution is specified. It includes solid geometric data, material property, and meshing. The analysis

results are obtained in the solution phase. In this phase the type of analysis, load data, and boundary constraints have to be specified. Then the finite element analysis is initiated to obtain the solution. The postprocessing phase of the ANSYS program follows the preprocessing and solution phases. In this phase the calculated results are shown in graphics display and/or tabular report form. A two-dimensional structural static analysis is used in this dissertation study. Solid models of objects are created by the modeling tools of ANSYS. The temperature-dependent material properties of the epoxy are established in a table. The SmartSize #2 and PLANE82 element is used for meshing. The load type is temperature variation. The constraints are axisymmetric. The first principal stresses of ceramic and the compressive stresses in x- or y-direction for web links are focused.

4.3.2 Temperature-Dependent Coefficient of Thermal Expansion

The coefficient of thermal expansion, α, is assumed as a constant in equation (4.14). If α is a function of temperature, it will become:

$$\varepsilon^{th} = \int_{T_{ref}}^{T} \alpha_{inst}(T)dT \tag{4.18}$$

where $\alpha_{inst}(T)$ is the instantaneous coefficient of thermal expansion. ANSYS uses a mean value of α. As with all materials, the properties of the photocurable resin change with variation in temperature and affect the shell structure deformation in the heating process. A summary of material properties of SL5170 resin including the coefficient of thermal expansion and Young's modulus is in Figure 4.7; the Poison ratio, ν_r, is 0.4 for SL5170 resin [Hague and Dickens, 1996]. In the range from the ambient temperature to about

60°C, there is a linear thermal expansion of approximately 88 × 10^{-6} mm/mm/°C. In the range from 65 to 150°C there is a two-fold increase in the thermal expansion to 181 × 10^{-6} mm/mm/°C. This sharp increase occurs around the glass transition temperature of the cured resin as the secondary bonds of the thermoset plastic melt. The material properties for the investment ceramic material used in this study are listed in Table 4.2 [Sandia, 1995]. In this FEA study the temperature-dependent properties are established in a table. The software looks up the property table and temperature to calculate the stress results.

Table 4.2 Investment ceramic material properties. [Sandia, 1995]

Young's modulus, E_c	5.09Gpa
Coefficient of thermal expansion, α_c	11.0 × 10^{-7} mm/mm/°C
Poison ratio, ν_c	0.016

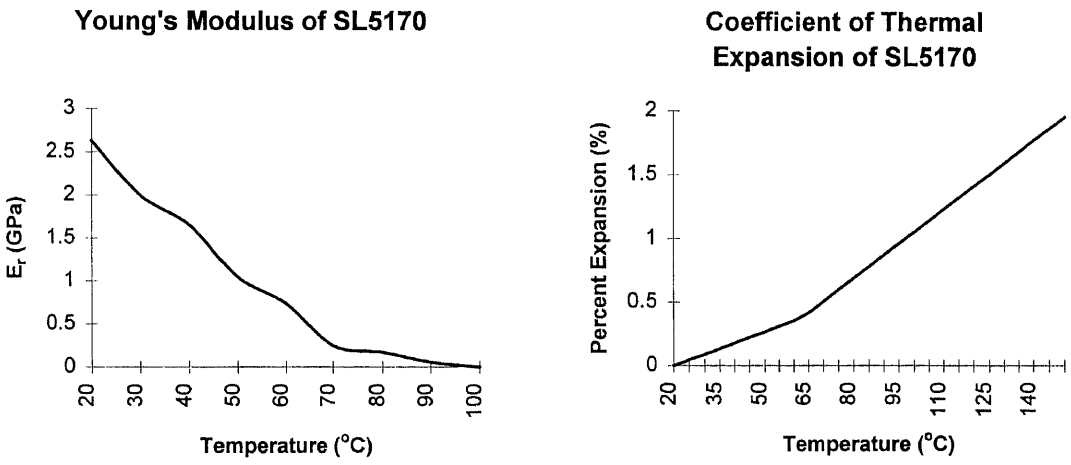

Figure 4.7 Thermal expansion (α_r) and Young's modulus (E_r) of SL5170 epoxy resin versus temperature. [Hague and Dickens, 1996]

4.3.3 Assumptions and Convergence Studies

In this analysis, a two-dimensional model of a ceramic shell with internal web structure as shown in Figure 4.2, under a heating process to a stepwise (or steady-state) isothermal temperature, is assumed. The principle of the buckling of a square frame is adopted to determine the temperature of web structure buckling (see Figure 4.4). To simplify the analysis, we do not consider transient heat transfer during the thermal expansion of the pattern and ceramic shell. A two-dimensional model is used to reduce the complexity of the geometry of the ceramic shell with internal web structure. The basis of the two-dimensional model is the "simple, topologically connected" internal web structure, i.e. two consecutive layers of the internal web structure are simply stacked without any interaction in the z-direction. Additionally, the temperature uniformity within the webbed pattern and the ceramic shell is assumed throughout this study. Practically it is difficult to keep the temperature uniform during the measurement of the specimens. For each step increase, the temperature is increased and kept long enough to reach the desired uniform temperature. The assumption of the buckling of the internal web structure is based on the confluence of a number of small square grids within the webbed pattern and the rigidity of the joints of the internal web structure to preserve the angles between various members [Wang, 1953]. Due to the thermal expansion, the resultant forces are likely to cause the individual square grids to buckle (see Figure 4.4). Our experimental observation gives a good agreement with the FEA results with the model of the buckling of a square frame. Our previous use of the buckling of a beam with two fixed ends was less accurate [Yao et al, 1996]. The buckling of frame model enables determining the buckling temperature of the internal web link structure.

A larger number of elements will give more accurate results in finite element analysis. However, the computational time and model size are also more expensive. For the convergence of the finite element analysis, several models with different numbers of elements, node numbers, and boundary conditions have been carefully examined. ANSYS provides a "SmartSizing" mesh generation feature in Version 5.3. SmartSizing is a meshing feature that creates initial element sizes for free meshing operations. It gives the mesher a better chance of creating reasonably shaped elements during automatic mesh generation. This feature, which is controlled by the SAMARTSIZE command, allows the user to choose the level of mesh, from coarse #10 to fine #1. To achieve accurate results, poor elements have to be avoided. Several mesh levels have been examined on the Part1t6 model. The result is shown in Table 4.3. A comparison of a full model and a quarter model is given in Table 4.4 and Figure 4.8. This ensures that the boundary condition is properly defined. The model used for convergence and symmetrical studies is Part1t6. The temperature rise is from 20°C to 50°C. The models used in this study are quarter models and they are automatically meshed in level #2 using the PLANE82 element and axisymmetric boundary condition.

Table 4.3 Convergence of stress with number of elements, Part1t6.

	Web			Shell		
Mesh level	#2	#5	#10	#2	#5	#5
Elements	1100	908	746	936	380	380
Stress(MPa)	-3.25	-3.30	-3.50	1.01	1.00	0.98

Table 4.4 Comparison of results with a full model and quarter model.

	Web		Shell	
	Full model	Quarter model	Full model	Quarter model
Mesh level	#2	#2	#2	#2
Elements	1100	374	936	783
Stress (MPa)	-3.25	-3.29	1.01	1.01

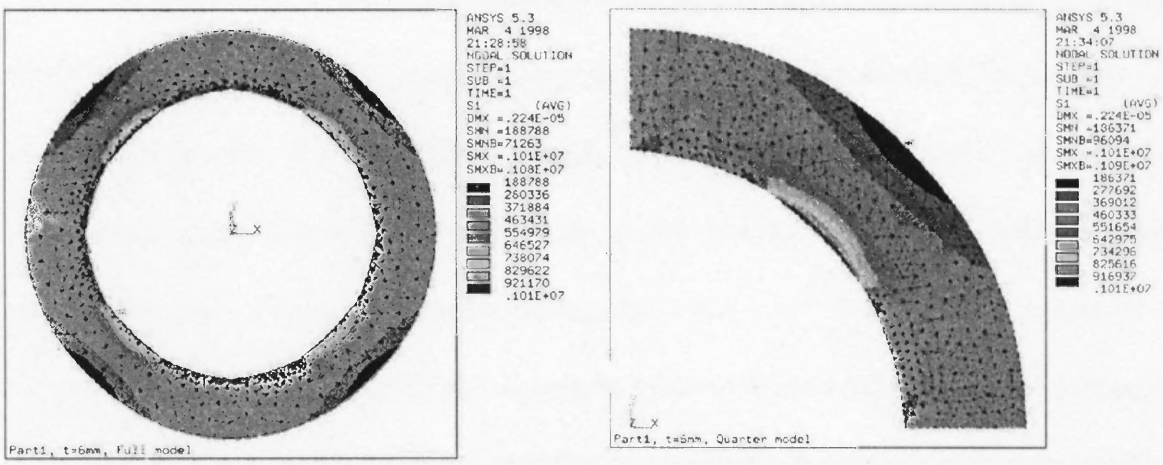

(a) Full size model. (b) Quarter model.

Figure 4.8 Hoop stress on ceramic shell of a full size model and a quarter model.

4.3.4 Two-Dimensional FEA Model

From the generalized Hooke's law, the stress-strain relations are as follows [Ugural and Fenster, 1995]:

$$\varepsilon_x = \frac{1}{E}[\sigma_x - \nu(\sigma_y + \sigma_z)] \qquad \gamma_{yz} = \frac{\tau_{yz}}{G}$$

$$\varepsilon_y = \frac{1}{E}[\sigma_y - \nu(\sigma_z + \sigma_x)] \qquad \gamma_{xz} = \frac{\tau_{xz}}{G}$$

$$\varepsilon_z = \frac{1}{E}[\sigma_z - \nu(\sigma_x + \sigma_y)] \qquad \gamma_{xy} = \frac{\tau_{xy}}{G}$$

A three-dimensional problem can be reduced to a two-dimensional problem by plane stress or plane strain approaches. A state of plane stress is said to exist when the elastic body is very thin and there are no loads applied in the thickness direction. The stress components associated with the thickness direction, σ_z, τ_{xz}, and τ_{yz} are very small and assumed to be zero, when the applied loads lie in the x-y plane. The state of plane strain occurs in members that are not free to expand in the direction perpendicular to the plane of the applied loads. Plane stress and plane strain problems are shown in Figure 4.9.

By theory, the semi-hollow structure is designed as a "simple, topologically connected" internal web structure. Therefore, two consecutive web structures are simply stacked with an offset. As a consequence, the force effect between two layers in the vertical direction is not significant. A typical layer of web pattern and shell is shown in Figure 4.2. The analysis can be simplified as a two dimensional plane stress problem. That is, σ_z, τ_{xz}, and τ_{yz} are taken to be zero. The above strain-stress relation can be reduced as follows:

$$\varepsilon_x = \frac{1}{E}[\sigma_x - \nu\sigma_y] \qquad \varepsilon_z = \frac{-1}{E}\,\nu(\sigma_x + \sigma_y)$$

$$\varepsilon_y = \frac{1}{E}[\sigma_y - \nu\sigma_x] \qquad \gamma_{xy} = \frac{\tau_{xy}}{G}$$

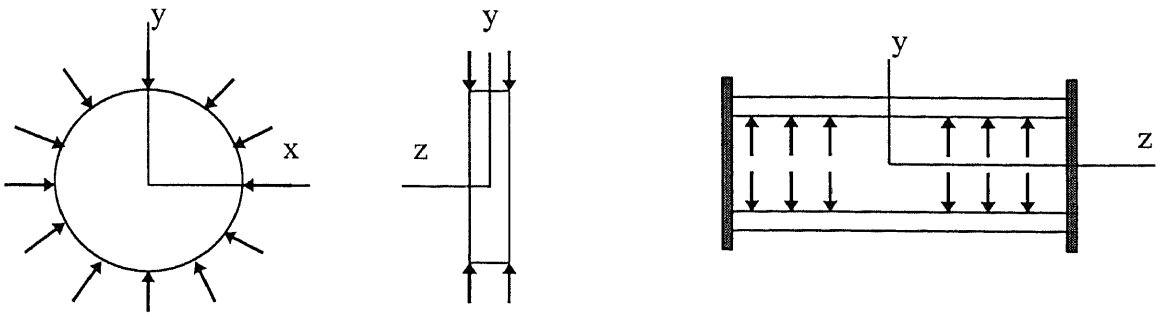

(a) A thin body in a state of plane stress.

(b) A cylinder under uniform internal pressure in a state of plane strain.

Figure 4.9 (a) Plane stress and (b) plane strain.

4.4 Simulation Results and Discussion

In this section, the results of numerical simulations corresponding to the burnout process of each sample in investment casting are presented. Solid and completely hollow patterns are first examined and compared with the results from Lames equations to ensure that the finite element model is correct.

4.4.1 Solid and Completely Hollow Patterns

It is rational to examine the extreme cases of solid and completely hollow SLA patterns, which always cause shell cracking and pattern break down during pattern burnout and

handling, respectively. Table 4.5 and Figure 4.10 show the FEA results for solid, hollow, and webbed pattern and the calculated results from Lames equation for the solid pattern. As can be seen in Figure 4.10, the computational results (×) gives a good agreement with the theoretical calculation (——) for the solid pattern.

As can be seen in Figure 4.10, the induced stresses of the ceramic shell are quite large for the solid pattern (——), and very small for the hollow pattern (-•-•-•-). It is rational to assume that there is a pattern between solid and hollow patterns to have induced stresses smaller than what the ceramic shell can withstand. This pattern can compromise the characteristics of rigidity and thermal sustainability. The webbed pattern was modeled to estimate the induced stresses. The dashed line (------) in Figure 4.10 is the generated stress profile on the ceramic shell with a webbed SLA pattern during the burnout process.

Table 4.5 Comparison of FEA results from ANSYS and analytical results from Lames equation for a solid pattern in the burnout process.

	Hoop Stress in Ceramic Shell (MPa)			
T(°C)	Lames Calculation	Solid Pattern	Hollow Pattern	Webbed Pattern
30	2.89	2.89	0.120	0.555
40	5.24	5.24	0.187	0.890
50	6.38	6.38	0.204	1.010
60	6.97	6.97	0.168	0.868
70	8.17	8.17	0.146	0.803
80	7.71	7.71	0.132	0.731
90	3.29	3.29	0.051	0.289

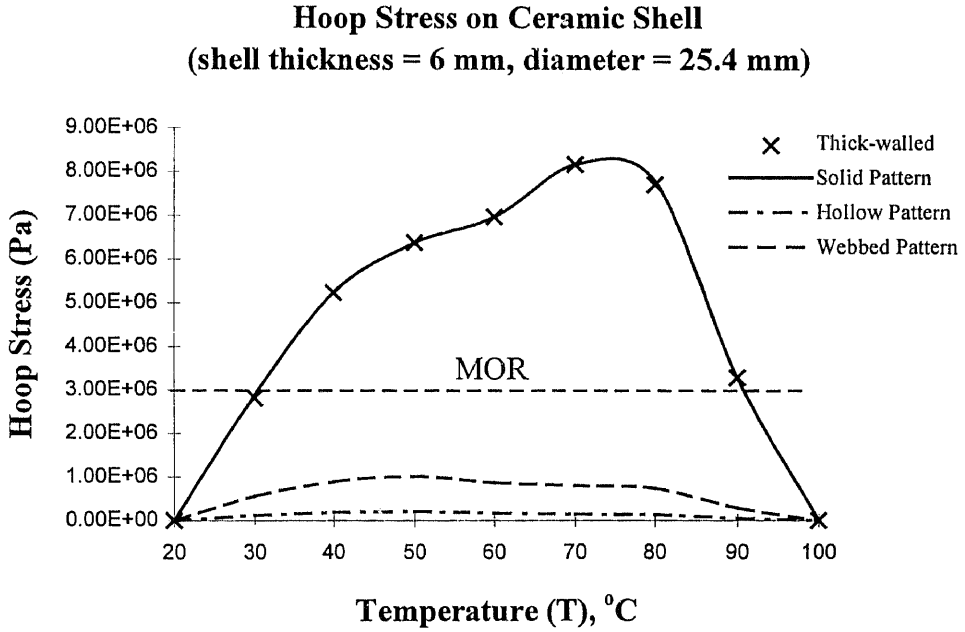

Figure 4.10 Hoop stress profiles on ceramic shell with solid, hollow and webbed SLA patterns.

4.4.2 Effect of Shell Thickness

An example of the computer simulation is used to illustrate how the shell cracking temperature and the pattern buckling temperature are determined. The finite element result of an SLA part coated with a 1 mm thickness ceramic shell is depicted in Figure 4.11, and the corresponding data is listed in Table 4.6. The σ_c and σ_x (or σ_y) represent the principal (hoop) stress in the ceramic shell and the compressive stress in the epoxy webbed pattern, respectively. The modulus of rupture (MOR) of the ceramic material is 3.0×10^6 Pa. The σ_c value is compared with MOR to define the rupture temperature of the ceramic shell. P_{cr} is the critical pressure that causes the web link to buckle. The critical pressure for the buckling of a square frame is given [Wang, 1954].

$$P_{cr} = \frac{16.47EI}{AL^2} \tag{4.1}$$

where A is the cross-sectional area of the web link, E is Young's modulus of the epoxy, I is the moment of inertia of web link cross-section, and L is the web link length. Here L equals 6.35 mm (0.25 inch). $A = b \times h$ and $I = \frac{hb^3}{12}$, where b is the width of the web link, and h is the height of the web link. The σ_x value is compared with P_{cr} to determine the buckling temperature of the web link. In this example, the results are $T_u = 35°C$, and $T_b = 52°C$ (see Table 4.6). Note Young's modulus of the epoxy resin is a function of temperature. $T_b = \infty$ or $T_u = \infty$ means no pattern buckling or no shell cracking at all. The same procedure is repeated for each test sample. The collective data of the test samples are listed in Table 4.7.

Hoop stress on the ceramic shell

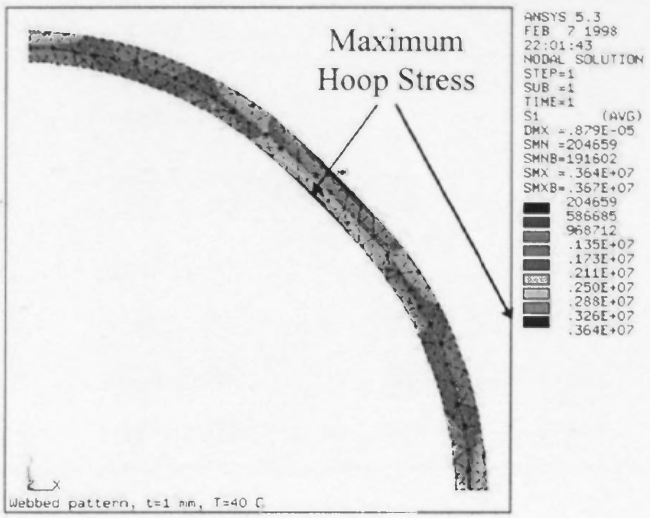

Stress within the webbed pattern

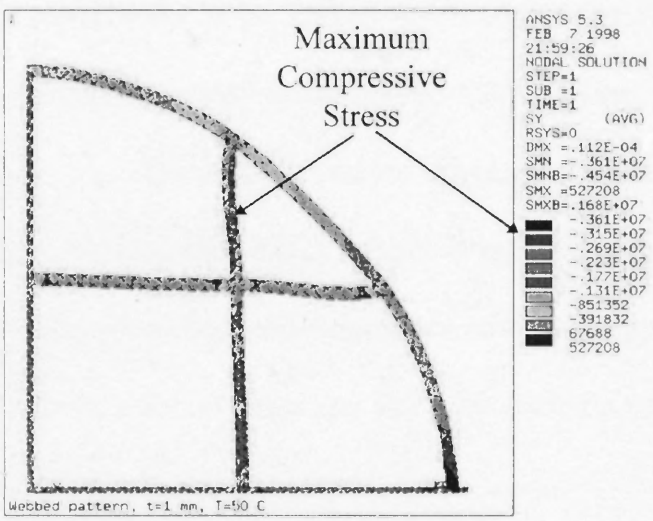

Figure 4.11 The stress profile from the result of the finite element simulation for Part1 with 1 mm ceramic shell.

Table 4.6 Comparison of analytical values of σ_c and σ_r with MOR and P_{cr}, respectively, to determine $T_u \approx 40°C$ and $T_b \approx 50°C$.

T (°C)	σ_c (Pa)	σ_x (Pa)	P_{cr} (Pa)
30	2.07×10^6	1.69×10^6	6.30×10^6
40	3.64×10^6	2.76×10^6	5.20×10^6
50	4.55×10^6	3.15×10^6	3.14×10^6
60	4.43×10^6	2.71×10^6	0.28×10^6
70	4.84×10^6	2.41×10^6	0.78×10^6
80	2.18×10^6	2.15×10^6	0.63×10^6
90	1.89×10^6	8.40×10^5	0.32×10^6

Figure 4.12 shows the numerical results for Part1. The calculated rupture temperature (T_u) for this part with 1 mm thickness is about 35°C, while the experimental result is about 40°C as shown in the figure. Similar trends can be seen for the effect of the ceramic shell thickness on the generated stresses in the shell. It is seen from Figure 4.12 that the hoop stress decreases as the shell thickness is increased. That is, a thicker ceramic shell can better resist the thermal expansion of the SLA epoxy pattern. In this study, 3 mm shell thickness is strong enough to hold the force exerted by the epoxy pattern due to thermal expansion. Figure 4.13 shows that the effect of shell thickness on the stress induced in the internal web structure is quite small.

Table 4.7 Predicted rupture temperature and buckling temperature of the test samples and their comparison with the glass transition temperature.

Sample I.D.	Rupture Temperature (°C)	Buckling Temperature (°C)	Glass Transition Temperature (°C)	Relationship
Part1t1	35	52	60 - 70	$T_g > T_b > T_u$
Part1t3	∞	51	60 - 70	$T_u > T_g > T_b$
Part1t6	∞	50.5	60 - 70	$T_u > T_g > T_b$
Part1t9	∞	50.5	60 - 70	$T_u > T_g > T_b$
Part2t6	∞	37	60 - 70	$T_u > T_g > T_b$
Part2t9	∞	37	60 - 70	$T_u > T_g > T_b$
Part3t3	∞	50.5	60 - 70	$T_u > T_g > T_b$
Part3t6	∞	50.5	60 - 70	$T_u > T_g > T_b$
Part4t3	∞	77.5	60 - 70	$T_u > T_b > T_g$
Part4t6	∞	77.5	60 - 70	$T_u > T_b > T_g$
Part4t9	∞	77.5	60 - 70	$T_u > T_b > T_g$
Part5t6	∞	51	60 - 70	$T_u > T_g > T_b$
Part5t9	∞	51	60 - 70	$T_u > T_g > T_b$
Part6t1	40	37	60 - 70	$T_g > T_u > T_b$
Part6t2	45	37	60 - 70	$T_g > T_u > T_b$

Note: Sample I. D. described in Table 4.1

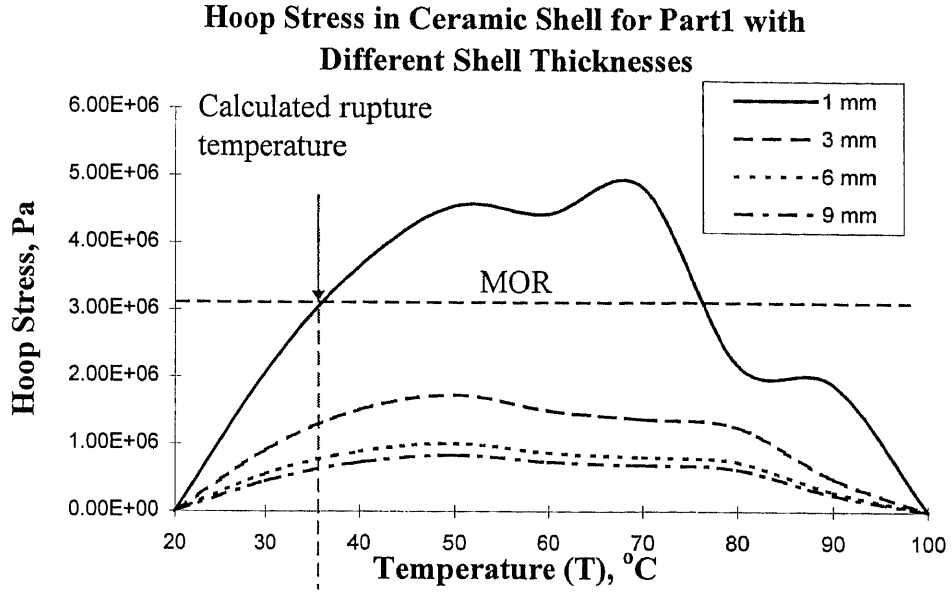

Figure 4.12 Hoop stress decreased as the shell thickness increased. The calculated rupture temperature for Part1 with 1 mm shell thickness is about 35°C, and the observed rupture temperature is about 40°C.

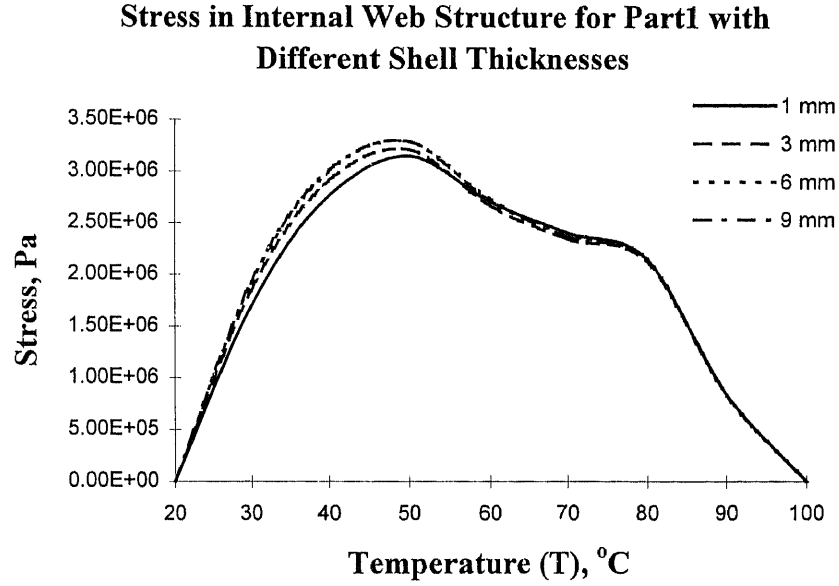

Figure 4.13 Stresses in the internal web structure for different shell thicknesses for Part1.

4.4.3 Effects of the Web Structure and Dimensions

The effect of the width and the span length of the web link structure are shown in Figures 4.14 and 4.15, respectively. As can be seen in Figure 4.14, a larger link width of the internal web structure exerts a larger stress on the ceramic shell. A larger web link width also has a larger moment of inertia. As a result, the internal web structure with a larger web width is more difficult to bend. In contrast, a pattern with a larger span length of the web link bends more easily. As can be seen in (4.1), the critical compressive pressure, $P_{cr} = \frac{16.47EI}{AL^2}$, is inversely proportional to the square of the web link span length. That is, the webbed pattern with a larger span of the web links is more likely to buckle.

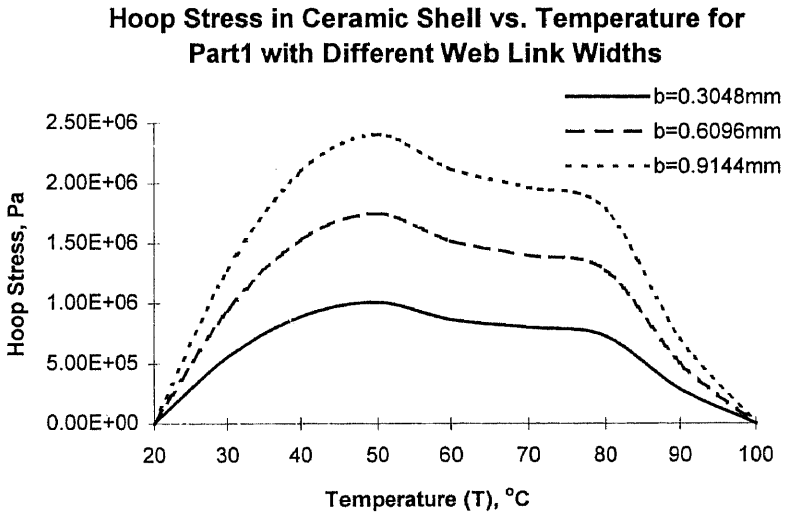

Figure 4.14 Hoop stress at various temperatures and web link widths; Part1, t=6 mm.

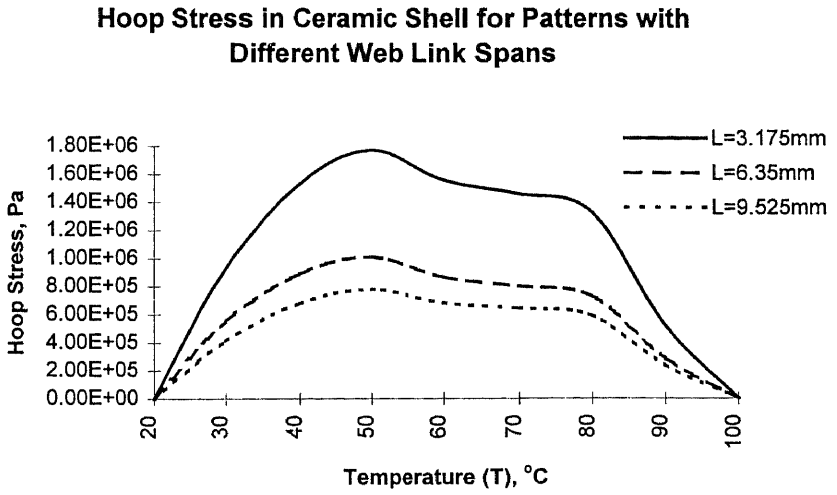

Figure 4.15 Hoop stress varies with different web link spans for Part1 (L=6.35 mm), Part2 (L=9.525 mm), and Part4 (L=3.175 mm), t=6 mm.

4.5 Equivalent Force Method

Practically, it is difficult to apply Lames equations to analyze the stresses in the ceramic shells and epoxy patterns due to the geometric complexity of the pattern. The finite element analysis is, of course, a route to estimate the stress profile for a complex model of the webbed structure. However, the geometric complexity of the web structure can exert large computational burden or even exhaust the computing capacity in running an FEA package for the stress analysis. An equivalent force technique is thus devised to replace the thermal effect of the web structure by a set of forces exerted on the skin of the epoxy pattern.

The equivalent forces acting on the ceramic shell by the web structure during the burnout process are estimated from the web geometry and the heating temperature using a simple method. A schematic drawing is shown in Figure 4.16. The stresses due to the thermal expansion of the web can be solved by regarding the web to consist of many

beams, each clamped at the two ends. The thermal effect due to temperature rise can thus be approximated by the thermal expansion of many decoupled, clamped-clamped beams.

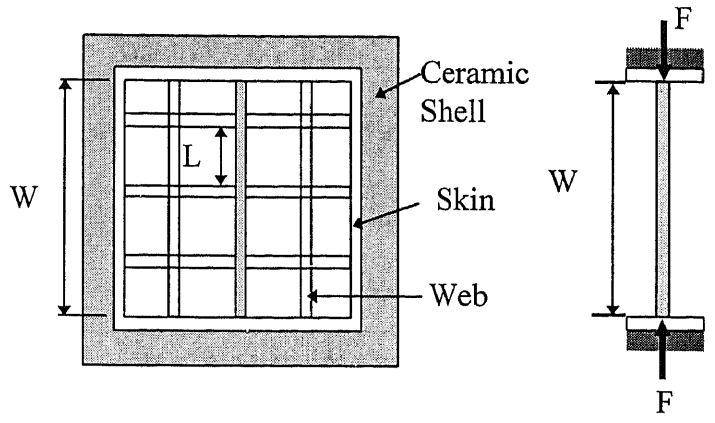

Figure 4.16 Reaction force on the web structure due to temperature rise.

As thermal expansion occurs due to temperature rise ΔT, the beam cannot elongate freely due to the end constraints. A compressive force F is thus developed in the beam when the temperature increases. The ceramic shell also expands slightly due to ΔT. The elongation of the beam relative to the ceramic shell due to the temperature increase is $(\alpha_r - \alpha_c)W\Delta T$, where α_r and α_c are the coefficients of thermal expansion of the epoxy resin and ceramic material, respectively. The compression of the beam due to the reaction force F is FW/EA, where E is Young's Modulus of the resin and A is the cross-sectional area of the beam. Equating the elongation and the compression gives

$$F = EA(\alpha_r - \alpha_c)\Delta T \tag{4.19}$$

The effect of thermal expansion in the web structure can thus be replaced by equivalent forces exerted on the skin surface of the pattern that are calculated using the

above equation. After finding F from this equation, the compressive stress and strain in the beam can be obtained as follows:

$$\sigma = F/A = E(\alpha_r - \alpha_c)\Delta T \tag{4.20}$$

$$\varepsilon = \sigma/E = (\alpha_r - \alpha_c)\Delta T \tag{4.21}$$

Here we used square and circular models as examples. With the internal web structure, the webbed pattern increases in rigidity compared to the hollow pattern. The stresses obtained for these patterns are shown in Figure 4.17. In the equivalent force model, the pattern is modeled as a skin having point forces acting on its surface. The FEA result of this model is shown in Figure 4.18. The nodal stresses in elements of the webbed structure model and equivalent force model are shown in Figure 4.19 and Table 4.8. The thermal stresses in the ceramic shell obtained using the method of equivalent forces are close to those obtained using the exact web structure in both magnitude and profile. Another example of circular model is shown in Figure 20 and Table 4.9. This strongly indicates the validity of the proposed method of equivalent forces. This equivalent force technique can be used to simulate a three-dimensional investment casting model.

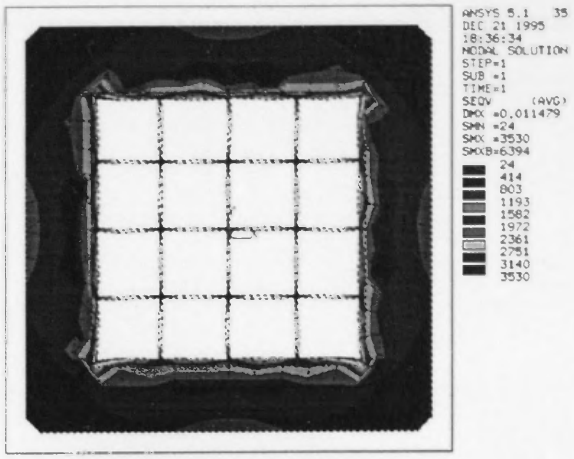

Figure 4.17 Stresses for the webbed pattern with 100°C temperature rise.

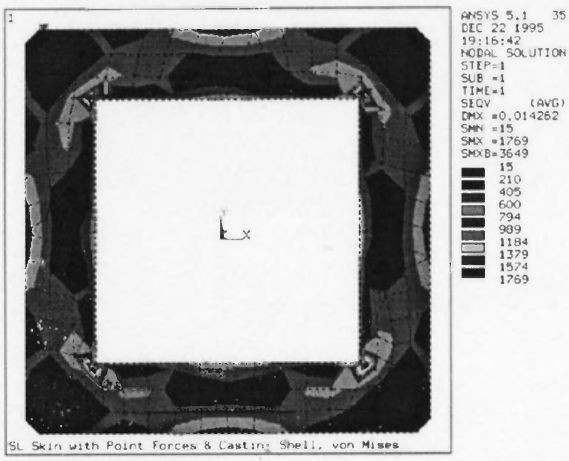

Figure 4.18 Stresses for the hollow pattern and equivalent forces with 100°C temperature rise.

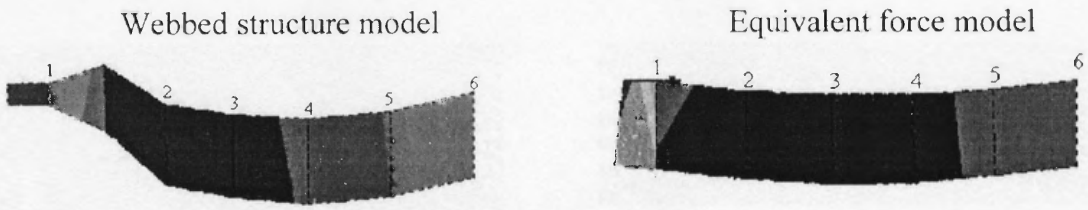

Figure 4.19 Stresses in the elements using the webbed model and the equivalent force model.

Table 4.8 Nodal stresses from FEA using the webbed and equivalent forces models.

	(psi)	1	2	3	4	5	6
Webbed	σ_x	-1060	-280	-140	-65	-17	3
Structure Model	σ_y	-1475	220	350	520	720	975
Equivalent	σ_x	-980	-322	-148	-69	-18	3
Force Model	σ_y	-1460	198	345	512	700	945

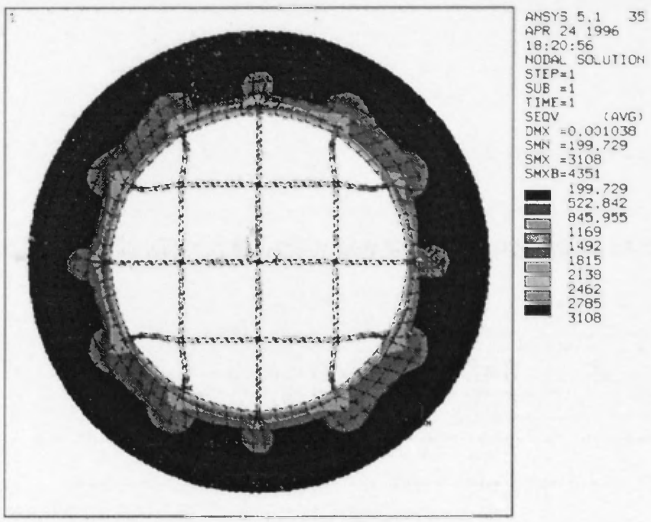

Figure 4.20a Stresses for the webbed pattern with 100°C temperature rise.

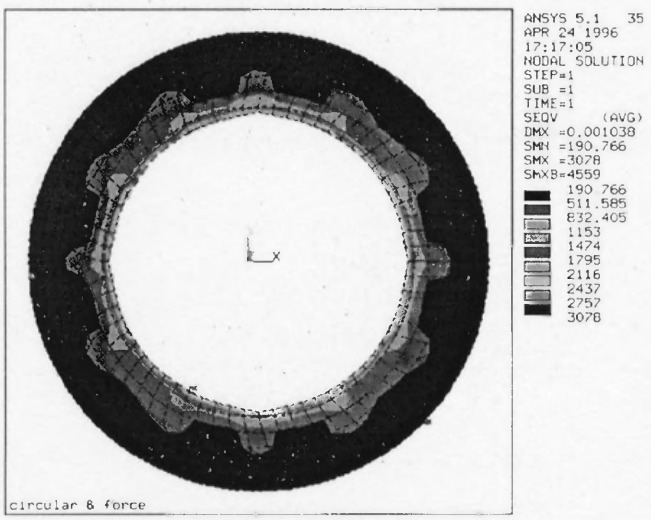

Figure 4.20b Stresses for the hollow pattern and equivalent forces with 100°C temperature rise.

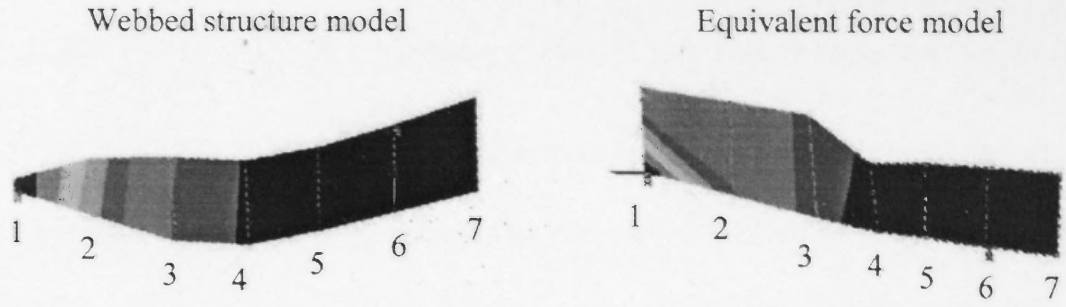

Figure 4.20c Stresses in the elements using webbed model and equivalent force model.

Table 4.9 Nodal stresses from FEA using the webbed and equivalent forces models.

	(psi)	1	2	3	4	5	6	7
Webbed Structure Model	σ_x	156	489	424	417	426	430	458
	σ_y	-1046	-420	-208	-132	-30	-34	0
Equivalent Force Model	σ_x	152	472	414	407	409	418	442
	σ_y	-1002	-371	170	-101	-64	-28	2

4.6 Modified Lames Thick-Walled Formula

In Section 4.2.3 Lames equations for a thick-walled cylinder were used to validate the induced hoop (σ_0) and radial (σ_{rad}) stresses from FEA for a ceramic shell with a cylindrical solid pattern. The pressure and stresses are

$$p = \frac{(\alpha_r - \alpha_c)\Delta T}{\frac{1}{E_r}(1 - \nu_r) + \frac{1}{E_c}(k + \nu_c)} \tag{4.10}$$

$$\sigma_{rad} = -p \tag{4.11}$$

$$\sigma_\theta = k\,p \tag{4.12}$$

where $k = \frac{(R+t)^2 + R^2}{(R+t)^2 - R^2}$, R is the radius of the circular SLA pattern, and t is the ceramic shell thickness. The formula cannot be directly applied to the investment casting with a webbed SLA pattern due to the complexity of the web structure. Therefore, it is necessary to perform finite element analysis. However, the operation of FEA is lengthy and costly for any change of web dimensions and shell thickness, thus an analogous formula will be helpful to quickly check the stress profiles in the ceramic shell and web structure. This approach is valuable when used with the previous empirical results of finite element analysis (in Section 4.4).

With the voids inside, the webbed SLA pattern can be treated as a porous epoxy material with modified material properties, including Young's modulus (E_r') and coefficient of thermal expansion (α_r'). The induced stress can be estimated by using the analogous material properties (E_r' and α_r') of the porous material in (4.10). The E_r' and α_r' are $E_r' = E_r$ / e-factor and $\alpha_r' = \alpha_r$ / c-factor. The adjustments, "e" factor and "c" factor can be selected based on the FEA data. Some examples and values of e-factor and c-factor are given in Figure 4.21. The results from the analogous formula are compared with the results of FEA. As can be seen, both the e-factor and c-factor are constant when the same pattern is used (despite different shell thickness). The "c" factor is a constant while the "e" factor varies when estimating the hoop stress in the ceramic shell. The "c" factors also varies when estimating the stress in the web.

These analogous formula is very useful in the practical web structure design for estimating the induced thermal stresses in the ceramic shell and web link with new dimensions of web structure or different values of shell thickness. The general curves of

"e" and "c" factors for the web span and width as variables are shown in Figure 4.22. When the web width equals 6.35 mm or when the web span equals 0.3048 mm, the pattern is considered as a solid, and the factors of "e" and "c" are unity. By using this approach, the general curve of "e" and "c" factors against void ratio can also be obtained.

t(mm)=	3	6	9
e-factor=	12.5	12.5	12.5
c-factor=	1	1	1

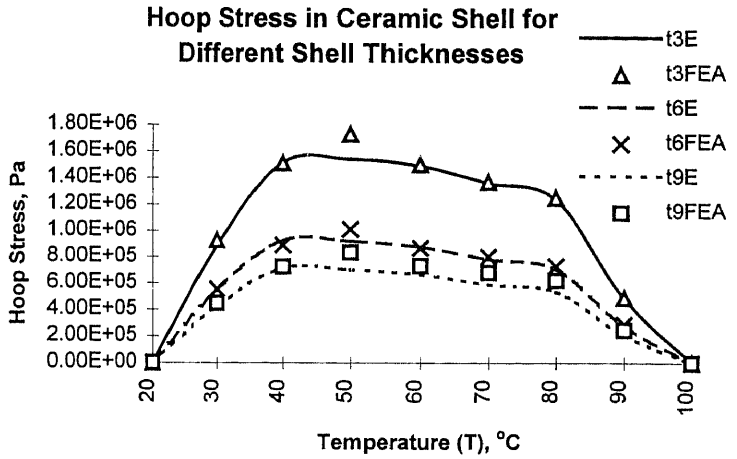

t(mm)=	3	6	9
e-factor=	12.5	12.5	12.5
c-factor=	0.112	0.1117	0.1115

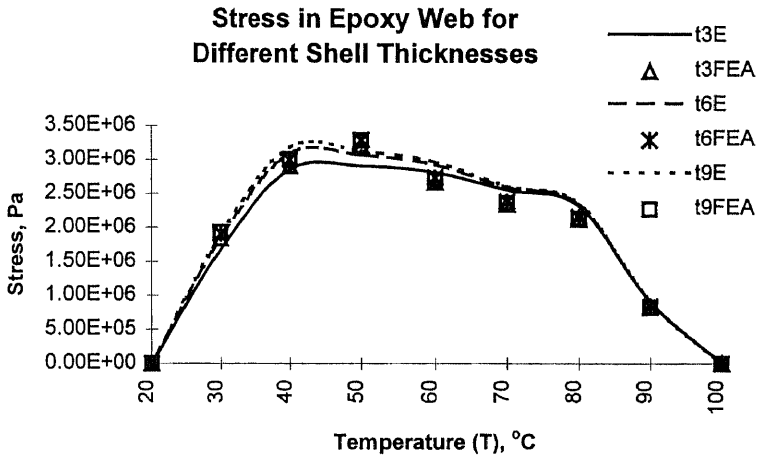

Figure 4.21a Stresses estimated by the analogous formula for various shell thicknesses.

b (mm)=	0.3048	0.609	0.9144
e-factor=	12.5	6.9	4.8
c-factor=	1	1	1

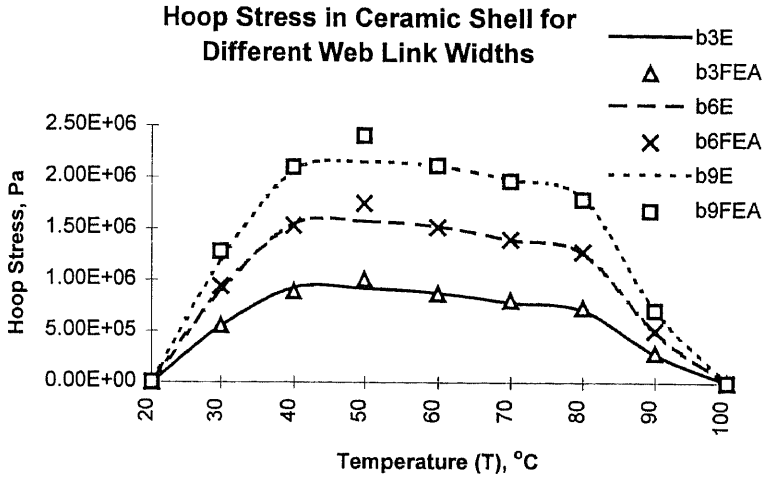

b (mm)=	0.3048	0.609	0.9144
e-factor=	12.5	6.9	4.8
c-factor=	0.12	0.2	0.27

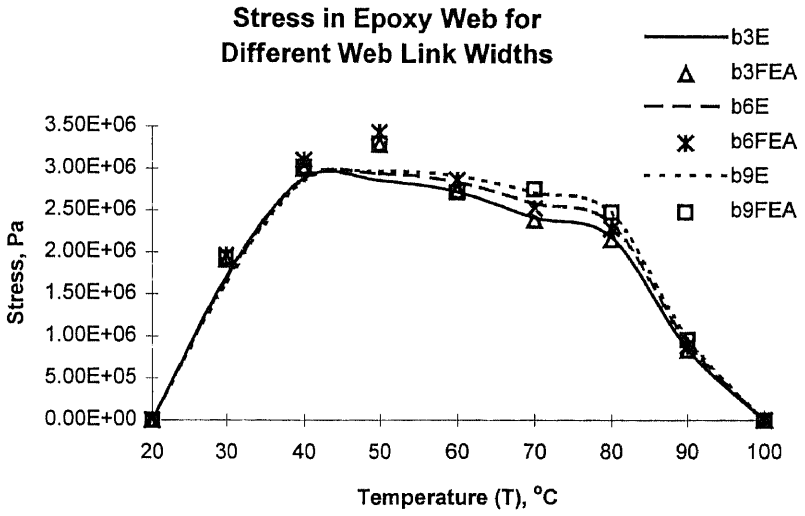

Figure 4.21b Stresses estimated by the analogous formula for various web link widths.

L (mm)=	3.175	6.35	9.525
e-factor=	6.75	12.5	15.5
c-factor=	1	1	1

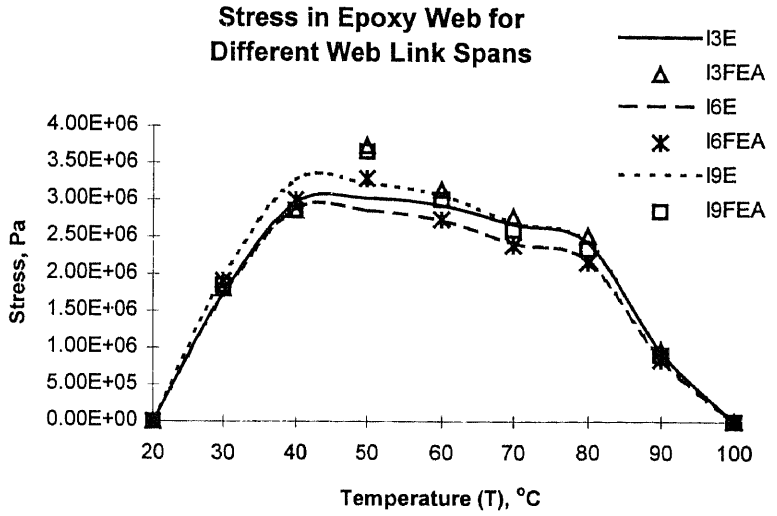

L (mm)=	3.175	6.35	9.525
e-factor=	6.75	12.5	15.5
c-factor=	0.198	0.12	0.087

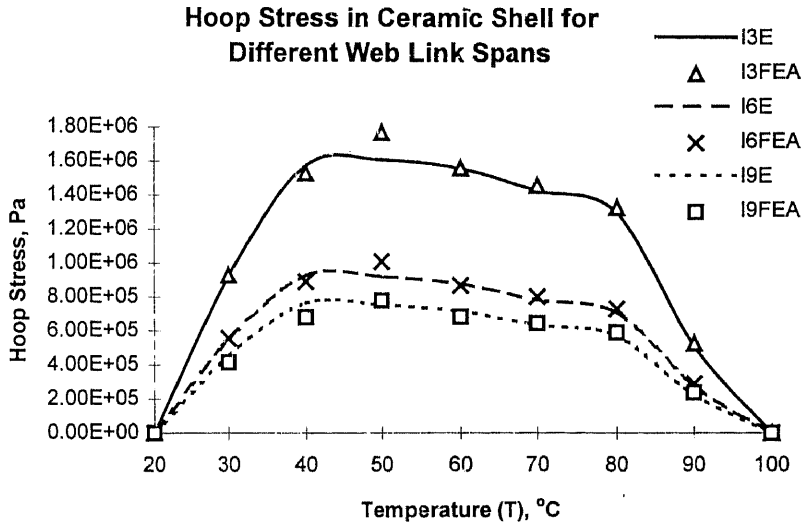

Figure 4.21c Stresses estimated by the analogous formula for various web link spans.

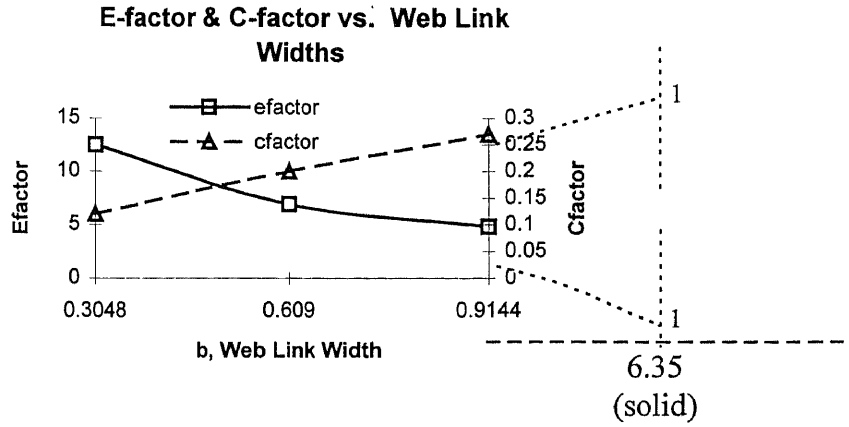

Figure 4.22a General curves of adjust factors for different web link widths.

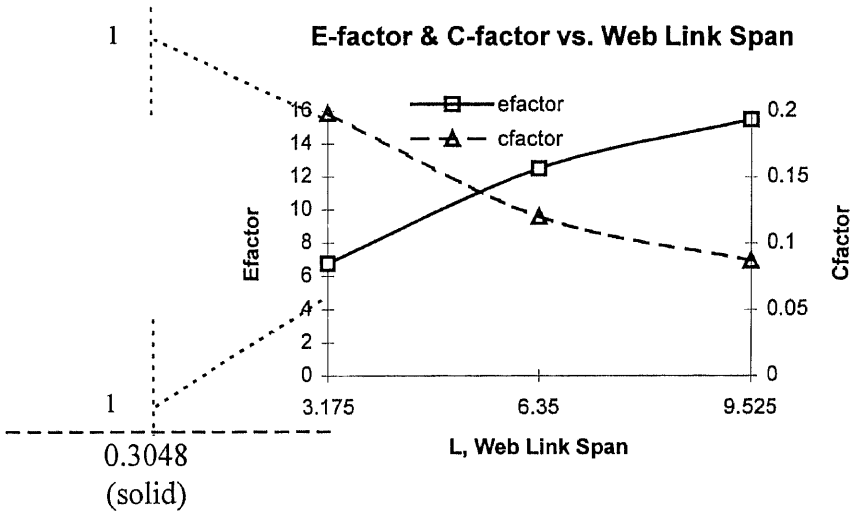

Figure 4.22b General curves of adjust factors for different web link spans.

4.7 Closure

This chapter presents an analytical and numerical approach to study the burnout of internally webbed SLA patterns in investment casting. This is done by comparing the temperatures of shell cracking, web buckling and glass transition of the epoxy material, so as to understand the cracking of ceramic shell and the buckling of internal web link. Four relationships of the temperatures of shell cracking, web link buckling and the glass transition of epoxy are identified, i.e $T_g > T_b > T_u$, $T_u > T_g > T_b$, $T_u > T_b > T_g$, and $T_g > T_u > T_b$. The different relationships result from different dimensions of the web structure and different shell thicknesses. The stress profiles and locations of maximum stress for each sample are obtained. The numerical simulations predict that the shell cracking and web link buckling may occur at lower temperatures than the glass transition temperature. The results reveal that shell cracking and web link buckling depend strongly on the shell thickness and the dimensions of the web links. These predictions will be validated in the next chapter qualitatively and quantitatively. An analogous formula is developed to estimate the induced stress in the shell and web link by considering the porous webbed pattern as a solid pattern with an equivalent Young's modulus and thermal expansion coefficient. The analogous formula provides a quick means to estimate the generated stresses in the ceramic shell and web link with new dimensions of web structure and shell thickness. An equivalent force technique is also developed and validated. This equivalent force technique simplifies the analysis of thermal stresses in the burnout of a complex shell model with a webbed pattern in investment casting.

CHAPTER 5

EXPERIMENTAL RESULTS AND DISCUSSION

This chapter presents experiments that are conducted to gain evidence for the analytical predictions and to develop a better understanding of the mechanisms of shell cracking and SLA pattern collapsing during the pattern burnout process in investment casting. It falls into two parts. First, qualitative experiments are made to observe the phenomena of the pattern burnout process. Secondly, the induced stresses on the shell are measured by a strain gauge instrument. Both the qualitative observation and the strain gauge based experimentation validate the predictions of FEA in the previous chapter.

5.1 Sample Preparation

The cross-sectional area of web structure and shell thickness are varied to investigate their effects on the temperatures of ceramic cracking and pattern buckling. Test samples are designed in order to get different shell cracking and pattern buckling combinations of temperatures with different sets of parameters. After numerical analysis, the test samples are geometrically designed with the Pro/ENGINEER package and built using an SLA 250 fabricator with the SL5170 photocurable epoxy resin from Ciba-Geigy. The internally webbed SLA samples used in this study have a simple cylindrical geometry of 25.4 mm (1 inch) diameter and 76.2 mm (3 inches) long. The dimensional specifications of the test samples are listed in Table 4.1. The dimensions of Part1 (L = 6.35 mm, b = 0.3048 mm, and h = 1.4732 mm) are the typical values used in the QuickCast build style. The SLA

build parts are coated by Sandia National Laboratories (SNL) with ceramic shells having the thicknesses of 1, 3, 6 and 9 mm. The samples are intentionally designed with one open end in order to observe the web structure during the burnout process. Therefore, these SLA parts need to be sealed with investment wax at the two ends prior to the ceramic slurry dipping, so as to prevent any slurry inside the webbed pattern during the ceramic coating process (see Figure 5.1). Otherwise, the slurry evaded inside the webbed pattern will lead to an unsuccessful investment shell. The procedure of dipping process in SNL is given in Table 5.1. Figure 5.2 illustrates a webbed SLA pattern with and without ceramic coating.

Table 5.1 The typical dipping process and materials of slurry and stucco in investment casting.

Dip Coat	Slurry	Stucco
1	"PrimeCoat" slurry: Colloidal silica Remasil 60 aluminosilicate Fused silica	70 grit alumina
2	PrimeCoat slurry (above)	54 grit alumina
3	"Backup" slurry Nalcoag 830 colloidal silica fused silica	54 grit alumina RG-2 fused silica
4	Backup slurry	RG-2 fused silica
5	Backup slurry	RG-2 fused silica
6	Backup slurry	RG-2 fused silica
7	Backup slurry	RG-2 fused silica
8	Backup slurry	RG-2 fused silica
9	Backup slurry	RG-2 fused silica
10	Backup slurry	RG-2 fused silica

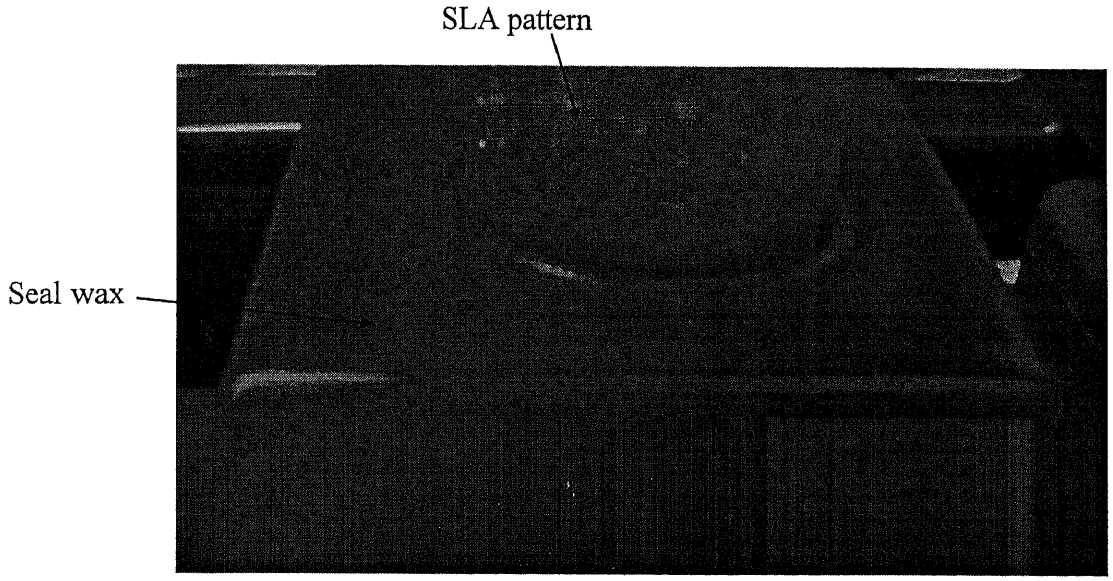

Figure 5.1 Pre-wax ends of SLA pattern to prevent any slurry inside the webbed pattern.

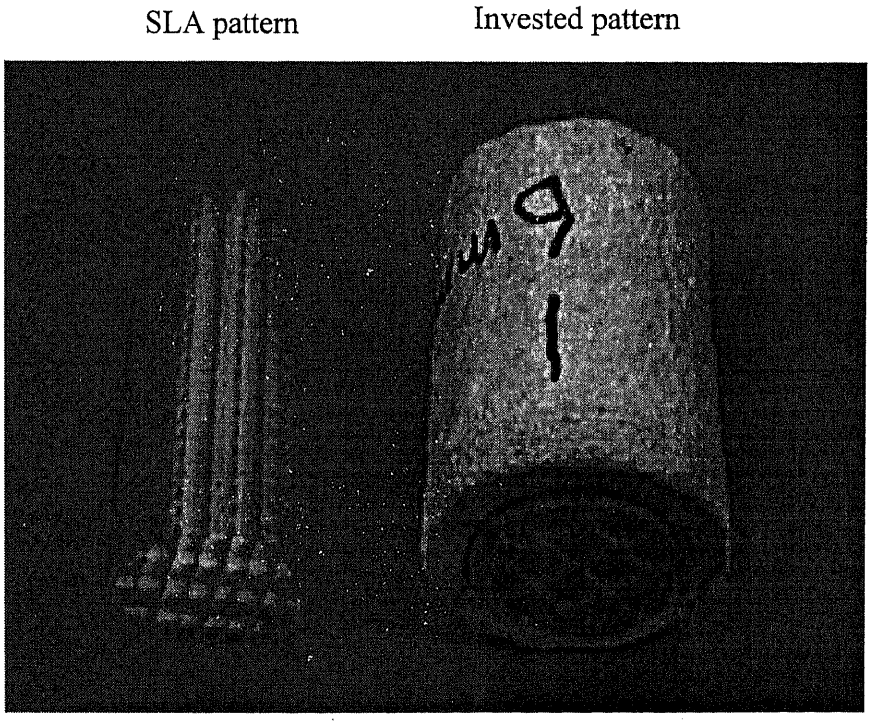

Figure 5.2 SLA pattern without and with ceramic shell.

5.2 The Experimental Procedure

The test samples are examined and recorded before being placed in the oven. The oven used for the pattern burnout experiment has its temperature controlled electrically (see Figure 5.3). The invested shell/pattern constructions are placed in the oven and gradually heated from 23°C up to 170°C, with a rate of 5°C/minute, to simulate the pattern burnout process in investment casting. The test samples are examined and recorded at intervals of ten degrees, up to 100°C. The observations of test samples are made with a magnifier and an imaging camera. The observations recorded include shell cracking, epoxy softening, and web link buckling. If the SLA webbed pattern collapses because of the bend of a web link, then the web has buckled. If the pattern fails because of softening, then the pattern will look "leathery".

Figure 5.3 Electric temperature controlled oven.

5.3 Experimental Observations and Discussions

5.3.1 Shell Cracked

Part1 is the test sample with the typical internal web structure (see Figure 4.3; L = 6.35 mm, b = 0.3048 mm, and h = 1.4732 mm) used in QuickCast. The samples that are invested with 1 mm ceramic shell, Part1t1, show no shell cracking until the temperature reaches 40°C. Its shell cracks and propagates along the diagonal corner when the temperature reaches 40°C (see Figure 5.4a). The web links still remain straight (see Figure 5.4b) because the shell has cracked already. When the temperature reaches the glass transition, 60 - 70°C, the epoxy material becomes somewhat sticky and leathery. When the temperature is increased to 100°C, the part becomes very dry and brittle. After 100°C and up, the test sample starts to vent smoke.

This observation indicates that the shell cracking occurs at the early stages of the burnout process in investment casting, when the invested shell is not strong enough to resist the exerted forces from the thermal expansion of the internal web structure. It agrees with the prediction of FEA. From FEA, the predicted rupture temperature is about 35°C, at which the induced stress exceeds the MOR of the ceramic material and thus fractural cracking occurs. The maximum stress occurs at the diagonal corners because the tensile forces and bending moments at the diagonal corners cause more stresses on the ceramic shell (see Figure 5.41a and 5.41b).

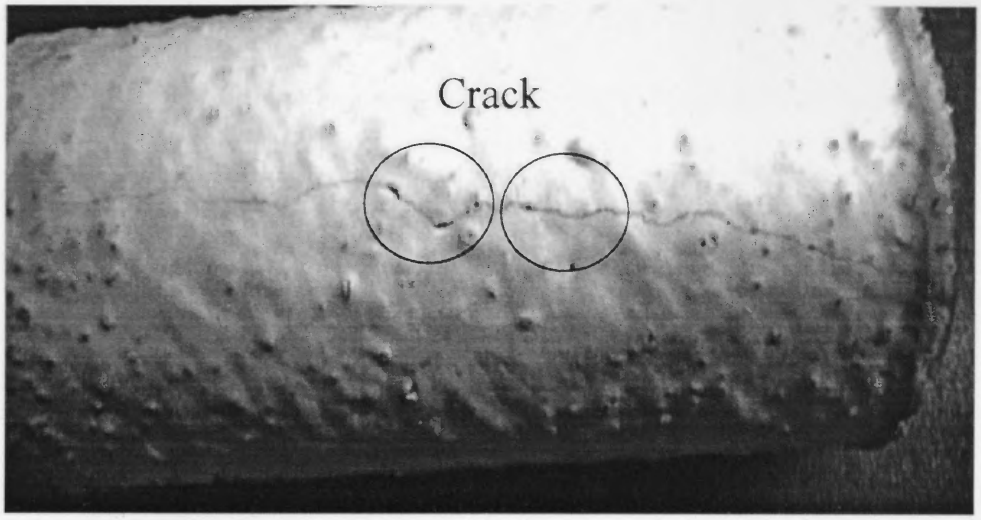

Figure 5.4a The shell of the test sample Part1t1 cracks at 40°C.

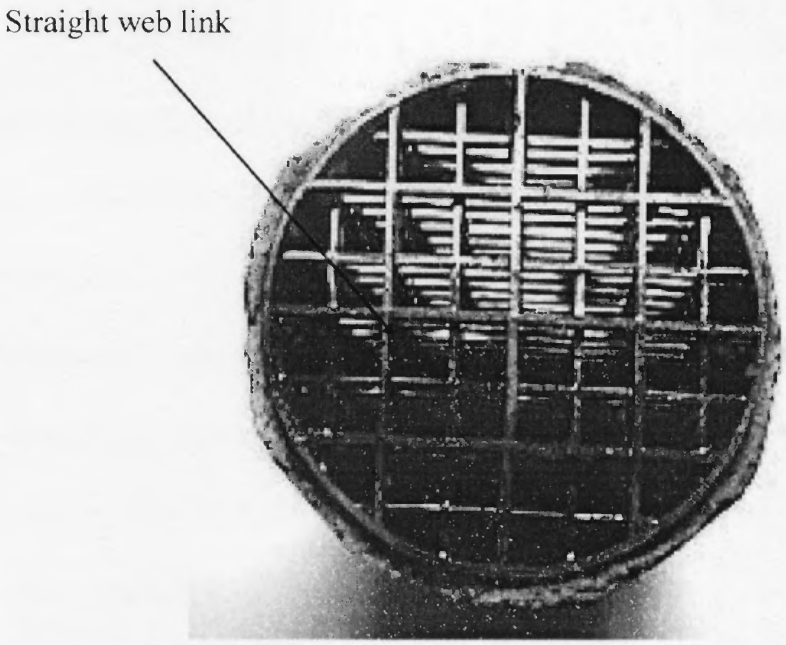

Figure 5.4b The internal web structure remains straight without wavy shape.

5.3.2 Web Link Slightly Buckled

The observations show that the web links of the test samples with the typical web structure (Part1) and 3, 6, 9 mm in shell thickness are slightly buckled when the temperature reaches 50°C (see Figures 5.5a,b). There is no occurrence of shell cracking at all, whereas the web link becomes brittle and collapsed after the glass transient temperature. Likewise, the web links of the samples, Part5, with a smaller web link height and coated with 6 and 9 mm thickness, appears slightly buckled (see Figure 5.6). Again, the results of FEA are confirmed by experimental observations. The FEA prediction indicates that the web links of those parts are buckled around 51°C (see Table 4.7). There is no occurrence of shell cracking at all because MOR is greater than the induced stress from thermal expansion. The Part3 has a web width larger than the typical internal web structure (Part1) by 50%. The experimental results show that the web structure exhibit slight buckling. Figure 5.7 shows the result of burning of Part3. In this group, the buckling temperature is lower than epoxy glass transition temperature and the rupture temperature is the largest ($T_u > T_g > T_b$). The results indicate that the shell of 3 mm thickness is thick enough to take the stress induced from the thermal expansion. The thicker the shell is, the better. However, coating a thicker ceramic shell is expensive and time consuming. It is too early to conclude that the 3 mm shell thickness is strong enough for practical shell investment casting. The FEA shows that variations in the induced stresses of the samples with 6 and 9 mm with temperature increases are quite small (see Figure 4.12).

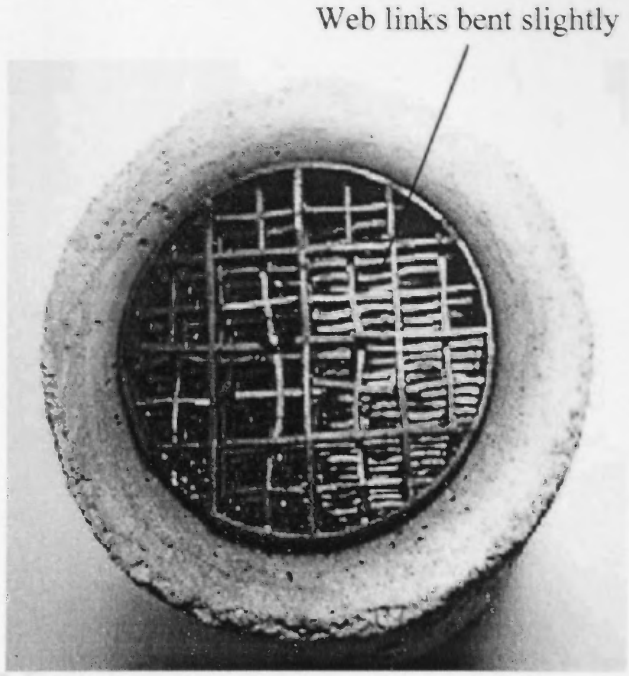

Figure 5.5a The web links of the test sample with 6 mm thickness. Part1t6 appears slightly wavy at 50°C and the web links are collapsed.

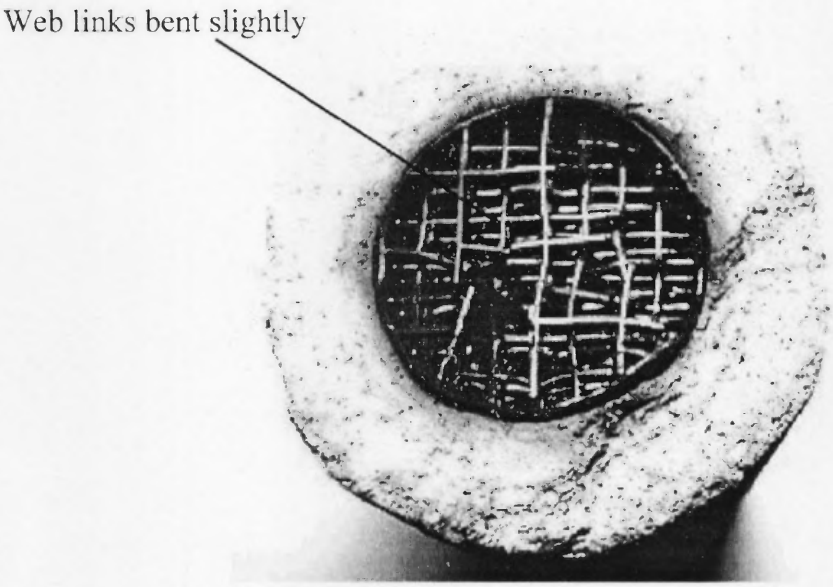

Figure 5.5b The web links of the test sample with 9 mm thickness. Part1t9 appears slightly wavy at 50°C and the web links are collapsed.

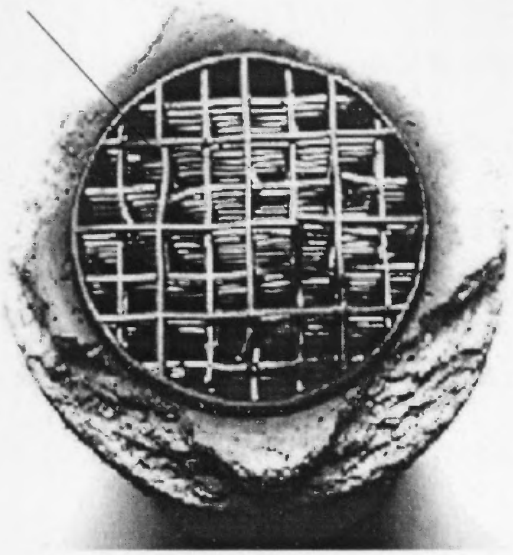

Figure 5.6 Larger web height part with 6 mm shell thickness. Part5t6 appears slightly buckled.

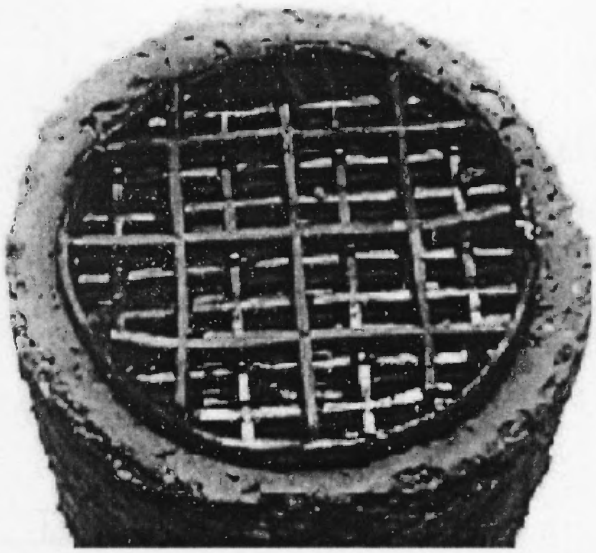

Figure 5.7 Larger web width part with 3 mm shell. Part3t3 appears slightly buckled.

5.3.3 Web Link Severely Buckled

The experimental results of Part2, which has 50% larger web link span than that of Part1, show that the web link becomes wavy when the temperature reaches around 40°C. Figures 5.8a and 5.8b show the internal web structure of Part2t6 (6 mm shell thickness) before and after heating. The temperature (37°C) at which the web link starts to bend is significantly lower than the glass transition temperature (60 - 70°C) of the epoxy material. The test samples show no shell cracking. The buckling temperature of Part2 (with a longer web link span) is lower than that of other patterns. It confirms the FEA prediction, $T_u > T_g > T_b$ (see Table 4.7). The predicted stress from FEA decreases as the web span length increases (see Figure 4.15). The induced stresses are smaller than MOR thus no shell cracking. This result leads to the conclusion that the temperature of web link buckling can be controlled via a proper selection of web link dimensions, leading to the prevention of shell cracking.

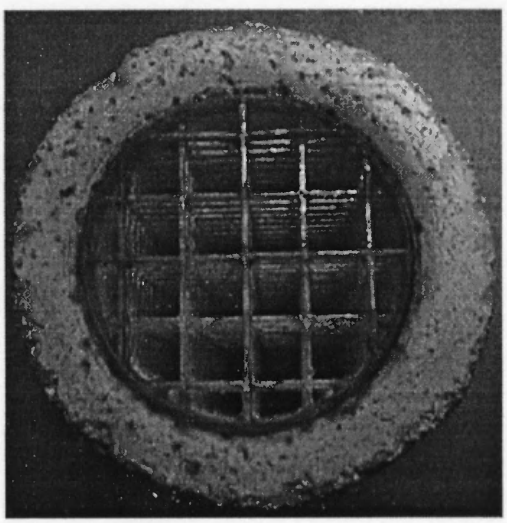

Figure 5.8a Test sample Part2t6 before heating.

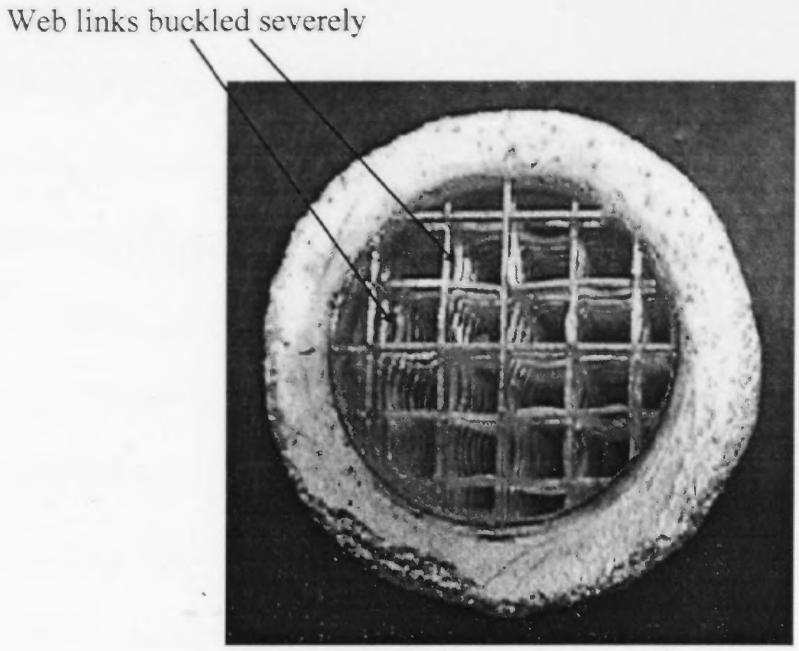

Figure 5.8b Test sample Part2t6 bends significantly after heating to 40°C.

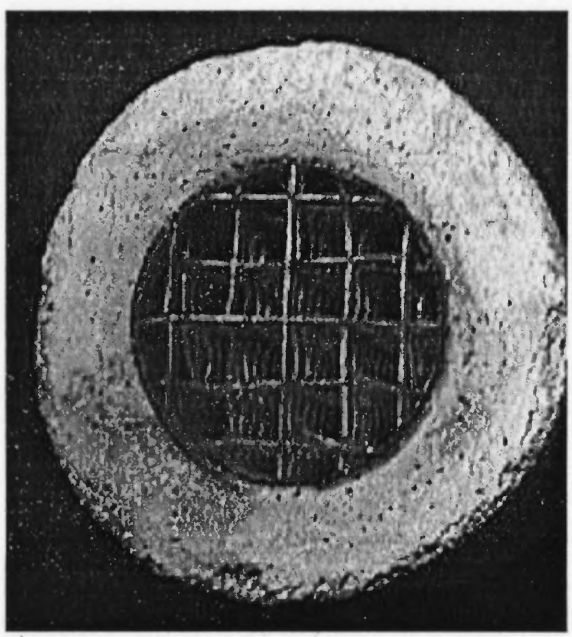

Figure 5.8c Web links of the test sample Part2t9 with 9 mm shell thickness bent significantly at 40°C.

5.3.4 No Buckling in Web Link

Figure 5.9 shows the results of burnout of Part4. At high temperatures (> 100°C) the web structure becomes brittle and breaks down, with no sign of web link bending. The Part4 has a web span length shorter than the typical web structure by 50%. From Table 4.7, the buckling temperature (78°C) is higher than the glass transition temperature. The experimental observations show that they hardly compared with other parts. Recall that the critical load (4.2) to cause the buckle of a square frame is inversely proportional to the square of the web link span. It confirms the numerical prediction and indicates that the web link span is essential to the buckling of web link.

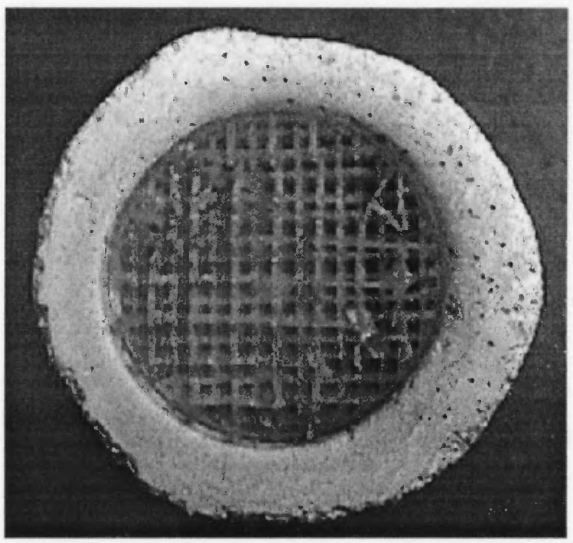

(a) Part4t6, shorter web link part with 6 mm shell thickness.

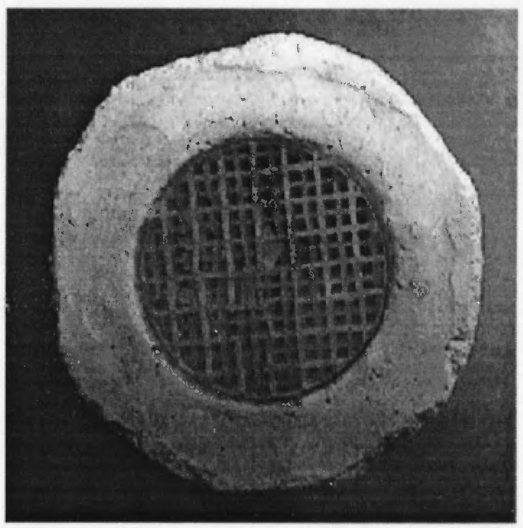

(b) Part4t9, shorter web link part with 9 mm shell thickness.

Figure 5.9 Parts with smaller web span length do not bend during the burnout process.

5.3.5 Web Link Buckled and Shell Cracked

The experimental observations of Part6t1 and Part6t2 show that the web links buckle but then the ceramic shell still cracks (see Figure 5.10). The FEA results (see Table 4.7) predict that for Part6t1 and Part6t2, the web link buckles and the shell cracks at about the same low temperatures. The dimensions of Part6 are the same as those of Part2 which has longer web link spans. The experimental result confirms the FEA prediction. It leads to the conclusion that shell thickness is essential to the prevention of shell cracking.

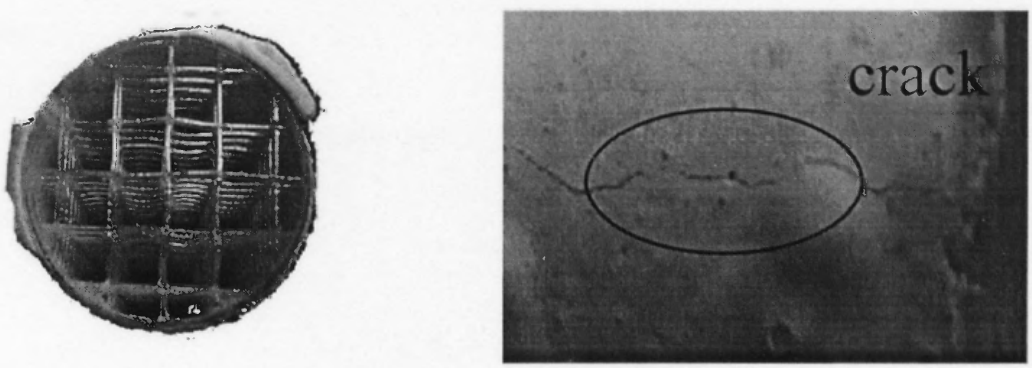

Web link buckled

Shell thickness of 1 mm is not enough to absorb induced stress

Figure 5.10 Part6t1, a long web span (9.525 mm) pattern with 1 mm shell thickness. The web links are buckled but the ceramics shell is still cracked.

5.4 Experimental Measurement with Strain Gauge

In the previous section, the qualitative experimental investigation provides the evidence for the situation under which the shell cracks and the internal web structure buckles. In Chapter 4, the computational simulations provide the predictions of shell cracking temperatures, web link buckling temperatures, induced stress profiles, and locations of maximum stresses in the ceramic shell and webbed pattern. Following the result of a

finite element stress analysis, a further experimental study with strain gauges is performed in order to provide a comprehensive understanding about the ceramic shell cracking and to identify effective ways for preventing the shell cracking.

Strain gauges and thermocouples were mounted on the test samples. An example of the test sample is shown in Figure 5.11a. After mounting the strain gauges on the surface of each pattern, the pattern is coated with investment ceramic slurry (see Figure 5.11b). The samples are then placed in the oven (see Figure 5.11b). The generated strains due to heat are recorded from 23°C to 100°C. Figure 5.12 shows the strain gauge instrument.

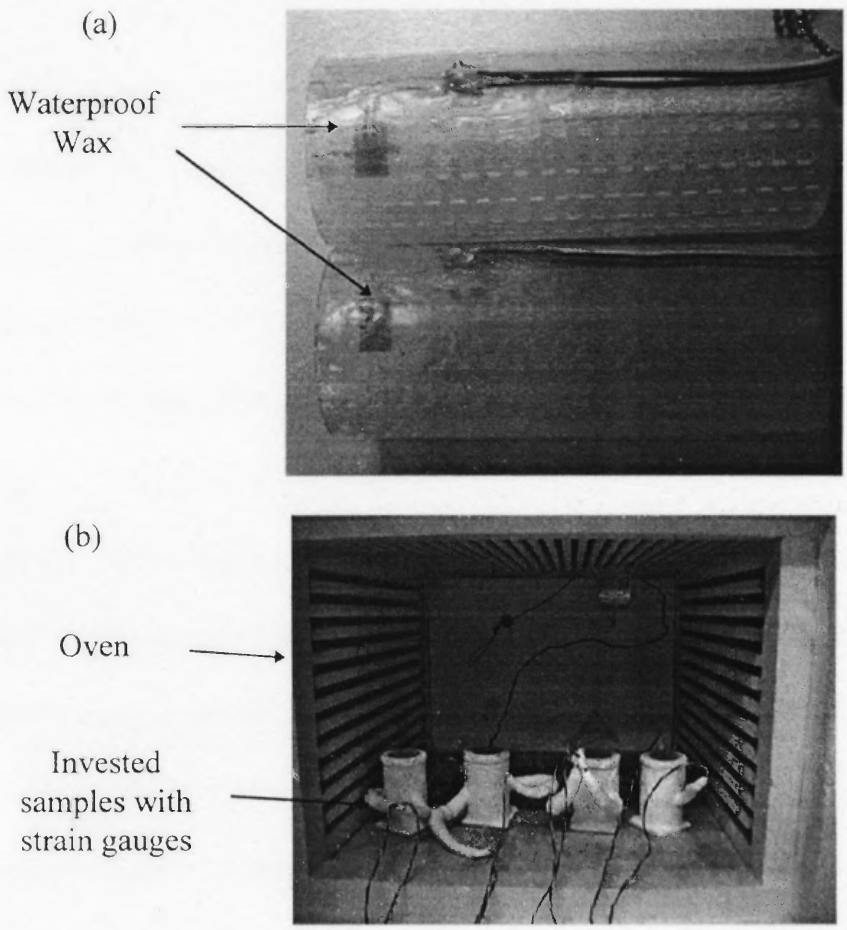

Figure 5.11 Samples mounted with strain gauges.

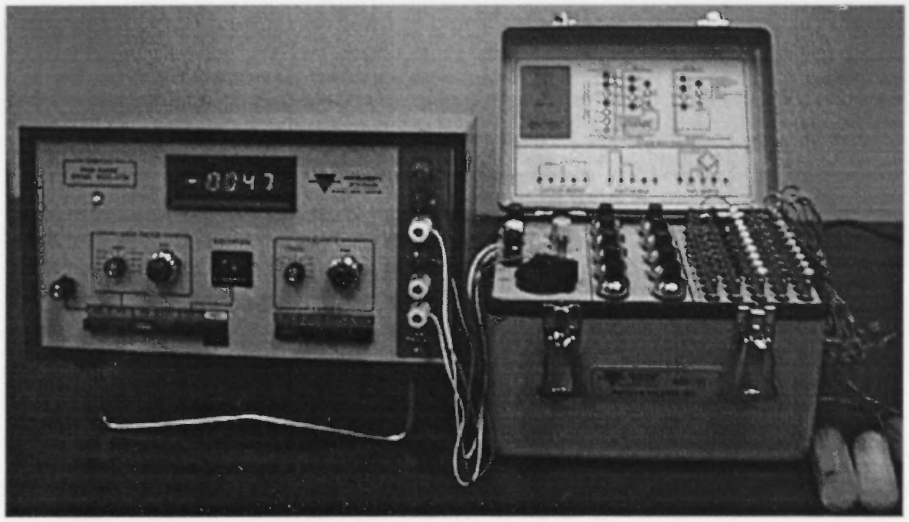

Figure 5.12 Strain gauge instrument.

The experimental results obtained from the strain gauges are shown in Figure 5.13. The results exhibit the same trends as the predictions from the finite element analysis. We only consider the thermal expansion of the shell/pattern construction in our numerical simulation. The property of thermal insulation of investment ceramic material causes the temperature lag in the epoxy pattern (see Figure 5.14). Therefore the measured stresses from the experiments are somewhat larger than the results of FEA. If we take the average of the temperatures at the interface and center, then the experimental data can be improved. If the heating rate is slower, the experimental measurements can also be improved. Figure 5.14b shows it takes about 9 minutes for the measured temperature to reach the target setpoint. From the analytical and experimental study, the stresses at low temperatures (below the epoxy glass temperature) are more important because the shell cracking and web link buckling may occur at low temperatures. After the glass transition,

the properties of epoxy change dramatically. Accordingly, the predicted and measured stresses are no longer very meaningful.

The data of the initial run of the experiment for each sample shows a negative (compressive) strain (see Figure 5.15). It is contrary to the real situation of the thermal expansion of the SLA pattern. The discrepancy is due to the significant thermal expansion of wax. Note that the wax is applied for the purpose of moisture-proofing the strain gauges during the slurry dipping process. This discrepancy can be eliminated by preheating the test samples to the melting point of the wax, about 70°C, for a certain time to "lose" the wax before recording the experiment result. The experiment also shows the epoxy material cannot be heated and cooled again to repeat the same experiment (see Figure 5.16).

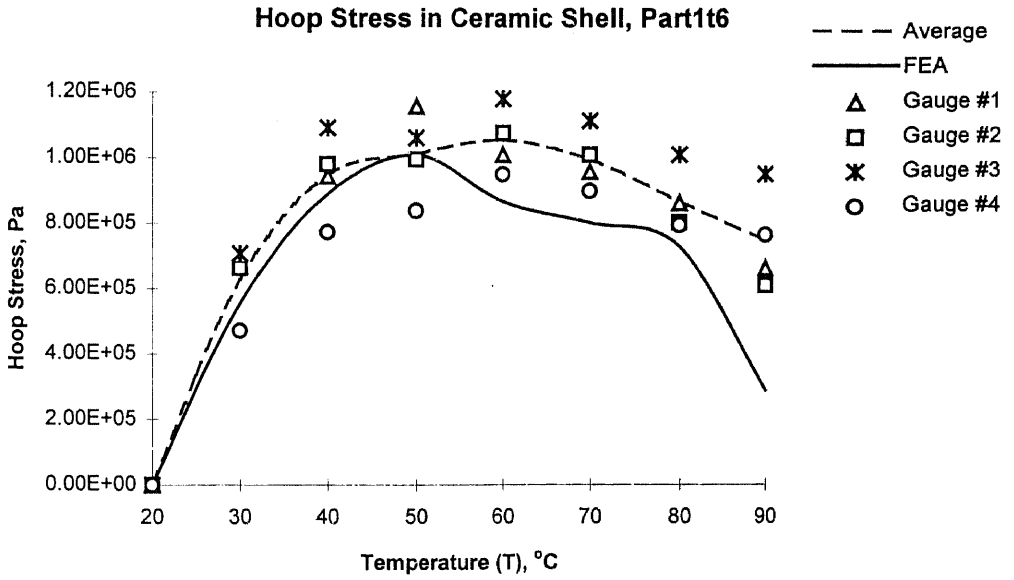

Figure 5.13a Hoop stress developed in Part1t6 under the influence of heat.

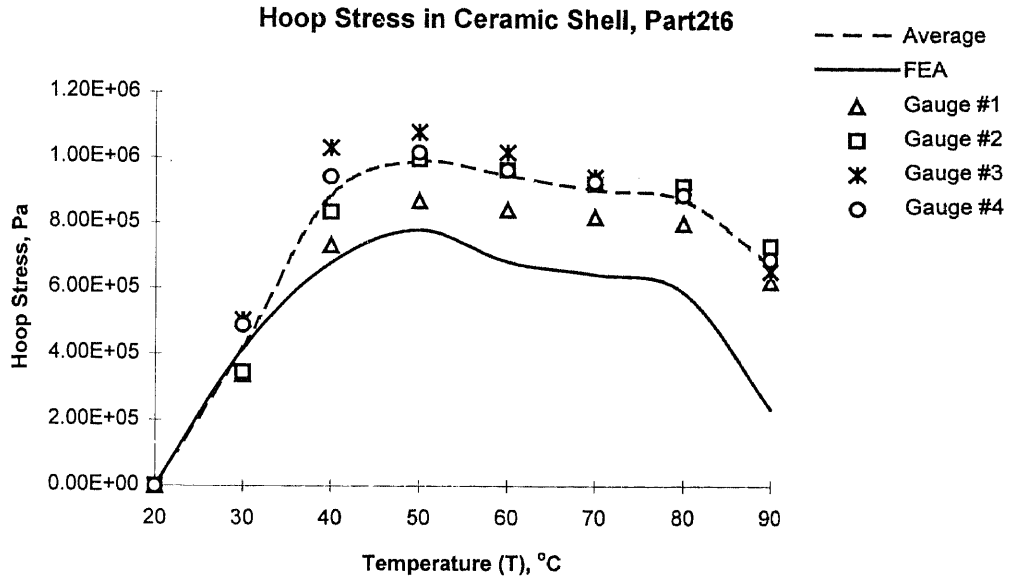

Figure 5.13b Hoop stress developed in Part2t6 under the influence of heat.

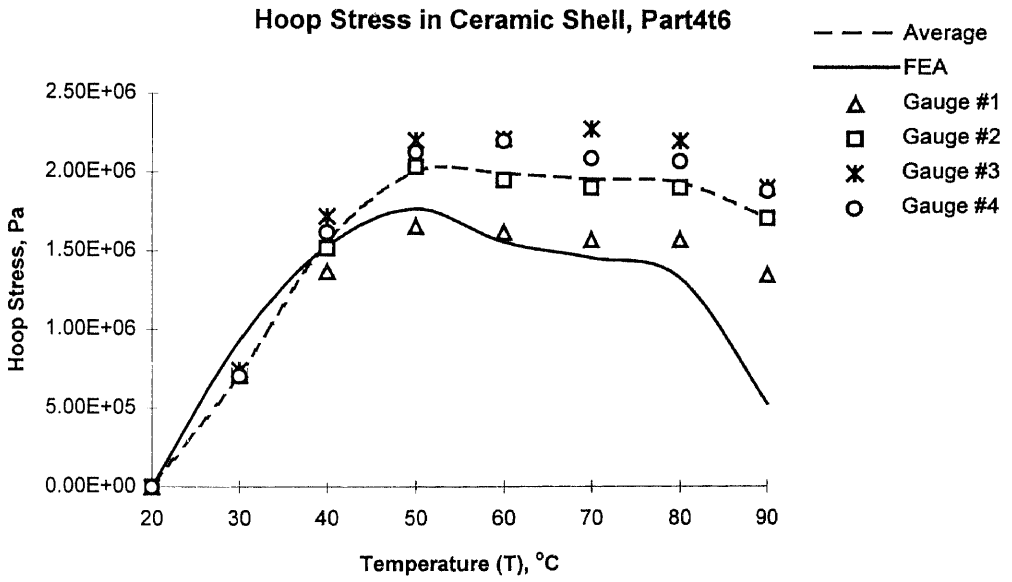

Figure 5.13c Hoop stress developed in Part4t6 under the influence of heat.

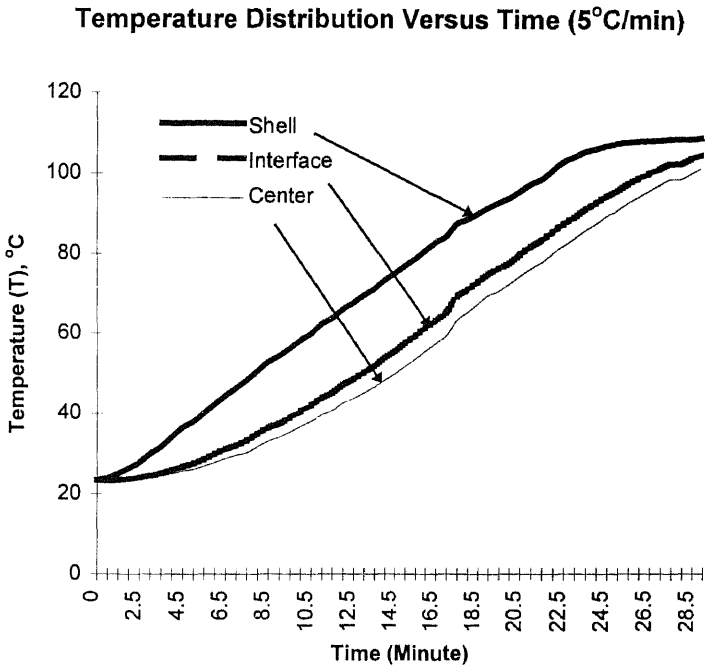

Figure 5.14a The thermal insulation of ceramics and epoxy causes temperature discrepancy.

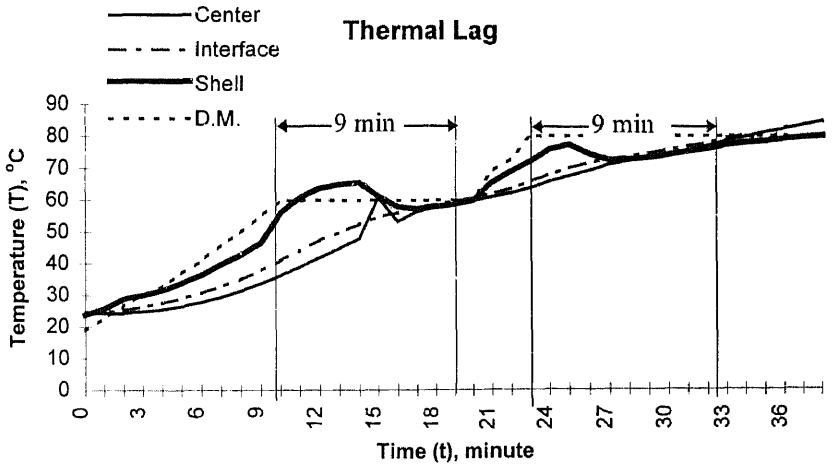

Figure 5.14b It takes longer time (about 9 minutes) to reach the pre-set temperature (DM) because of thermal lag.

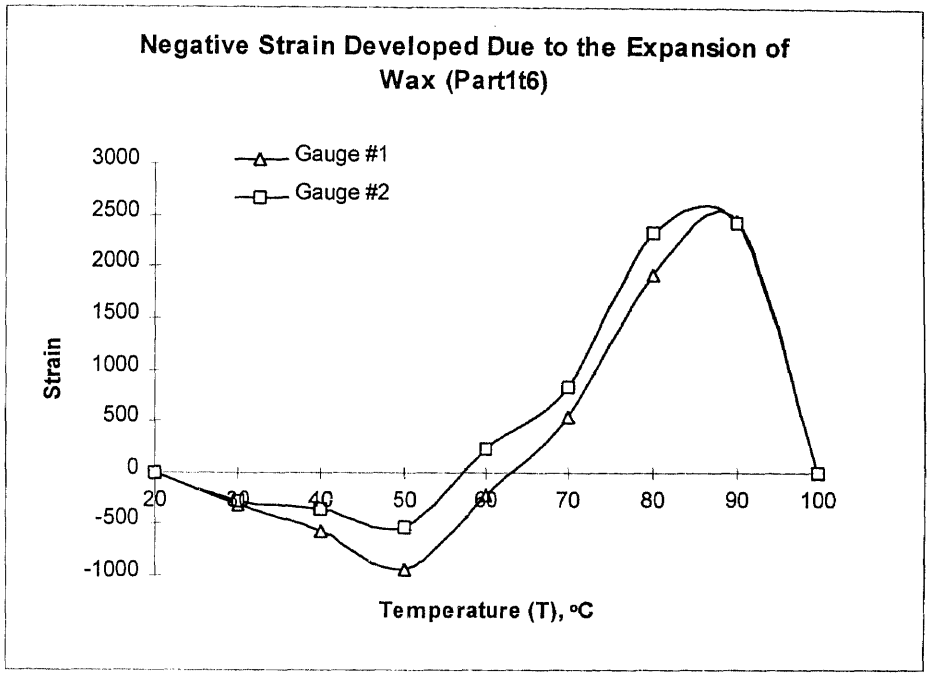

Figure 5.15 Initial strain is negative when the fresh sample is being heated.

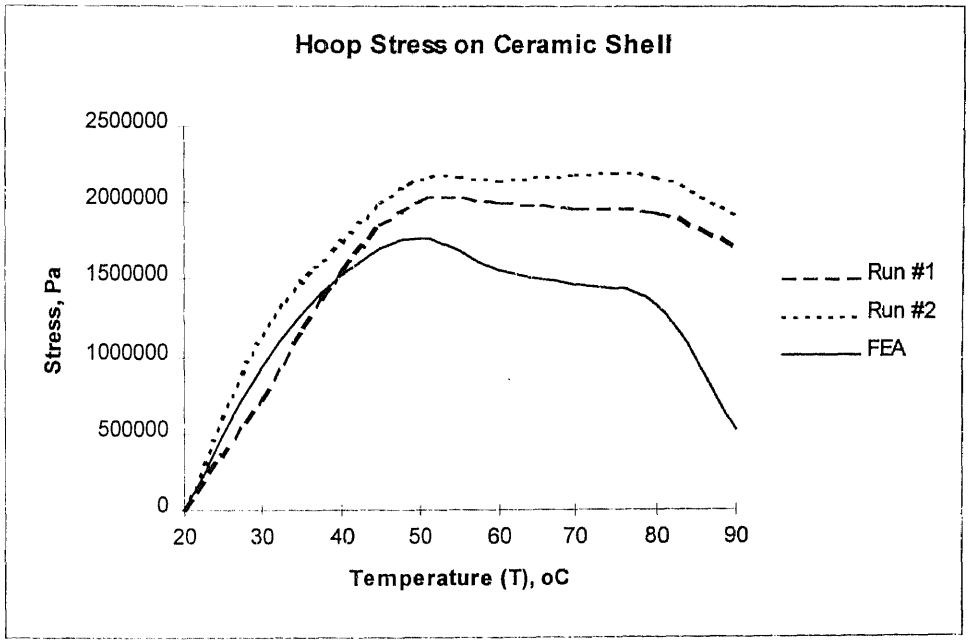

Figure 5.16 Stress increased in Run #2 because the epoxy material has been hardened.

5.5 Findings and Lessons Learned

This chapter presents the experimental results of the SLA pattern burnout process. It reveals the mechanism of shell cracking and provides useful information about how to prevent the shell cracking. These experimental results have good agreement with the FEA predictions in the previous chapter. The following is a summary of the findings of these experiments and comparisons with FEA predictions:

1. The experiments confirm the FEA predictions and show that investment shell cracks at a low temperature before the glass transition temperature of epoxy.
2. The links of webbed SLA patterns are observed to have various degrees of wavy shape, i.e. slightly buckled, or severely buckled, or no buckling.
3. The experiments and FEA simulations indicate that the mechanisms of shell cracking and web link collapsing are strongly related to the dimensions of web structure and the investment shell thickness.
4. The experiments and FEA simulations demonstrate that the webbed pattern with a longer link span length and smaller link width can bend or buckle more easily.
5. When the test samples are bent or buckled, the interior angles of the rectangular frames are preserved. This supports the model of using the buckling of a rectangular frame for analysis.
6. The experiments and FEA simulations show that the induced stress decreases dramatically when the internal web link buckles.
7. The results of strain gauge measurements show reasonable agreements with the FEA predictions. The discrepancy comes from thermal insulation,

uncertainty of material property, and additional expansion of wax and adhesive material.

8. The expansion of the moisture-proof wax and additional adhesive material for strain gauge installation contributes to some experimental errors. Pre-lost wax can help eliminate this discrepancy.

CHAPTER 6

DESIGN OF INTERNAL WEB STRUCTURE

The analytical and experimental studies described in Chapters 4 and 5 are based on a pattern with an internally square web structure, which is generated by an existing build style of SLA for shell investment casting tooling. In this chapter, the control of shell cracking and webbed pattern buckling via the design of new geometrical shapes of internal web structure is presented. The purpose is to provide a possibility of designing a new build style of internal web structure which provides better features for shell investment casting tooling.

6.1 Geometrical Shape of Internal Web Structure

6.1.1 Background

The challenge of building SLA patterns as thermally expendable patterns in shell investment casting is to address simultaneously the issues of rigidity and collapsibility. That is, the SLA pattern must be strong enough for pattern handling and downstream processing, such as surface finishing, shipping and slurry coating. Meanwhile, the pattern must be able to collapse on itself without breaking the shell during the pattern burnout process in investment casting.

A quasi-hollow build style of SLA patterns was designed by 3D Systems, based on Jacobs' observation that the yield of invested shells with SLA patterns is a function of

void ratio. In order to build quasi-hollow SLA patterns for investment casting tooling, the requirements for an internal web structure are as follows:

- high void ratio, to increase the yield of successful investment shells
- large web link span, to increase void ratio
- negligible deflection of the surfaces, to achieve high accuracy
- large open cells, to allow fast drainage
- large interior angle, to reduce the residual liquid resin
- good collapsibility, to enable the pattern collapsing inwards during the burnout process

Consequently, investigations and developments of quasi-hollow patterns with different internal web structures are undertaken. Triangular, square, and hexagonal honeycomb internal structures are considered here (see Figure 6.1). The first two web structures were developed by 3D Systems. The focus here is on the development and analysis of a hexagonal web structure of SLA pattern and comparison with the other two structures for investment casting tooling.

6.1.2 Triangular Internal Web Structure

In early 1992 the development of a quasi-hollow pattern for shell investment casting was introduced to solve the problem of solid SLA pattern for shell investment casting. A completely hollow pattern was found to deform too easily under normal handling. Also, walls which are long and thin would actually bow inwards even under the relatively low hydrostatic pressure levels experienced during the coating of slurries to form investment

shells. Thus, the quasi-hollow pattern has been developed to have a thin outer skin (0.014 to 0.018 inch, or 0.35 to 0.45 mm thick), supported by a "simple, topologically connected" internal web structure, such that the rigidity of the SLA pattern is enough to withstand the compressive load during the dipping process.

In order to obtain a high-quality pattern, the uncured liquid resin must be drained completely from the interior of the pattern. The cells within the pattern should be open to allow the uncured liquid resin to flow freely from any one location to another. If the internal web structure consisted of closed cells complete drainage would not be possible without venting and draining each and every cell. The concept of topologically simple connections enables uncured resin at any location of the pattern to flow freely within the limits of gravity, viscous drag, and surface tension forces.

In 1993, the triangular web structure was designed and released as an in the early quasi-hollow build style. The web structure consists of a series of equilateral triangles having the altitude of to 3.8mm (0.15 inch). These triangles are built on the top of one another for a specified height, with an offset so that the vertices of the new group of equilateral triangles lie directly above the centroids of the previous group of equilateral triangles. Serious problems such as poor upfacing surface quality, incomplete pattern drainage, lower void ratio, and occasional shell cracking during the burnout process are encountered.

Triangular web structure, a = 9.65 mm

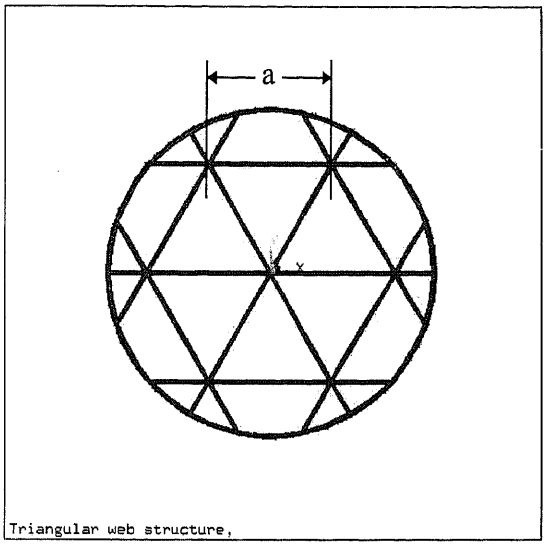

Square web structure, b = 6.35 mm

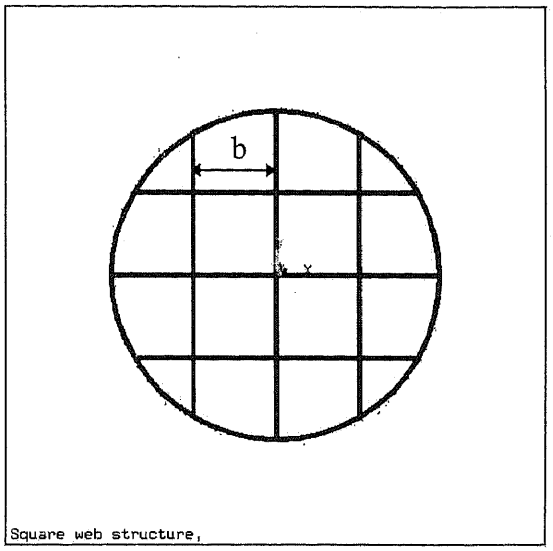

Hexagonal web structure, c = 3.94 mm.

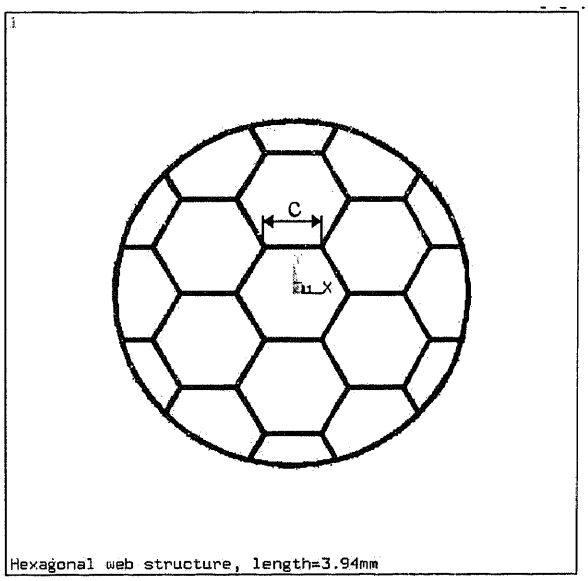

Figure 6.1 Three geometric shapes of internal web structure: triangular, square and hexagonal shapes, with constant area (A) for the same drainage rate. Their web link length are a, b, and c, respectively.

6.1.3 Square Internal Web Structure

The triangular internal web structure, despite much improvement, still has a lot of shortcomings for the shell investment casting process. The design of square internal web structure was introduced and released in 1995. It addressed the shortcomings of triangular internal web structure. The new features include thick upfacing and downfacing skin layers, large link span, high void ratio, large interior angle, and selectable vents and drains. The feature of the thick upfacing and downfacing skin mitigates the pinhole problem that results from the support removal in the triangular build style. Additionally, the thick upfacing and downfacing skin layers increase not only the strength but also the facing quality of the quasi-hollow pattern. With the enhanced thick skin, a glass-like upfacing surface can be fabricated by the QuickCast 1.1 build style. The quality of the upfacing surface finish is also improved.

Reports from the foundries indicate that the foundry yield of successful castings is a monotonically increasing function of the void ratio [Jacobs, 1996]. Since the cured linewidth of laser exposure can be expressed as

$$L_w = B\sqrt{C_d / 2D_p} \tag{6.1}$$

where L_w is the linewidth, B is the laser spot diameter, C_d is the cured depth, and D_p is the penetration depth. The cured linewidth does not depend upon the web link spacing. Accordingly, the increase of web link spacing will increase the void ratio. Unfortunately, the longer span of the web link may cause a bigger "sag" of the span. For a simply supported beam the maximum deflection can be calculated from

$$\delta_{max} = \frac{5qL^4}{384EI} \tag{6.2}$$

where I is equal to $\frac{bh^3}{12}$, and q is the uniform load. Thus the deflection of a uniformly loaded beam is directly proportional to the fourth power of the span, and inversely proportional to the cube of the thickness. However, with the triple upfacing skin of the QuickCast build style, the quality of the upsurface is not affected. This is due to the fact that the first skin layer acts as a support for the second layer, and then the combined first and second skin layers act as a support for the third and final upfacing skin. The void ratio increases as the web link span becomes longer. Consequently, it increases the yield of successful foundry shell investment castings, without increasing the deflection of the surface. That is, it does not influence the quality of the upfacing and downfacing surfaces. The design of a square web structure thus enhances parts quality, void ratio, and better drainage by increasing the web span, interior angle, and skin layers.

6.1.4 Guidelines

The development of internal web structure is still undergoing changes to overcome the problematic drainage, collapsibility, rigidity, and surface quality of the quasi-hollow SLA pattern for successful investment casting. The studies of the internal web structure in the previous research works have led to the design guidelines for a new internal web structure for investment casting tooling as follows:

1. The SLA pattern with an internal web structure has to be structurally rigid for handling and subsequent operations.

2. The internal web structure has to be easily collapsible during the burnout process in investment casting.
3. The internal web structure must provide a large void ratio for high yields of successful foundry castings without sacrificing the pattern.
4. The geometrical shape of internal web structure must provide large open areas and interior angles for the uncured liquid to drain out, leaving very little residual liquid resin at the corner of the web cell.

6.2 Design of Hexagonal Web Structure

6.2.1 Rheological Analysis

To fabricate quasi-hollow patterns for the shell investment casting, the uncured liquid resin captured within the internal web cells must drain out. Otherwise, it will increase the solid thickness after the postcuring process. Consequently, it is more likely to cause the shell cracking to occur. Therefore, to drain out the uncured liquid resin thoroughly and rapidly is a major task. The drainage of the epoxy resin is a laminar flow, because the Reynolds number of the epoxy resin is in the range of 10^{-2} to 1 [Jacobs, 1995]. The Hagen-Poiseuille equation of the laminar flow of a viscous fluid in a tube is [Schlichting, 1995]:

$$Q = \frac{\pi R^4}{8\mu l}(p_1 - p_2) \tag{6.3}$$

where $(p_1 - p_2)$ is the pressure drop, R is the radius, and μ is the viscosity of the fluid. The volumetric flow rate is proportional to the fourth power of the radius of the tube, or is

proportional to the square of the area. Therefore, to improve resin drainage it is important to increase the cell size.

Another problem of incomplete drainage is the effect of liquid resin capillary and viscous forces to form a natural meniscus at the corners of an internal web cell. The size of meniscus is related to the interior angle. The larger open interior angle will generate a larger meniscus shape. Consequently, the residual liquid resin will be diminished.

From the standpoint of rheology, the internal web cell must have a large open area with a large open interior angle to achieve a high yield of successful investment casting shells. A comparison is made for triangular, square and hexagonal web structures with the same area (A), with the web link lengths for equilateral triangles, squares and hexagons being a, b, and c, respectively. Then b is equal to 1.52a, and c is equal to 0.62a. Table 6.1 shows the area, length, circumference, and void ratio for triangular, square and hexagonal structures. The basis of analysis is keeping the area constant in order to have the same drainage rate for the triangular, square and hexagonal web structures.

Table 6.1 Comparison of triangular, square and hexagonal structures, with the area constant for the same drainage rate.

	Interior Angle	Web Link Length (mm)	Area (mm^2)	Circumference (mm)	Void Ratio
Triangle	60°	9.65	40.323	28.95	0.73
Square	90°	6.35	40.323	25.4	0.83
Hexagon	120°	3.94	40.323	23.64	0.89

6.2.2 Stress Analysis

Finite element analysis is used to compare the thermal stress in the various web structures. The web width is 0.3048 mm for all of the structures. The material properties are the same as those described in Chapter 4. The dimensions of each structure are given in Table 6.1. The numerical results of the FEA are shown in Table 6.2. The stress profiles are shown in Figure 6.2. As shown, the void ratio has increased to 0.89 for the hexagonal web structure from 0.79 for the triangular web structure and 0.83 for the square web structure. The induced stress on the ceramic shell for the hexagonal structure is reduced by 32% and 22% compared with the triangular structure and square web structures, respectively.

The webbed SLA patterns are subjected to a hydrostatic pressure (1 Pa in this FEA analysis) during the ceramic slurry dipping process. SLA patterns may cause certain degrees of deformation under the hydrostatic pressure. A comparison of deformation of patterns for different web structures is made and shown in Figure 6.3. The results of FEA indicate that the pattern with hexagonal web structure deforms larger than others. The maximum deformations of patterns with hexagonal, square and triangular web structure are 0.302×10^{-6} mm, 0.282×10^{-6} mm, and 0.185×10^{-6} mm, respectively. That is, the pattern with hexagonal web structure is more fragile.

Table 6.2 Stress for different web structures, with 6 mm of ceramic shell thickness.

	Stress (Pa)		
T (°C)	Triangular	Square	Hexagonal
30	6.26E+05	5.55E+05	4.49E+05
40	1.02E+06	8.90E+05	7.12E+05
50	1.17E+06	1.01E+06	7.91E+05
60	1.02E+06	8.68E+05	6.66E+05
70	9.48E+05	8.03E+05	5.92E+5
80	8.63E+05	7.31E+05	5.37E+05
90	3.40E+05	2.89E+05	2.10E+05

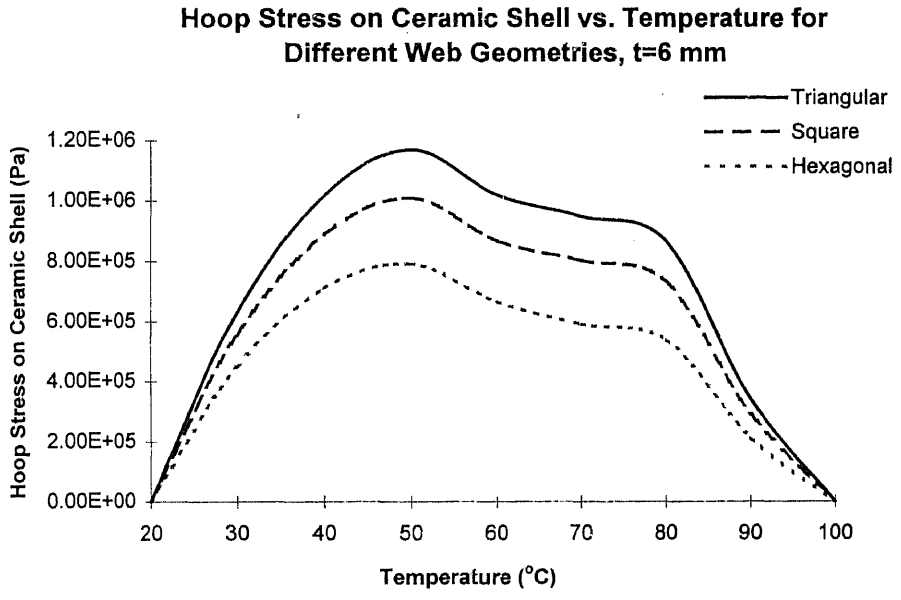

Figure 6.2 Comparison of stress profiles on ceramic shell with different geometrical web structures.

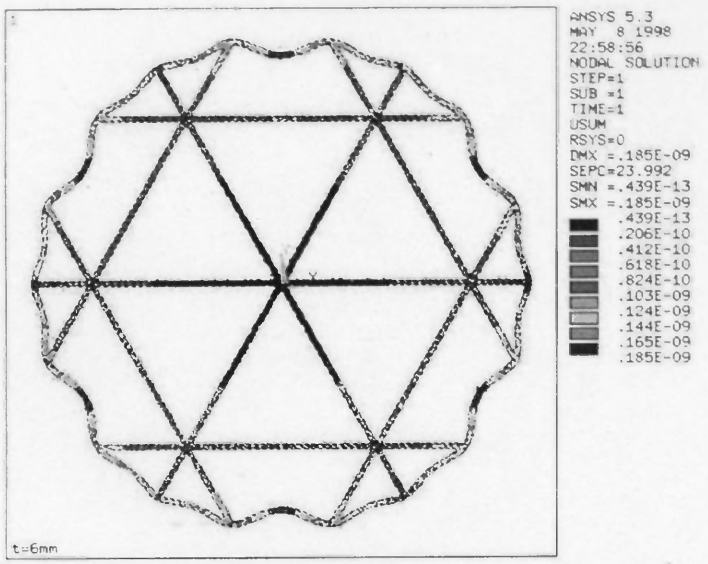

Figure 6.3a Pattern with triangular web deforms 0.185×10^{-6} mm under 1 Pa hydrostatic pressure.

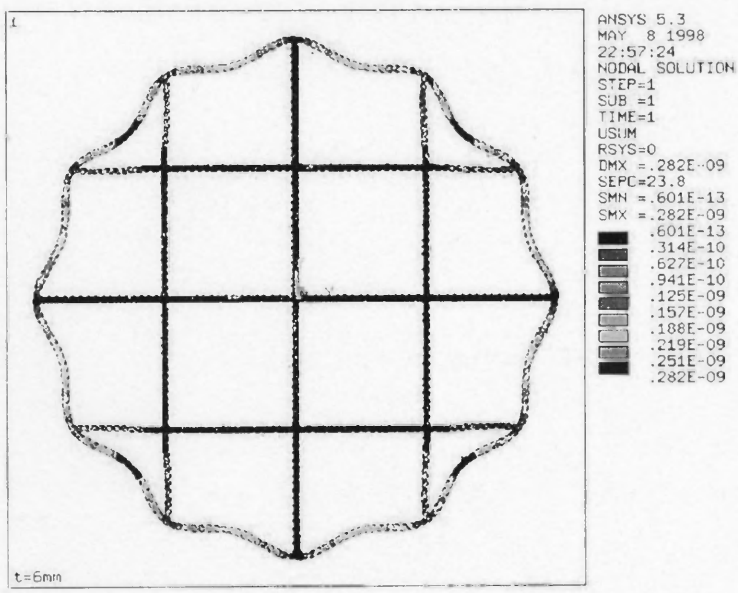

Figure 6.3b Pattern with square web deforms 0.282×10^{-6} mm under 1 Pa hydrostatic pressure.

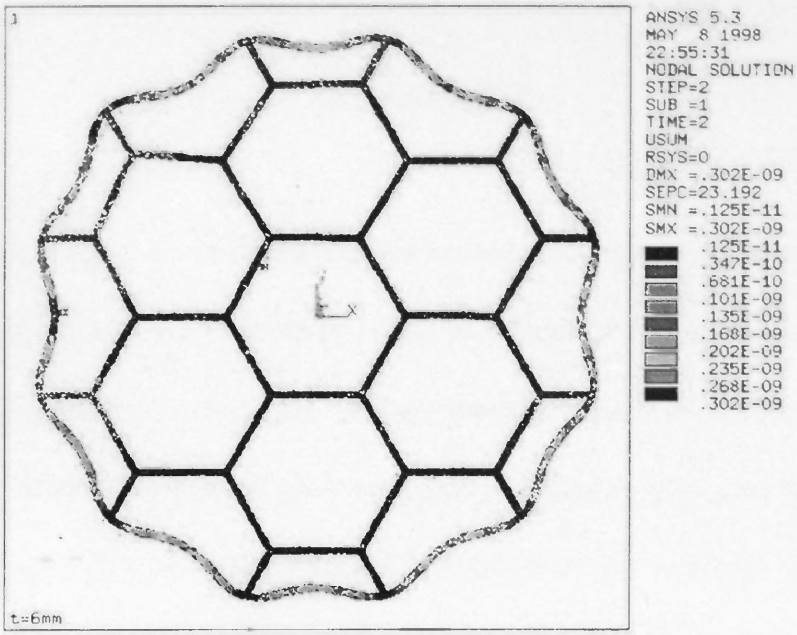

Figure 6.3c Pattern with hexagonal web deforms 0.302×10^{-6} mm under 1 Pa hydrostatic pressure.

CHAPTER 7

CONCLUSION

The numerical model and instrumented experimentation show that the induced stresses on the ceramic shell reduced dramatically after the internal web links buckle during the pattern burnout process in investment casting. However, the shell mold still cracks while the web links buckle in some samples which have long web spans and thin shells. Shell cracking and web link buckling occur at temperatures (40 - 60°C) below the glass transition temperature of epoxy (60 - 70°C). Shell thickness is an important factor for the prevention of shell cracking. The dimensions of web link structure are the main determining factors of web link buckling. A pattern with a longer web link span or a smaller web width buckles more easily. The prevention of shell cracking during the pattern burnout process can be achieved by buckling of the epoxy pattern or softening of the epoxy material.

A finite element model for investment casting with SLA webbed patterns is presented. It can be used to identify at what temperatures the shell cracks and the web link buckles, and to predict the generated stresses in the investment shell and in the web link during the SLA pattern burnout process. The predicted temperatures of shell cracking and web link buckling and the magnitudes and locations of maximum stresses in the investment shell and web link show reasonable agreement with the measured quantities. The discrepancy between the numerical predictions and experimental data is not

substantial and can be further reduced if the effects of heat transfer of the ceramics and epoxy materials are considered.

An analogous formula for estimation of thermal stresses in the investment shell and webbed pattern is developed. The development is based on the Lames equation for the thick-walled cylinder, using the FEA obtained stresses to determine the equivalent Young's modulus and coefficient of thermal expansion for the quasi-hollow SLA pattern (regarded as a part with porous material). Instead of FEA with the sophisticated pattern geometry, the equivalent force method developed can be used to efficiently simulate the thermal stresses in the pattern burnout process for the prevention of shell cracking in investment casting.

The hexagonal web structure appears to have the potential to resolve the problems of existing triangular and square web structures for investment casting tooling using SLA rapid prototyping technology. The void ratio has been increased to 0.89 from 0.79 for the triangular web structure and 0.83 for the square web structure. The FEA results show that the induced stress has been reduced by 32% and 22% compared with the triangular and square web structures, respectively. The drainage of uncured liquid resin has been increased by increasing the interior angle to reduce the meniscus.

REFERENCES

Atwood, C. L., Maguire, M. C., Pardo, B. T., and Bryce, E. A., "Rapid Prototyping Applications for Manufacturing," *SAMPE Journal*, v 32 n 1, pp. 935-948, (1996).

Beaman, J. J, and et. al., *Solid Freeform Fabrication: A New Direction in Manufacturing*, Kluwer Academic Publishers, Morwell, MA, (1997).

Blake, P., Baumgardner, O., Haburay, L., and Jacobs, P. F., "Creating Complex Precision Metal Parts Using QuickCast," *Proceedings of SME–Rapid Prototyping and Manufacturing*, 1994 Conference, Dearborn, MI, April 26-28, (1994).

Burns, M., *Automated Fabrication*, PTR Prentice Hall, Englewood Cliffs, NJ, (1993).

Conley, J. G., and Marcus, H. L., "Rapid Prototyping and Solid Free Form Fabrication," *Journal of Manufacturing Science and Engineering*, v. 119, n. 4, pp. 811-816, ASME, (1997).

Deckard, C. R., and Beaman, J. J., "Recent Advances in Selective Laser Sintering," *Proceedings of the 14th Conference on Production Research and Technology*, National Science Foundation, Ann Arbor, MI, (1987).

Denton, K. R., and Jacobs, P. F., "QuickCast Tooling: A Case History at Ford Motor Company," *Proceedings of SME–Rapid Prototyping and Manufacturing*, Dearborn, MI, April, (1993).

Dunham, G. D., "Rapid Prototyping Through Investment Casting," *ANTEC Conference Proceedings of the 52nd Annual Technical Conference*, pp. 1094-1096, (1994).

Friedrich, B. P., et al., *JTEC/WTEC Panel Report on Rapid Prototyping in Europe and Japan*, SME Press, ITRI of Loyola College in Maryland, Baltimore, MD, (1997).

Gere, J. M., Timoshenko, S. P., *Mechanics of Materials*, 2nd edition, Brooks/Cole Engineering Division Monterey, CA, (1984).

Greenbaum, P. Y. and Khan, S., "Direct Investment Casting of RP Parts," *Conference Proceedings of Rapid Prototyping and Manufacturing*, Dearborn, MI, (1994).

Hague, R., and Dickens, P. M., "Stresses created in ceramic shells using QuickCast models," *Proceedings of The First National Conference on Rapid Prototyping and Tooling Research*, Buckinghamshire College, UK, Nov. 6-7, 1995, pp. 89-100, (1995).

REFERENCES
(Continued)

Hague, R., and Dickens, P. M., "Requirements for the successful autoclaving of stereolithography models in the investment casting process," *Proceedings of The Second National Conference on Rapid Prototyping and Tooling Research*, Buckinghamshire College, UK, Nov. 18-19, 1996, pp. 77-92, (1996).

Hosni, Y. A., Nayfeh, J., and Sundaram, R., "Investment Casting Using Stereolithography: Case of Complex Objects," *Conference Proceedings of 6th Industrial Engineering Research* , pp. 843-849 (1997).

Jacobs, P. F., "QuickCast 1.1 & Rapid Tooling," *Proceedings of the North American Stereolithography User Group Conference and Annual Meeting*, 1995, Tampa, FL, March 12-16, (1995).

Jacobs, P. F., *Rapid Prototyping and Manufacturing: Fundamentals of Stereolithography*, SME, Dearborn, MI, (1992).

Jacobs, P. F., "Enhanced Stereolithography Patterns for Investment Casting and Rapid Tooling," *Conference Proceedings of the 27th International SAMPE Technical Conference*, v. 17, Albuquerque, NM, pp. 980-995, (1995).

Jacobs, P. F., *Stereolithography and Other RP&M Technologies*, ASME Press, New York, NY, (1996).

Johnson, J. L., *Principles of Computer Automated Fabrication*, Palatino Press, Irvine, CA, (1994).

Kalpakjian, S. *Manufacturing Processes for Engineering Materials*, Chapter 5, (1991).

Kassimali, A., *Structural Analysis*, PWS Publishing Company, Boston, MA, Chapters 5 & 12, (1995).

Kennerknecht, S., and Sarkis, B., "Rapid Prototype Casting (RPC): The Fundamentals of Producing Functional Metal Parts from Rapid Prototype Models Using Investment Casting," *Proceedings of the Fifth International Conference on Rapid Prototyping*, University of Dayton, Dayton, OH, June 12-15, (1994).

Koch, M., "Rapid Prototyping & Casting," *Proceedings of the 3rd European Conference on Rapid Prototyping & Manufacturing*, (1994).

REFERENCES
(Continued)

Krikorian, G., "Practical Comparison of Rapid Prototyping and Tooling Options", *Wescon Conference Record Proceedings of the 1996 Wescon Conference*, Anaheim, CA, pp. 312-316, (1996).

Menon, U., and Koch, M., "Rapid Prototyping for Foundry Tool Making," *Proceedings of Solid Freeform Fabrication Symposium*, pp. 95-101, Austin, TX, (1991).

Merz, R., Prinz, F., B., Ramaswami, K., Terk, M., and Weiss, L. E., "Shape Deposition Manufacturing," *Proceedings of the Solid Freeform Fabrication Symposium*, The University of Texas at Austin, Austin, TX, August 8-10, (1994).

Pang, T. H., "Advances in Stereolithography Photopolymer Systems," *Stereolithography and other RP&M Technologies*, SME Dearborn, MI, July 1996, Chapter 2, (1996).

Prioleau, F. R., "Applications of Stereolithography in Investment Casting," *Conference Proceedings of the Second Internaltional Conference on Rapid Prototyping* , University of Dayton, Dayton, Ohio, (1991).

Ramaswami, K., and Prinz, F. B., "CNC Cutter Path Generation in Shape Deposition Manufacturing," *Proceedings of Concurrent Product and Process Engineering Symposium*, ASME International Mechanical Engineering Congress and Exposition, San Francisco, CA, Nov. 12-17, (1995).

Richerson, D. W., *Modern Ceramic Engineering: Properties, Processing, and Use in Design*, Marcel Dekker, New York, 1982, Chapters 2-3, (1982).

Sachs, E., et al., "Micro-Constructive Manufacturing by 3D Printing," *Proceedings of NSF Design and Manufacturing Grantees Conference*, Cambridge, MA, Jan. 5-7, (1994).

Sandia National Laboratories, Properties of Investment Ceramic, *Internal Report*, (1995).

Schlichting, H., *Boundary Layer Theory*, McGraw Hill, New York, NY, Fourth Edition, pp. 10-11, (1995).

Sarkis, B., "Rapid Prototyping for Non-Ferrous Investment Casting," *Proceedings of SME Rapid Prototyping & Manufacturing*, 1994 Conference, Dearvorn, MI, (1994).

Segerlind, L. J., *Applied Finite Element Analysis*, John Wiley and Sons, New York, Chapter 23, (1984).

REFERENCES
(Continued)

Taylor, P. R. "Lost wax casting - a short illustrated review," *Metals and Materials*, v 2, n 11, pp. 705-710, (1986).

Ugural, A. C. and Fenster, S. K., *Advanced Strength and Applied Elasticity*, PTR Prentice Hall, Englewood Cliffs, NJ, Chapter 8, (1995).

Wang, C. T., *Applied Elasticity*, McGraw-Hill, New York, Chapter 9, pp.. 209-239, (1953)

Yao, W. L., Wong, H., and Leu, M. C., "Analysis of Thermal Stresses in Investment Casting with Epoxy Patterns," *Proceedings of North America Stereolithography Users Group Meeting and Conference*, 1996, San Diego, CA, March 10-14, (1996).

Yao, W. L., Wong, H., Leu, M. C. and Sebastian, D. H., "An Analytical Study of Investment Casting with Webbed Epoxy Patterns," *The proceedings of the 1996 ASME Manufacturing Science and Engineering Winter Conference and Annual Meeting*, MED-Vol. 4, Atlanta, GA, November, (1996).